European Union's Seventh Framework Programme

Grant Agreement Nº: 603521

Project Acronym: **PREFACE**

Project full title: **Enhancing prediction of tropical Atlantic climate and its impacts**

Instrument: Collaborative Project

Theme: ENV.2013.6.1-1 – *Climate-related ocean processes and combined impacts of multiple stressors on the marine environment*

Start date of project: 1 November 2013 Duration: 48 Months

Deliverable D4.2: "Eastern Atlantic interannual to decadal variability: Analysis of historical in-situ and remote sensing data with regard to the Eastern Atlantic interannual to decadal variability and Benguela Nino"

Lead work package for this deliverable: UCT

Lead contractor for this deliverable: UCT

Due date of deliverable: 30.04.2016

Actual submission date: 29.04.2016

Project co-funded by the European Commission within the Seven Framework Programme (2007-2013)		
Dissemination Level		
PU	Public	X
PP	Restricted to other programme participants (including the Commission Services)	
RE	Restricted to a group specified by the Consortium (including the Commission Services)	
CO	Confidential, only for members of the Consortium (including the Commission Services)	

Contribution to project objectives – with this deliverable, the project has contributed to the achievement of the following objectives (see Annex I / DOW, Section B1.1.):

N.º	Objective	Yes	No
1	Reduce uncertainties in our knowledge of the functioning of Tropical Atlantic (TA) climate, particularly climate-related ocean processes (including stratification) and dynamics, coupled ocean, atmosphere, and land interactions; and internal and externally forced climate variability.	x	
2	Better understand the impact of model systematic error and its reduction on seasonal-to-decadal climate predictions and on climate change projections.		x
3	Improve the simulation and prediction TA climate on seasonal and longer time scales, and contribute to better quantification of climate change impacts in the region.	x	
4	Improve understanding of the cumulative effects of the multiple stressors of climate variability, greenhouse-gas induced climate change (including warming and deoxygenation), and fisheries on marine ecosystems, functional diversity, and ecosystem services (e.g., fisheries) in the TA.		x
5	Assess the socio-economic vulnerabilities and evaluate the resilience of the welfare of West African fishing communities to climate-driven ecosystem shifts and global markets.		x

Authors of this deliverable:

Mathieu Rouault (UCT), Peter Brandt (GEOMAR), Marek Ostrowski (IMR), Volker Mohrholz (IOW), Anja v.d. Plas (NatMIRC, MFMR)

Deviation from planned efforts for this deliverable:

No deviation.

Contents

Executive Summary

The present deliverable (D4.2) is a report on analyses of historic in situ and remote sensing data with regards to the internanual to decadal variability in the Eastern Atlantic. Belonging essentially to Task 4.2 “Monitoring variability along the southern hemisphere coastal wave guide”, it focuses on the eastern equatorial Atlantic and the coastal upwelling region of the southern hemisphere. Thus it encompasses a region of particular strong climate variability and at the same time strongest SST bias in coupled climate models. The report is divided into 6 sections, which are briefly described in the extended summary below. The results are based on the analysis of observations in the coastal and equatorial wave-guides and the application of models based on linear wave theory. The key findings can be summarised as follows.

1. Annual and semi-annual variations in the equatorial ocean circulation are dominated by the second and fourth baroclinc modes, which are resonantly excited.

2. Moored long-term velocity observations for the first time give insight into the mean state, intra-seasonal to seasonal variability and transport of the Angola Current. Preliminary analysis suggests that contrary to previous literature, there is no steady southward flow at the continental slope off Angola at 11°S. Instead, the time series is dominated by alternating bands of southward and northward velocities that can last for a few months.

3. Remotely forced coastal Kelvin waves dominate the interannual upper ocean variability in the Angola-Benguela region, explaining approximately 50% of the sea surface height variations and all the major Benguela cold and warm events during the period 1998-2012, including the 2010-11 event.

4. Furthermore, these Kelvin wave signals drive meridional currents in the Benguela region that control the water mass properties in this region on seasonal to interannual timescales.

5. Importantly the variations in the Benguela-Angola region can be well reproduced by linear ocean models forced by equatorial wind variations. This suggests a potential to predict these events with a 1 month lead time off Angola.

6. On longer timescales, decadal shifts in the ocean temperature and circulation of the Benguela region were linked to changes in the marine ecosystems.

The results regarding observed variability in the Benguela upwelling region on seasonal and longer time scales will be used for comparison with forced ocean simulations (WP5), coupled climate simulation (WP7) and for the interpretation of tropical Atlantic variability (WP9). It also contributes to Task 4.3, where a comparison is to be drawn between northern and southern hemispheres.

Extended summary of report sections

In section 1 **Annual and semi-annual cycle of equatorial Atlantic circulation associated with basin mode resonance**, we use multi-year, full depth velocity measurements from the central equatorial Atlantic to analyze the vertical structure of annual and semi-annual variations of zonal velocity. A baroclinic modal decomposition finds that the annual cycle is dominated by the 4^{th} mode and the semi-annual cycle by the 2^{nd} mode. Similar local behavior is found in a high-resolution general circulation model. This simulation reveals that the annual and semi-annual cycles of the

respective dominant baroclinic modes are associated with characteristic basin-wide structures. Using an idealized linear reduced-gravity model to simulate the dynamics of individual baroclinic modes, it is shown that the observed circulation variability can be explained by resonant equatorial basin modes. Corollary simulations of the reduced-gravity model with varying basin geometry (i.e. square basin versus realistic coastlines) or forcing (i.e. spatially uniform versus spatially variable wind) show a structural robustness of the simulated basin modes. A main focus of this study is the seasonal variability of the Equatorial Undercurrent (EUC) as identified in recent observational studies (see also D4.1). Main characteristics of the observed EUC including seasonal variability of transport, core depth, and maximum core velocity can be explained by the linear superposition of the dominant equatorial basin modes as obtained from the reduced-gravity model.

In section 2**, Intraseasonal to interannual variability of the eastern boundary circulation and hydrography off Angola,** we briefly describe the mean state of the alongshore flow across a number of monitoring lines along the path of the Angola Current inferred from moored and shipboard observations, as well as the evolution of subsurface temperature anomalies from 1995 to 2015. Furthermore, moored long-term velocity observations, for the first time, give insight into the mean state, intra-seasonal to seasonal variability and transport of the Angola Current.

In section 3, **Role of Interannual Kelvin wave propagations in the equatorial Atlantic on the Angola Benguela current system,** we investigate the link between equatorial Atlantic Ocean variability and the coastal region of Angola and Namibia from 1998 to 2012. We found a correlation of 0.68 between monthly dynamic height anomalies derived from the Prediction and Research Moored Array in the Tropical Atlantic (PIRATA) and monthly sea surface height anomalies (SSHA) derived from altimetry while the correlation with an Ocean Linear Model SSHA is 0.65. Major warm and cold events in the Angola-Benguela current system are remotely forced by ocean-atmosphere interactions in the tropical Atlantic. Wave dynamics along the equatorial wave guide are at the origin of their development. Weaker than normal easterlies wind stress in the Western Equatorial Atlantic triggers equatorial downwelling Kelvin waves that propagate eastward along the equator and polewards along the African coast initiating a warm event. Conversely, cold events are forced by stronger than normal wind stress that triggers upwelling Kelvin waves. An Ocean Linear Model can be easily implemented in real time using satellite estimate or model output. PIRATA data and altimetry data are also available in real time and can be used in an early warning system. An Index based on PIRATA data at [0 S, 0 N] seems to work better than an index based on Wind stress anomalies in the Western Tropical Atlantic along the equator. Altimetry derived SSH link the equatorial propagation to the coastal region. It seems that local forcing has little to do with the generation of most of major cold and warm events although they could modulate their intensity. The PIRATA array of mooring is crucial to the observation of those Kelvin waves and must be maintained. Finally, the study opens the possibility to forecast the start of Benguela Niños and Niñas in Angola with one month to two lead time, especially from October to April, using an Ocean Linear Model forced by wind speed, altimetry and PIRATA data.

In section 4, **Origin, development and demise of the 2010-2011 Benguela Niño**, we study in detail this warm event. A Benguela Niño developed in November 2010 and lasted for 5 months along the Angolan and Namibian coastline in the Angola Benguela current system. Maximum amplitude was reached in January 2011 with an interannual monthly SST anomaly larger than 4ºC at the Angola Benguela front. Consistent with previous Benguela Niños, this event was generated by a relaxation of

the trade winds in the western equatorial Atlantic, which triggered a strong equatorial Kelvin wave propagating eastward along the equator and then southward along the south-west African coast. In the equatorial band, the associated ocean subsurface temperature anomaly clearly shows up in data from the PIRATA mooring array. The dynamical signature is detected by altimetry derived Sea Surface Heights and well reproduced by an ocean Linear Model. In contrast to previous Benguela Niños, the initial propagation of subsurface temperature anomalies along the equator started in October and the associated warming in the Angolan Benguela Front Zone followed on as early as November 2010. The warming was then advected further south in the Benguela upwelling system as far as 25°S by an anomalously strong poleward subsurface current. Demise of the event was triggered by stronger than normal easterly winds along the Equator in April 2011 leading to above normal shoaling of the thermocline along the Equator and the south-west African coastline off Angola a month later.

In section 5, **Seasonal to interannual variability of water mass characteristics and currents on the Namibian shelf**, we analyse an unique data set comprising more than 85 months of temperature and salinity and 68 months of current meter records across 13 years (2002 - 2015) measured with an oceanographic mooring on the Namibian shelf. The study highlights the importance of the meridional advection for the water mass characteristics in the Benguela system on seasonal to interannual time scales. The annual flow reversals of the meridional velocity around March and October are concurrent with Kelvin wave induced changes in the sea level anomaly. The occurrence of extreme warm and cold events in the Benguela upwelling system is strongly related to the alongshore advection that in turn is in balance with the coastal sea level anomaly. During the extreme warm event in austral fall 2011 the monthly mean temperature in the water column exceeded the climatological values by about 2.4 K.

In section 6, **Ecosystem change in the southern Benguela and the underlying processes**, the focus is on coastal climate change and variability in the Benguela system and potential role on ecosystem change in the region. Overfishing and human-induced climate changes are putting severe pressure on marine ecosystems. In the southern Benguela, most of South Africa's commercial fisheries have a long history of exploitation and this, coupled with spatio-temporal changes in key species over the last three decades has severely impacted some of South Africa's fisheries and ecosystems. In almost all cases these changes have taken place since the 1980s. Spatial shifts in species have either involved an eastward expansion of cool-water species, including kelps, rock lobster and pelagic fish, or a retraction of warm-water species such as the brown mussel, suggesting a cooling of inshore waters along the south-west coast since the 1980s. This suggested cooling is revealed in ocean temperature for the south-west coast region during the same period.

Report on the deliverable

1. Annual and semi-annual cycle of equatorial Atlantic circulation associated with basin mode resonance

Brandt P., Claus M., Greatbatch R., Kopte R., Böning C.W., Toole J. and Johns W. (2016) Annual and semi-annual cycle of equatorial Atlantic circulation associated with basin mode resonance. In revision, J Phys Oceanogr.

1.1 Introduction

The mean tropical Atlantic circulation manifests a superposition of the wind-driven and thermohaline circulations that are focused in the upper ocean and near the western boundary (Schott et al. 2004; Schott et al. 2005). At the equator below the surface wind drift associated with the equatorial easterlies, the Equatorial Undercurrent (EUC) flows eastward along the equator contributing to the Atlantic meridional overturning circulation and to the wind-driven subtropical cells (Hazeleger and de Vries 2003; Hazeleger et al. 2003). The EUC is among the strongest currents in the tropical Atlantic and flows down the depth-dependent eastward pressure gradient. While nonlinearities contribute to its mean characteristics (Charney 1960; Qiao and Weisberg 1997), the EUC is essentially governed by linear dynamics with the meridional momentum equation being approximated by the geostrophic balance (Stommel 1960; McCreary 1981). The main focus of the study is the seasonal cycle of the zonal velocity that is the dominant variability in the upper layer of the central equatorial Atlantic particularly modulating the mean eastward flow of the EUC. A question to be addressed is whether the flow variations can be understood as a linear wave response to annual and semi-annual wind forcing? Using a general circulation model (GCM), Philander and Pacanowski (1986) found that the western part of the equatorial Atlantic is dominated by a local response to the annual wind forcing, while the central and eastern Atlantic shows a stronger semi-annual cycle only partially attributable to the local wind forcing. The downward propagation of energy supplied by periodic wind forcing at the sea surface can be conceptually described by equatorial beams. Eastward and westward propagating beams are found analytically as the sum of low-order baroclinic mode equatorial Kelvin and Rossby waves, respectively (McCreary 1984). In the tropical Atlantic, such beams are most pronounced at the annual period; the associated upward phase propagation can be identified in direct current observations as well as in high-resolution GCM simulations (Brandt and Eden 2005). In relation to the relative strength of the annual and semi-annual wind forcing of the tropical Atlantic, the semi-annual cycle of the velocity field is enhanced compared to the annual cycle. Using idealized and realistic simulations of the tropical Atlantic, Thierry et al. (2004) found that the propagation of second baroclinic mode equatorial Kelvin and Rossby waves are in resonance with the semi-annual wind forcing. Due to the downward energy propagation and the generally dissipative character of the basin resonance, bottom reflections or the presence of the Mid-Atlantic Ridge do not appear to affect the general structure of the semi-annual cycle of the velocity field. The spatial and temporal structure of such resonance phenomena are best described by equatorial basin modes (Cane and Moore 1981). These modes are low-frequency standing equatorial modes composed of equatorial Kelvin and long Rossby waves in the context of a shallow-water model with a given gravity wave speed characteristic of a specific baroclinic mode. The total travel time of both types of waves across the basin defines the period of the gravest basin

mode. In the inviscid case, the analytical solution by Cane and Moore (1981) has a singularity in mid-basin due to Rossby wave focusing. The introduction of lateral diffusion and/or mean flow can prevent such focusing, which makes solutions more realistic in comparison to observations (Greatbatch et al. 2012; Claus et al. 2014).

The concept of equatorial basin modes has been applied to explain the dynamics of observed intraseasonal, seasonal and interannual variability in the three equatorial basins (see, e.g., Johnson and Zhang 2003; Fu 2007; Ding et al. 2009). At semi-annual time scale, variability in both the Atlantic and Indian Ocean appear consistent with a resonance of the 2nd baroclinic mode that can be approximated by an equatorial basin mode (Jensen 1993; Han et al. 1999; Thierry et al. 2004; Ding et al. 2009). A subsequent study of basin mode resonance in the Indian Ocean by Han et al. (2011) highlighted the influence of wave damping and the shape of the equatorial basin on the spatial structure of these modes, while the existence of equatorial basin modes was found to be a robust feature in simulations with models of very different complexity. Here, we explore the role of the gravest equatorial basin modes of different baroclinic modes in shaping the seasonal cycle of equatorial Atlantic zonal velocity with a particular focus on the EUC. While a basin mode description of semi-annual variability was discussed in previous studies, we will show evidence of a resonant basin mode at the fourth baroclinic mode, annual period. During the recent decade, an enhanced equatorial observing system consisting of subsurface current meter moorings deployed in cross-equatorial arrays at different longitudes, i.e. 23°W, 10°W, and 0°, has been maintained, and the resulting data used to document the seasonal behavior of the Atlantic EUC (Brandt et al. 2014; Johns et al. 2014). Some of the identified characteristics such as the annual cycle of EUC deepening and shallowing and the semi-annual cycle of EUC core velocity have not been dynamically explained so far. Here we use full-depth velocity observations taken at the equator at 23°W to analyze the vertical structure of the seasonal cycle. Further, we compare these results to simulations with a primitive equation numerical model that reveals the horizontal structure of the dominant baroclinic modes in a realistic setting. The obtained horizontal structure resembles that of equatorial basin modes as simulated with a reduced-gravity model. Gravest equatorial basin modes have their strongest zonal velocity oscillations at the equator in mid-basin and might thus be well sampled by the 23°W moored observations. The reduced-gravity model is further used to study the structural dependence of the basin modes on the basin geometry (i.e. square basin versus realistic coastlines) and forcing (i.e. spatially uniform versus realistic wind forcing). The skill of the linear reduced-gravity model in replicating the dominant features of the seasonal cycle of the zonal velocity in the equatorial Atlantic demonstrates that a large part of the seasonal variability may be explained by equatorial wave dynamics associated with just two equatorial basin modes.

1.2 Mooring and CTD data

The zonal velocity observations were obtained from current meter moorings deployed at the equator at 23°W from February 2004 to April 2014 (Fig. 1.1). This data set represents an update of that published by Brandt et al. (2011) and Brandt et al. (2012). Here, we use mooring data from seven successive deployment periods of approximately 1.5-year duration. The moorings were equipped with two ADCPs. The upper one was a 300 kHz or a 150 kHz ADCP installed at 100 to 230 m depth and profiled upward from just below the EUC. The lower instrument was a 75 kHz ADCP that either profiled downward from just beneath the upper instrument or upward from about 600 to 650 m depth. We applied a 40-h low-pass filter to hourly-interpolated current data (ADCP sampling rates

varied typically between 0.5 and 1 per hour, but it was set to about 3 samples per day during one mooring period) to eliminate tidal currents and the de-tided data were subsequently subsampled to 12-hourly resolution. Between 600 and 1000 m during several mooring periods, a few single point current meters of different type were installed. Deeper in the water column, a McLane Moored Profiler (MMP) was programmed to sample the depth range between 1000 m and 3500 m. The installed profilers acquired data during three of the seven mooring periods, with a somewhat reduced measurement range during the third and seventh mooring periods (see Fig. 1.1). The MMPs were programmed to occupy profiles in bursts of two one-way traverses every 4 or 6 days, with the one-way profiles initiated 6 hours apart. No temporal filter was applied to the acquired velocity data. Given the length of the time series, the impact of measurement noise on the derived amplitude of the annual and semi-annual cycles can be regarded as negligible.

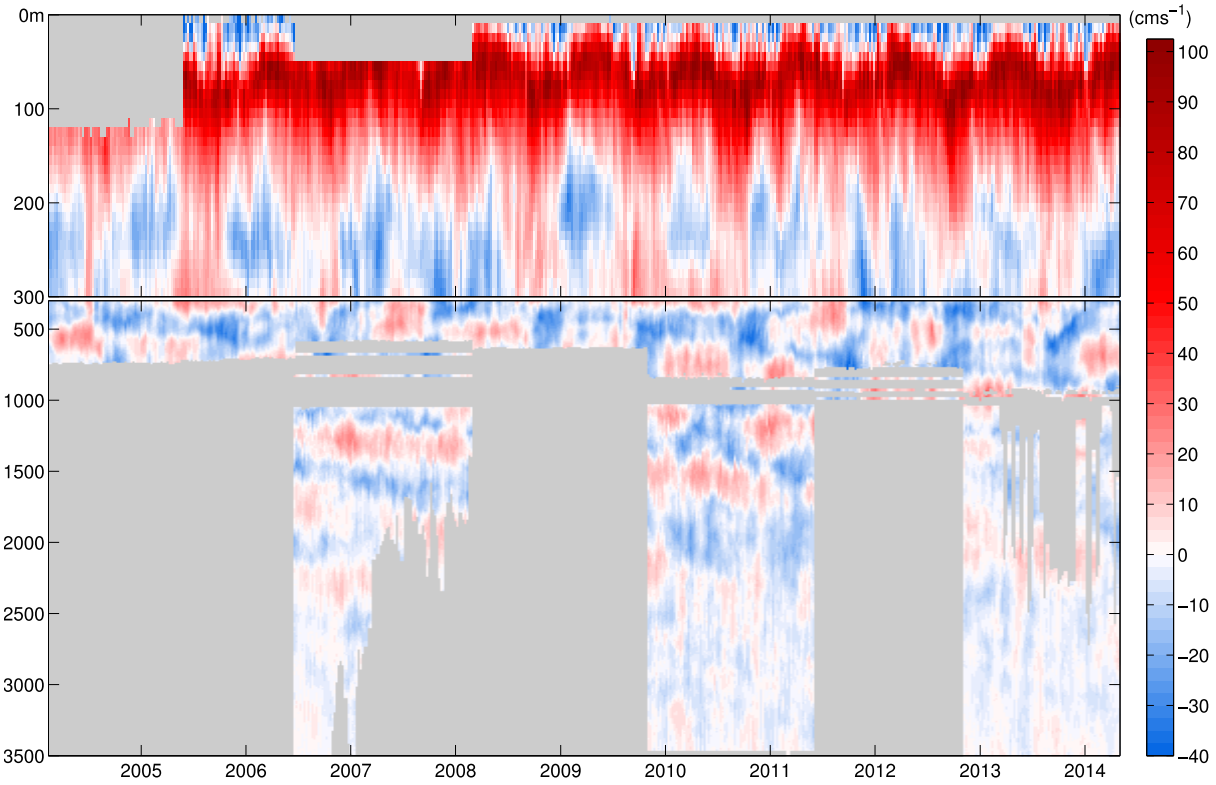

Figure 1.1: Observed zonal velocity from the equator, 23°W and above 3500 m depth. Velocity data above about 600 m are from moored acoustic Doppler current profilers, those between 600 and 1,000 m are from single-point current meters, and those below 1,000 m are from moored profilers. The gray areas mark depths not sampled by the deployed instrumentation. The upper 300 m are enlarged compared to the deeper part of the time series.

The time series has been used so far to study equatorial deep jets that are visible as bands of eastward and westward velocity characterized by downward phase propagation and a periodicity of about 4.5 years (Brandt et al. 2011) as well as the seasonal and interannual variability of the EUC (Brandt et al. 2014). Here we further exploit the data to study the seasonal circulation variability taking particular advantage of the nearly full depth velocity measurements to decompose the velocity field according to baroclinic modes at selected frequencies.

Table 1.1: Characteristics of the baroclinic mode decomposition of the mean Brunt–Väisälä frequency profile derived from CTD casts during mooring service cruises. The gravest basin mode period (4L/c) is calculated for a width of L=5.8 ×10^6 m.

Baroclinic mode	Phase velocity, c (m s^{-1})	Gravest basin-mode period (days)	Depth of first zero-crossing (m)	Depth of second zero-crossing (m)
1	2.47	109	1410	-
2	1.32	203	295	2220
3	0.95	284	85	795
4	0.74	361	65	400
5	0.57	473	50	270

For the decomposition of the moored velocity data into baroclinic modes we used vertical structure functions for a flat bottom derived from a mean Brunt–Väisälä frequency profile that was obtained by averaging individual Brunt–Väisälä frequency profiles calculated from shipboard CTD measurements taken during the mooring service cruises. The structure functions of the low baroclinic modes change only marginally when taking into account the variability about the mean Brunt–Väisälä frequency profile; however, some variations in the depth of zero-crossings of the profiles result when considering different ocean depths. To have a consistent analysis regarding the vertical structure of observed and simulated velocity variability, we decided to use one set of structure functions derived from the observed mean Brunt–Väisälä frequency profile for a water depth of 4500 m for both the analysis of the zonal velocity from moored observations as well as from the GCM. The main characteristics of the baroclinic modes are given in Table 1.1; the two modes of particular interest in the present study, i.e. the 2nd and 4th baroclinic mode, together with the mean zonal velocity in the upper 300 m derived from the moored time series are presented in Figure 1.2.

1.3 Model simulations

The GCM builds on a global configuration (TRATL01) of the NEMO (Nucleus for European Modelling of the Ocean) code (Madec 2008) in which the grid resolution of 0.5° is refined to 0.1° in the Atlantic Ocean between 30°N and 30°S via two-way nesting (Debreu and Blayo 2008). It includes 46 vertical levels, with increasing thickness from 6 m at the surface to 250 m at depth. With an interannually-varying forcing given by the Coordinated Ocean-ice Reference Experiments (CORE) (Griffies et al. 2009) reanalysis data over the period 1948-2007, the TRATL01 configuration was applied in Duteil et al. (2014) to study the circulation mechanisms responsible for the ventilation of the oxygen minimum zone in the eastern tropical Atlantic. A particular finding of that study was the improved realism of the equatorial current system owing to the higher resolution of the TRATL01 model compared to a 0.5° resolution model. Here, we use the output from the TRATL01 simulation over the period 1995- 2007, as well as three-year sub-sets of the time series, to assess the strength of the interannual variability that might be present in the moored observations covering periods of at least 3 years at the different longitudes.

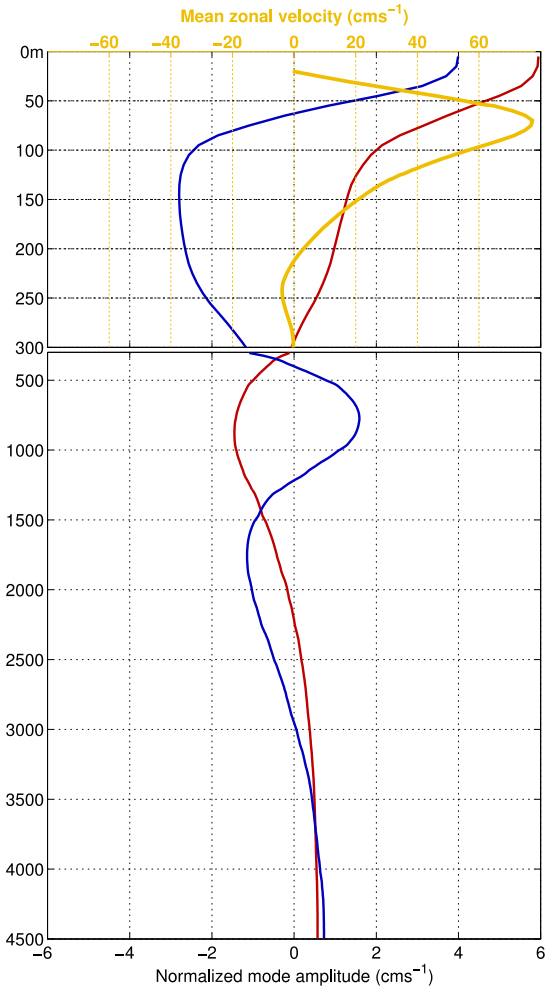

Figure 1.2: Normalized vertical structure function of the 2nd (red) and 4th (blue) baroclinic mode as derived from a mean Brunt–Väisälä frequency profile from the equator, 23°W. Normalization is performed with regard to the standard deviation of the structure functions. In the enlarged upper 300 m depth range also the mean zonal velocity (yellow) is shown.

Based on current meter moorings along meridional sections at 23°W, 10°W and 0°E deployed from October 2007 to June 2011, Johns et al. (2014) described the mean and the seasonal cycle of the EUC transport across the basin (Fig. 1.3).

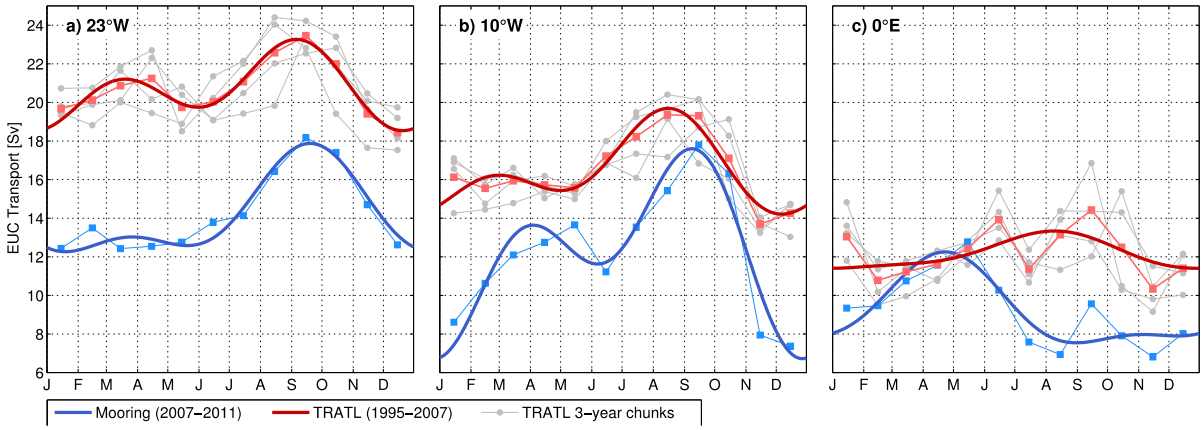

Figure 1.3: Monthly means (squares) of the 30–300 m EUC transport at 23°W, 10°W, and 0°E from observations taken from October 2007 to June 2011 (Johns et al. (2014), blue) and the TRATL01 model output derived for the whole model period, 1995-2007 (red) as well as for four successive three-year subsets of the time series (grey). Bold solid lines represent the mean seasonal cycles derived from annual and semi-annual harmonic fits of the observations (blue) and simulations (red).

At 23°W, the strongest EUC transport is observed in boreal autumn during the period of maximum easterly wind stress that varies dominantly at annual period. At 10°W, the EUC transport shows a semi-annual cycle with maxima in boreal spring and autumn. Further to the east, the wind forcing is dominated by its semi-annual component. However, the observed EUC transport at 0°E has only a single maximum in boreal spring. A comparison of simulated and observed EUC transport (Fig. 1.3) shows that (i) the model's annual mean EUC transport is generally overestimated and decreases more with distance from west to east as compared to observations (the interannual variability, delineated by the successive three-year subsets of the time series, is not able to account for these differences), (ii) within the seasonal cycle the timing of the boreal autumn maximum in the EUC transport is well represented at 23°W and 10°W, and (iii) there is only a weak simulated seasonal cycle at 0°E with the observed boreal spring maximum not represented. At 23°W, the simulation is found to capture the main characteristics of the seasonal velocity variability observed on the equator including amplitude and phase of the annual harmonic of zonal velocity (Fig. 1.4) and the spectral behavior (Fig. 1.5). In particular, the accurate representation of the observed seasonal cycle of zonal velocity in the central equatorial Atlantic, i.e. close to mid-basin where gravest equatorial basin mode velocity oscillations are strongest (Cane and Moore 1981), encourages us to focus on a baroclinic modal decomposition analysis at annual and semi-annual period. To further the dynamical understanding, we consider single baroclinic mode solutions by applying a linear reduced-gravity model in spherical coordinates. For governing equations and further details of the model see Greatbatch et al. (2012). The internal gravity wave speeds of the reduced-gravity model are taken from the baroclinic mode decomposition of the observed mean Brunt–Väisälä frequency profile described above (Tab. 1). The lateral eddy viscosity is set to 300 $m^2 s^{-1}$, which yields the most realistic results with regards to the meridional structure of high baroclinic mode waves (Greatbatch et al. 2012; Claus et al. 2014). The governing equations are applied to a rectangular as well as a realistic coastline domain with northern and southern boundaries at 20°N/S respectively. Sponge layers at the northern and southern boundaries prevent Kelvin wave propagation along those boundaries. The latitudes of the northern and southern boundaries in the reduced gravity model are chosen to be far

enough away from the equator to have little influence on the structure of the simulated equatorial basin modes. The horizontal resolution is the same as used in the GCM (1/10° in both longitude and latitude). Periodic wind stress forcing is applied to the momentum equations (either annually or semi-annually) and all simulations with the reduced-gravity model are run for 100 years in order to obtain a stable, periodically-oscillating solution. We note that the resulting oscillation amplitude will depend on different aspects of the model configuration, including the applied damping, the basin geometry, the strength of the basin mode resonance and, most importantly, the projection of the wind forcing onto the different baroclinic modes. Here, we use similar wind coupling coefficients as e.g. in Shankar et al. (1996) or Han et al. (1999). However, the annual and semi-annual oscillation amplitudes derived by the linear reduced-gravity model are scaled using the ratio of observed and simulated amplitudes of the annual and semi-annual oscillations on the equator at 23°W. This adjustment was performed to counter any misrepresentation of damping or forcing in the reduced-gravity model with respect to the simulated oscillation amplitude. The reduced-gravity model is then used to quantify the horizontal structure of the amplitude and phase of the annual and semi-annual cycle throughout the tropical Atlantic. Three sets of reduced-gravity model simulations are presented. The first uses an idealized rectangular domain with a basin width of 52.8° in longitude forced by spatially uniform zonal wind stress at annual or semi-annual period. The second set of simulations is identical except that the model domain is defined by the observed 1000 m isobath of the equatorial Atlantic basin at the eastern and western boundaries. For both sets of simulations with spatially uniform wind forcing, in addition to the amplitude scaling, a spatially uniform phase shift is applied to the simulated annual and semi-annual oscillations over the whole domain to achieve agreement between simulated and observed phases on the equator at 23°W. Following this approach, the adjusted model output is independent on the amplitude and phase of the wind forcing. The third set of simulations is the same as the second one except that we use a spatially varying, harmonically oscillating wind forcing derived from the NCEP-DOE AMIP-II Reanalysis product (Kanamitsu et al. 2002). In this third set of simulations we use zonal and meridional wind forcing. Specifically, the amplitude and phase of the annual and semi-annual wind forcing are obtained by harmonic fits at the corresponding period. In this most realistic set of simulations with the reduced-gravity model, only the amplitudes of simulated velocity oscillations are scaled according the observed values on the equator at 23°W; no phase adjustment is done as we expect the phase of the oscillations to be well-determined by the applied wind forcing.

1.4 Results

1.4.1. Characteristics of the annual and semi-annual cycle

The dominant signals in the zonal velocity field observed at the 23°W equatorial mooring (Fig. 1.1) are the seasonal cycle and the interannual variations associated with the equatorial deep jets. By analyzing an early subset of the mooring data, Brandt et al. (2006) identified strong annual cycle amplitudes above and below the mean core depth of the EUC that are in phase opposition. Deeper in the water column, sizable annual amplitudes were also found.

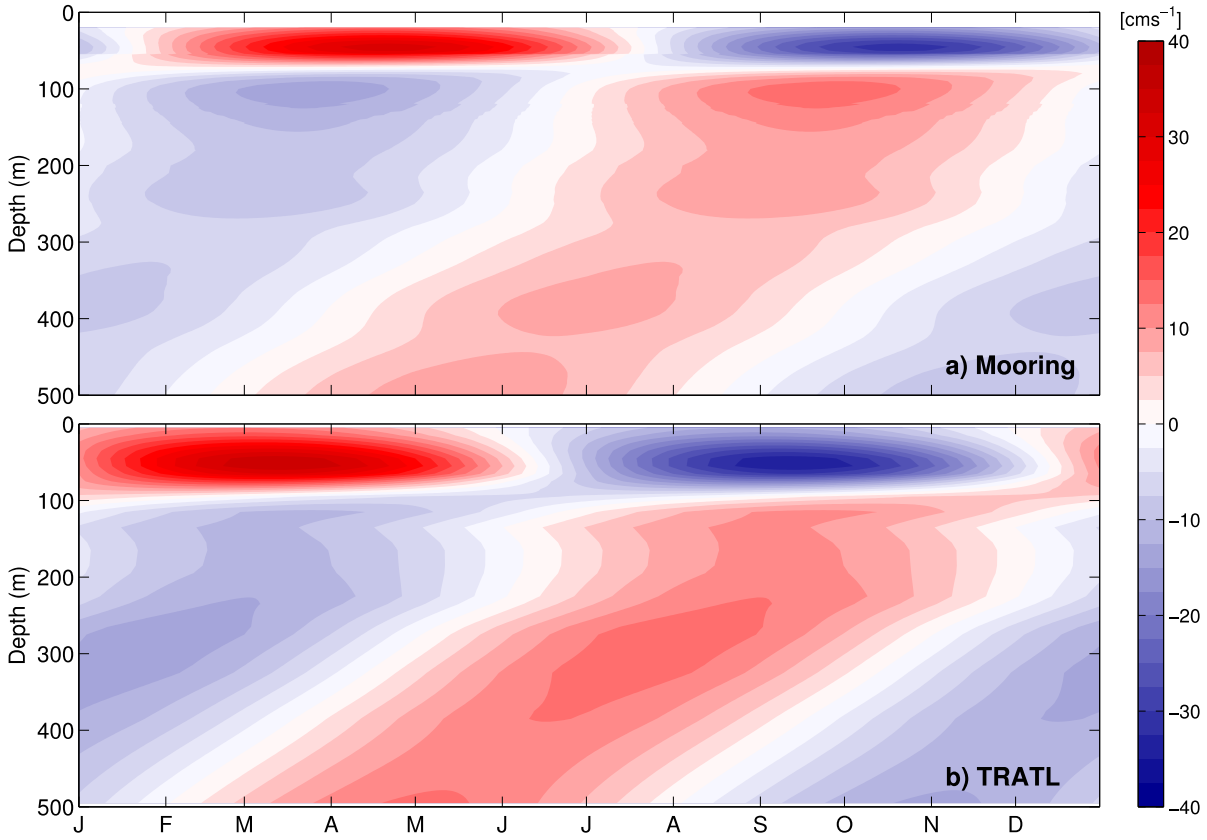

Figure 1.4: Annual cycle of zonal velocity in cm s^{-1} from the equator, 23°W as reconstructed using only the annual harmonic fit applied to moored velocity data (a) and the TRATL01 model output (b).

A reconstruction of the mean annual cycle from a harmonic fit of the moored velocity data (Fig. 1.4a) shows a clearly-visible phase jump at about 70 m depth associated with zero amplitude. Around 100-m depth, another maximum in the annual amplitude is found corresponding to the lower part of the EUC. This pattern represents the upward and downward movement of the EUC velocity core during the year, being shallowest in boreal spring and deepest in autumn. Below the EUC, upward phase propagation is evident that, according to linear equatorial wave theory, is associated with downward energy propagation. The simulation with the TRATL01 model (Fig. 1.4b) shows a very similar behavior. Main differences compared to the observations are the slightly deeper depth of the phase jump and the larger amplitude (with a maximum at about 300 m) below the EUC core. Note that the depth of maximum eastward velocity of the annual mean EUC at 23°W is about 70 m in the observations and about 85 m in the TRATL01 simulation, which following McCreary (1981) is indicative of too large vertical diffusion in the TRATL01 simulation. To derive a frequency spectrum from the irregularly-sampled moored velocity dataset we performed harmonic fits of the available data at each depth and averaged the derived amplitude vertically over the whole depth range (Fig. 1.5a). The obtained spectrum clearly shows very distinct peaks at annual and semi-annual periods with another weaker peak at about 120 days. The broad amplitude maximum at 4-5 year period is associated with the EDJs (Brandt et al. 2011; Ascani et al. 2015). The strong peaks in the zonal velocity amplitude suggest the presence of strong forcing at these periods and/or a resonant behavior or, possibly, indicate influence from flow instabilities (not discussed further here).

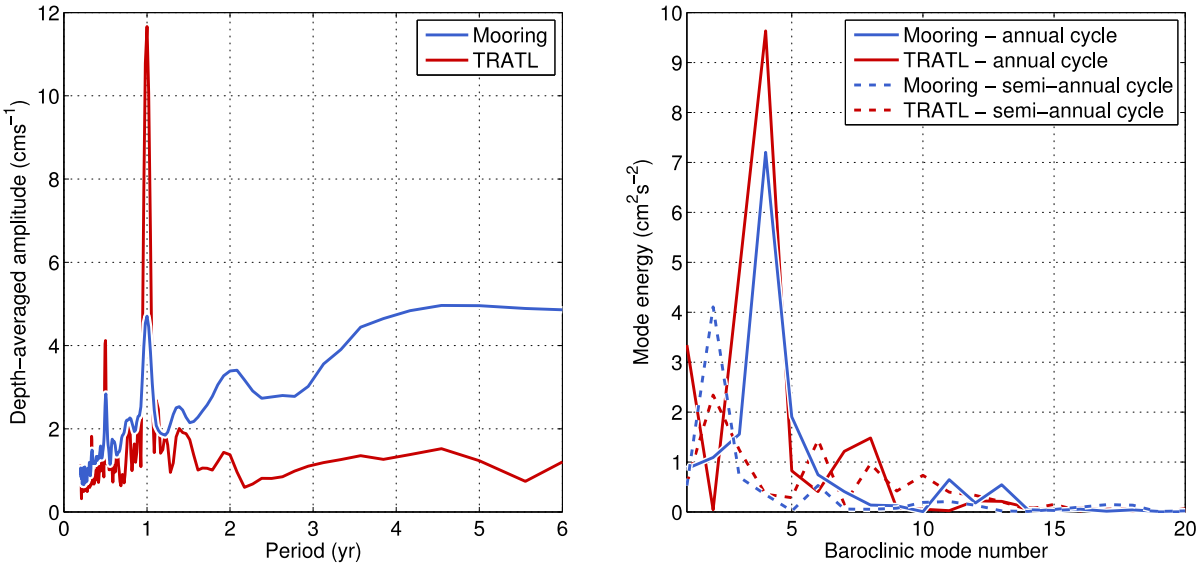

Figure 1.5: Frequency spectra of observed zonal velocity from the equator, 23°W (left panel) and baroclinic mode spectra of the annual (solid) and semi-annual (dashed) cycles (right panel) derived from the equatorial mooring (blue) and the TRATL01 model (red). The spectra of observed zonal velocity in (a) was derived by fitting harmonic functions to the available data at each depth level, followed by vertical averaging.

Similar calculations performed using the TRATL01 model velocity data also reveal spectral peaks at annual, semi-annual and 120-day periods with the peak at annual period being substantially stronger by a factor of 2 to 3 compared to observations. Enhanced amplitudes at interannual time scales are missing in the TRATL01 solution, pointing toward a well-known deficiency of such models in representing the EDJs (Ascani et al. 2015). To analyze the vertical structure of the annual and semi-annual cycle, we performed a baroclinic modal decomposition of the reconstructed annual and semi-annual cycles (Fig. 1.5b) at each discrete time step. The mode energy is then obtained by averaging the square of the derived coefficients over a whole cycle. As expected from previous studies (Thierry et al. 2004; Ding et al. 2009), the semi-annual energy density peaks at the 2nd baroclinic mode. More unexpected is the strong peak of the annual cycle at the 4th baroclinic mode. The vertical structure function of the 4th baroclinic mode has its first zero-crossing at 65 m depth (Table 1.1), which is close to the depth of the mean EUC core (Fig. 1.2). Thus the phase shift of the annual cycle within the EUC (Fig. 1.4a) is associated with the dominance of this baroclinic mode. Note the weak annual amplitudes at about 400 m depth (Fig. 1.4) that correspond to the second zero-crossing of the 4th baroclinic mode (Table 1.1) suggesting also a significant contribution of that baroclinic mode to the velocity variability below the EUC. The TRATL01 simulation has very similar characteristics: the peak of the 2nd baroclinic mode semi-annual cycle is slightly weaker than observed and the peak of the 4th baroclinic mode annual cycle is slightly stronger (Fig. 1.5b). We also note that the amplitude of the 3rd/5th baroclinic mode annual cycle is higher/lower in the TRATL01 simulations compared to the observation, which indicate a shift of the simulated annual cycle to lower modes having deeper first zero-crossings compared to higher modes (Table 1.1). This is consistent with our findings from the comparison of reconstructed annual cycles (Fig. 1.4), where the phase shift in the annual cycle between the upper and lower part of the EUC is deeper in the simulations compared to the observations. In a next step, TRATL01 output (which reproduces the main characteristics of the seasonal velocity variability on the equator at 23°W) is taken to calculate the horizontal pattern associated with the 2nd baroclinic mode semi-annual cycle and the 4th

baroclinic mode annual cycle (Fig. 1.6). These patterns reveal (i) an elongated amplitude maximum along the equator in mid-basin, (ii) general westward phase propagation off as well as at the equator, and (iii) a meridionally-broader pattern of the semi-annual cycle relative to the annual cycle. Both patterns have similarities with equatorial basin modes as theoretically described by Cane and Moore (1981), but reveal at the same time an asymmetry with respect to the equator. In a next step, we compare the pattern simulated using TRATL01 with idealized simulations using the reduced-gravity model.

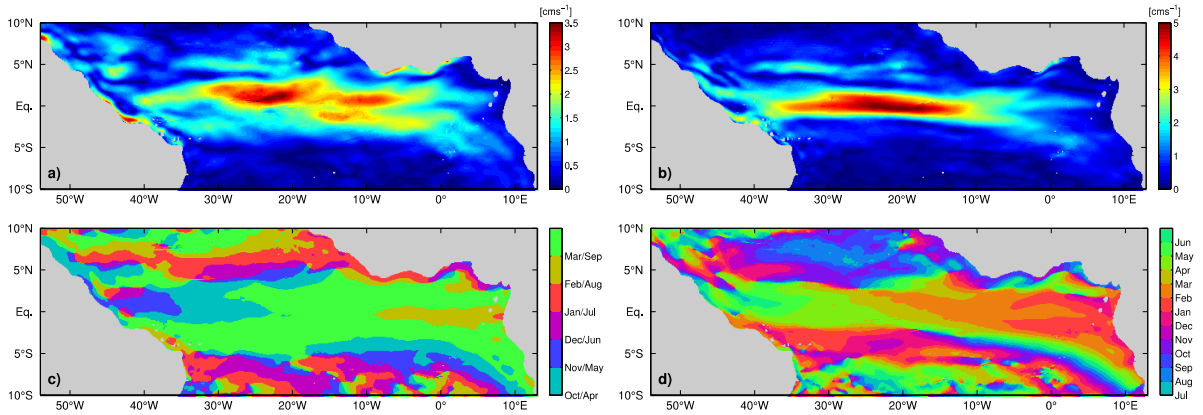

Figure 1.6: The amplitude (upper panels) and phase (lower panels) of the 2nd baroclinic mode, semi-annual cycle (left panels) and of the 4th baroclinic mode, annual cycle (right panels) of zonal velocity from the TRATL01 model. To derive the 3D zonal velocity field associated with the specific baroclinic mode, the amplitudes has to be multiplied by the corresponding vertical structure functions shown in Fig. 1.2. The phase is given in month of the year when maximum eastward velocity occurs at the surface.

1.4.2. Equatorial basin modes as simulated with the reduced-gravity model

In a first step, the reduced-gravity model is applied to study the resonance behavior of the equatorial ocean forced with spatially uniform zonal forcing of fixed amplitude but different oscillation periods. The simulations are performed for the square basin as well as for the basin with realistic coastlines. Following previous studies (Greatbatch et al. 2012; Claus et al. 2014), we chose the RMS of the zonal velocity along the equator calculated by excluding values near the eastern and western boundary within 10° in longitude offshore in the stable, periodically-oscillating state to identify the resonance of the equatorial basin modes (Fig. 1.7).

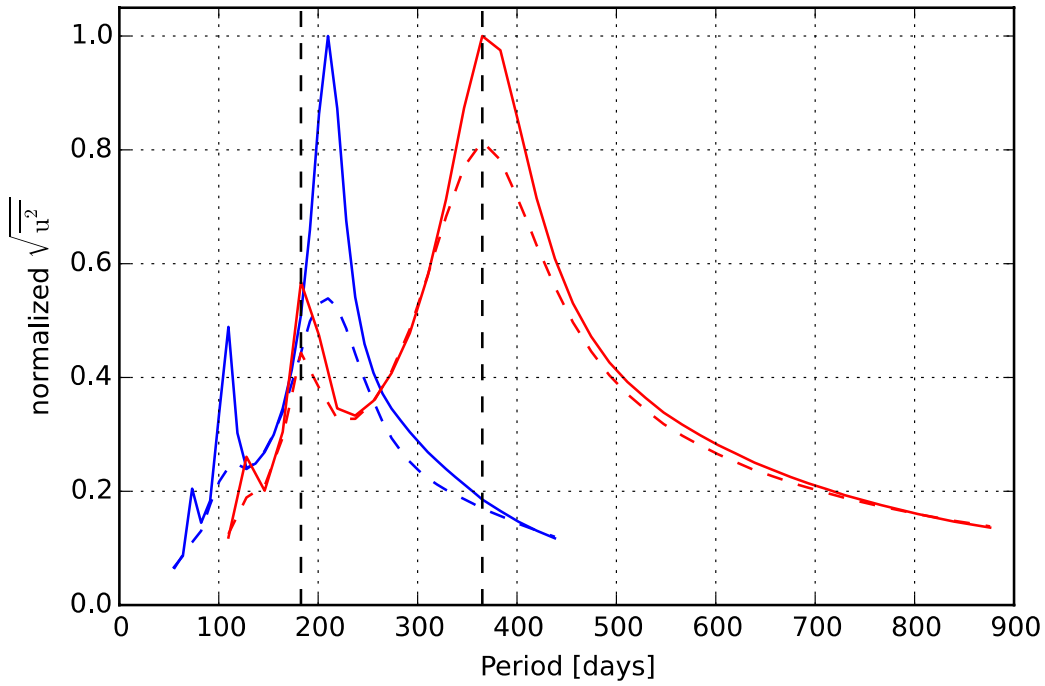

Figure 1.7: RMS of the zonal velocity along the equator calculated by excluding values near the eastern and western boundary within 10° in longitude offshore for the final complete oscillation cycle as a function of the period of the applied spatially uniform zonal forcing for simulations with the reduced-gravity model. Simulations are performed for the square basin (solid lines) as well as for the basin with realistic coastlines (dashed lines). The velocity in the ordinate for the 2nd baroclinic mode (blue) and the 4th baroclinic mode (red) simulation is normalized by the maximum amplitude of the respective simulation for the square basin. Vertical dashed lines mark the period of the semi-annual and annual cycles.

Here the estimate is taken over the final complete oscillation cycle. The simulations indicate resonance of the 2nd baroclinic mode near the semi-annual period at about 210 days and resonance of the 4th baroclinic mode almost exactly at the annual period. At the resonance periods, the amplitudes of the zonal velocity oscillations are somewhat reduced in the case of a basin with realistic coastlines compared to a square basin. This likely is the result of the slanting western boundary reducing the amplitude of the reflected Kelvin wave in comparison to a straight meridional boundary (Cane and Gent 1984) and possibly also a consequence of the Gulf of Guinea coastline shape in the east. Note that Fig. 1.7 indicates secondary resonances near 100 days for the 2nd baroclinic mode and near the semi-annual period for the 4th baroclinic mode. Several effects that could impact the resonance periods are neglected in the reduced gravity model. For example, in the real ocean the resonance periods might be reduced in comparison to the idealized simulation presented here due to the presence of a mean flow as shown for equatorial basin modes of higher baroclinic modes (Claus et al. 2014) or due to the nonlinear increase of the propagation speed of equatorial waves (Boyd 1980; Greatbatch 1985). Different runs with the reduced-gravity model sought to identify the structure of the basin modes in a uniformly-forced rectangular ocean and to study the influence of realistic coastlines and wind forcing. Similar to the TRATL01 simulation, the amplitude and phase of the 2nd baroclinic mode semi-annual cycle and the 4th baroclinic mode annual cycle in the reduced-gravity model shows an elongated amplitude maximum along the equator in mid-basin and generally westward phase propagation (Figs. 1.8-1.10). The solutions of the reduced-

gravity model for a square basin and spatially uniform zonal forcing are symmetric with respect to the equator. The main difference between the solutions for the 2nd baroclinic mode semi-annual cycle (Fig. 1.8a,c) and the 4th baroclinic mode annual cycle (Fig. 1.8b,d) is the meridionally broader pattern of the 2nd baroclinic mode semi-annual cycle; in the case of the semi-annual cycle, regions farther away from the equator are more affected by the basin mode oscillations than for the annual cycle.

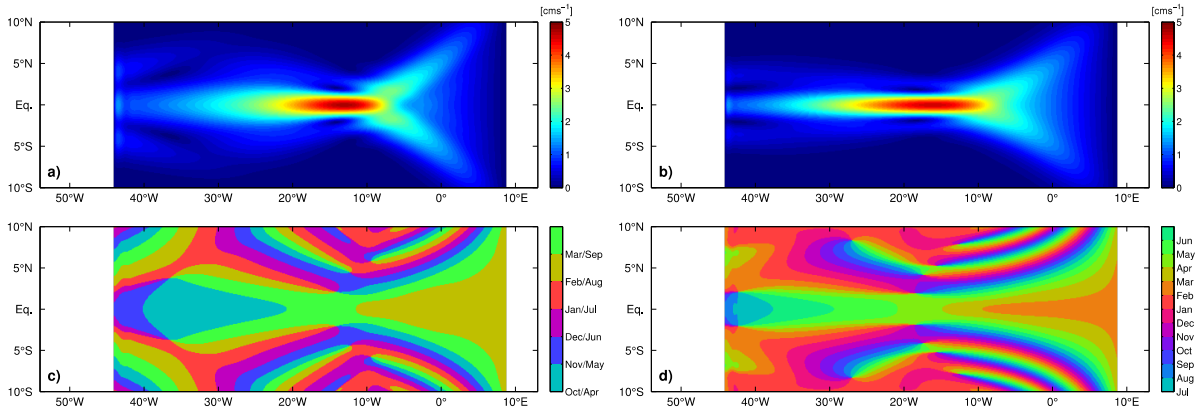

Figure 1.8: Same as Fig. 1.6, but simulated with the reduced-gravity model for the rectangular domain using a gravity wave speed c=1.32 m s^{-1} corresponding to the 2nd baroclinic mode (left panels) and c=0.74 m s^{-1} corresponding to the 4th baroclinic mode (right panels).

The introduction of realistic coastlines and the associated change of basin geometry induce an asymmetry in the meridional structure of the basin modes, i.e. in the western part of the domain the amplitude maximum is shifted northward whereas in the east, the amplitude in the southern lobe is enhanced and that in the northern lobe, reduced. Consistent results were found for the basin mode of the 2nd baroclinic mode semi-annual cycle using a GCM with realistic basin geometry (Thierry et al. 2004) that showed notable meridional asymmetry in the deeper circulation pattern. Here, the 2nd baroclinic mode semi-annual cycle is more strongly influenced by the introduction of realistic coastlines compared to the 4th baroclinic mode annual cycle. This could be expected due to the smaller meridional scale associated with the 4th baroclinic mode compared to the 2nd baroclinic mode. Interesting to note are the amplitude maxima at the northeastern boundary (Fig. 1.9a,b) that are likely associated with the propagation of coastal-trapped waves around the Gulf of Guinea. Somewhat similar maxima are also found in the TRATL01 solution (Fig. 1.6), especially for the 2nd baroclinic mode semi-annual cycle case.

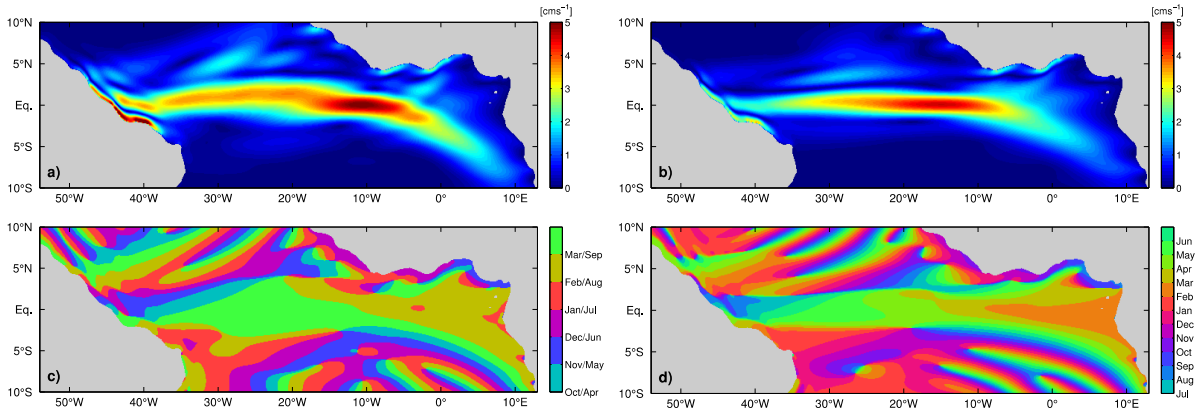

Figure 1.9: Same as Fig. 1.8, but for the realistic coastline domain.

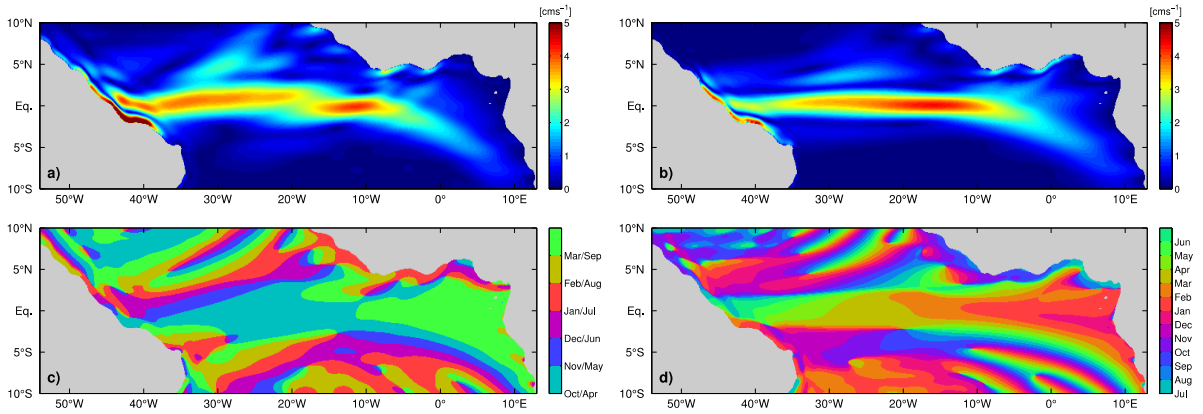

Figure 1.10: Same as Fig. 1.9, but with spatially varying forcing.

The final set of simulations with the reduced-gravity model was performed using a realistic spatial pattern of annual and semi-annual wind forcing. Contrary to the first two sets of simulations that were forced with spatially uniform winds, we only adjust the amplitude of the simulated basin mode in comparison to the moored observations on the equator at 23°W. The simulated phase was unaltered. With the more realistic wind forcing, the 2nd baroclinic mode semi-annual cycle develops two separate amplitude maxima in space (Fig. 1.10a), one centered on the equator at about 10°W and the second, slightly north of the equator west of 20°W. A similar structure can be found in the TRATL01 simulation (Fig. 1.6a). The main difference for the 4th baroclinic mode annual cycle when changing from reduced-gravity model simulations with spatially uniform to realistic wind forcing is a shift in the phase along the equator of up to 2 months suggesting a deficiency of the reduced-gravity model in the most realistic setup with an unaltered phase. Again, there is good agreement between the linear, reduced gravity model and the TRATL01 model in this case (Figs. 1.10b,d and Figures 1.6b,d). Overall, the regular oscillations produced by the reduced-gravity model are suggestive of equatorial basin modes. Realistic coastlines and realistic wind both induce meridional asymmetry in the basin mode structure; the influence being stronger for the lower baroclinic mode semi-annual cycle compared to the annual cycle. Confirming previous results using models of different complexity applied to the Indian and Atlantic Oceans (Thierry et al. 2004; Han et al. 2011) our results also show that the general structure of a resonant equatorial basin mode is fairly robust (similar structures are

observed in the various reduced-gravity model simulations (Figs. 1.8-1.10) as well as the GCM (Fig. 1.6)).

1.4.3 EUC variability associated with equatorial basin modes

A question that arises from the above results is, to what extent can the observed seasonal behavior of the EUC be explained by linear equatorial basin modes? Using the basin mode solutions from the reduced-gravity model, we reconstruct the 3D structure of the velocity anomaly field by applying the vertical structure functions of the corresponding baroclinic modes (Fig. 1.2). By adding the reconstructed simulated velocity anomalies to the mean velocity from meridional shipboard sections at different longitudes (Johns et al. 2014), we obtain time series of zonal velocity that can be analyzed in similar fashion as the observed time series. In particular, EUC transports are calculated following Johns et al. (2014), i.e. integrating only eastward velocities within the latitudinal range from 1°12'S to 1°12'N and the depth range from 0 to 300 m. Here, the reconstruction obtained from the reduced-gravity model simulations only includes the velocity variability associated with the 2^{nd} baroclinic mode semi-annual cycle and the 4^{th} baroclinic mode annual cycle, and is derived for all three cases: the square basin, realistic geometry, and realistic wind forcing. The comparison of observations with the reconstructed seasonal cycle (Fig. 1.11a, b, c) shows that i) at 23°W the observed pronounced EUC transport maximum in the seasonal cycle in September is found only slightly later in the reconstruction, ii) at 10°W very good agreement is achieved with EUC transport maximum in August/September, a secondary maximum in March/April and weakest EUC transport in December, and iii) there is only weak or no correspondence between observations and the reconstructions at 0°E with the former exhibiting a spring transport maximum whereas the reconstructions have a weak late boreal summer maximum, similar to what is seen in TRATL01 (Figure 1.3c). The difference between the three different reduced-gravity model reconstructions, i.e. square basin, realistic coastlines, realistic wind forcing, is relatively small, suggesting a robust behavior of the equatorial basin modes. For the reconstructed seasonal cycle of the EUC transport at the three longitudes, the contributions of the annual harmonic cycle and the semiannual harmonic cycle are of similar importance (Fig. 1.11d, e, and f). To further examine the vertical structure of the seasonal EUC transport variability, zonal transport profiles are calculated by integrating the reconstructed zonal velocity (only eastward velocities following Johns et al. (2014)) over the width of the EUC between 1°12'N and 1°12'S (Fig. 1.12), which can be directly compared to observations by Johns et al. (2014; their Figure 1.11). While in general the three different reconstructions are very similar, we note the influence of realistic coastlines compared to the square basin in producing a well-separated and shallower transport maximum at 35°W in boreal spring, and a slight weakening of the semi-annual transport maxima in the eastern equatorial Atlantic when introducing realistic wind forcing. The reconstructed transport profiles obtained by using the 2^{nd} baroclinic mode semi-annual cycle and the 4^{th} baroclinic mode annual cycle show several similarities with the observed total transport profiles (Johns et al. 2014): (i) there is a pronounced semi-annual cycle in the shallow part of the transport profile (about upper 100 m) and (ii) the EUC is shallow in boreal spring and deep in boreal autumn. Differences between simulations with the reduced-gravity model and observations are particularly evident in the flow below the EUC core. In the simulations, it is the deep extension of the EUC during August/September at 0°E (Fig. 1.12) that is chiefly responsible for the EUC transport maximum in boreal autumn (Fig. 1.11c). In the observations, the deep extension of the EUC at 0°E is strongest during May shortly after the shallow spring maximum, both together producing the EUC

transport maximum in boreal spring (Fig. 1.11c). The deep extension of the EUC at 10°W and at 23°W is about one month later in the simulations compared to the observations. Other parameters that characterize the seasonal EUC variability are its core depth and latitude as well as its maximum velocity (Fig. 1.13). These parameters were determined from moored observations at 23°W by Brandt et al. (2014). Comparison of the reduced-gravity model reconstructed fields with the observational curves shows that the semi-annual cycle in the EUC core velocity and the annual cycle in the EUC core depth can be largely reproduced with the superposition of the two dominant equatorial basin modes. The contribution of the semi-annual cycle to the seasonal cycle in the EUC core velocity is stronger than the contribution from the annual cycle (Fig. 1.13b) because the 2nd baroclinic mode has larger amplitude than the 4th baroclinic mode at the core depth of the mean EUC (Fig. 1.2). At the same time, the 4th baroclinic mode annual cycle very efficiently influences the seasonal cycle of the EUC core depth. With the first zero-crossing of the 4th baroclinic mode at about the core depth of the mean EUC (Fig. 1.2), the strengthening/weakening above/below the EUC core during boreal spring and vice versa during boreal autumn (Fig. 1.13d) results in a vertical movement of the EUC core during the annual cycle. The semi-annual cycle does not change sign in the depth range of the EUC and thus does not contribute significantly to the vertical movement of the EUC core. The latitude of the EUC core is not so well represented by the simple basin modes. Other effects that might play a role in setting this parameter not accounted for in the simulations are the seasonally varying shallow meridional circulation forced by the meridional wind stress at the equator and the quasi-stationary meandering of the EUC east of the North Brazil Current retroflection, likely responding to the strong seasonal cycle in the retroflection.

1.5 Summary and discussion

We have analyzed a multi-year velocity time series from the equator, 23°W, covering (with some gaps, see Fig. 1.1) the whole water column with respect to the seasonal variations of the zonal velocity. Distinct peaks in frequency-baroclinic mode space emerged, the most pronounced being the 2nd baroclinic mode at semi-annual period and the 4th baroclinic mode at annual period (Fig. 1.5). Similar peaks are found in the TRATL01 simulation. The associated horizontal pattern as obtained from the TRATL01 model is consistent with the presence of equatorial basin modes, as confirmed using a linear, reduced-gravity model (Figs. 1.7-1.10). The general agreement in the horizontal pattern as obtained from TRATL01 and the different runs with the reduced-gravity model also suggest that other effects not accounted for in the reduced-gravity model, like e.g. the seasonal variability in the stratification associated with a vertical displacement of the mean zonal velocity profile, play only a minor role in producing zonal velocity anomalies of the specific baroclinic mode analyzed here. By using a linear reduced-gravity model for the simulation of equatorial basin modes for a series of different baroclinic modes, we were able to show that linear wave dynamics provides a simple explanation for several characteristics of the observed zonal velocity seasonal variability including that of the EUC. Besides equatorial beams that are often used to describe the seasonal variability in the equatorial ocean (McCreary 1984; Lukas and Firing 1985; Thierry et al. 2004; Brandt and Eden 2005), equatorial basin modes represent a powerful alternative means of describing equatorial ocean dynamics (Cane and Moore 1981; Jensen 1993; Han et al. 1999; Ding et al. 2009; Han et al. 2011). Equatorial basin modes are associated with basin resonances occurring at periods defined by the phase speeds of equatorial Kelvin and long Rossby waves of specific baroclinic modes and the basin geometry. In conjunction with the spectra of the wind forcing, basin resonance appear

to explain the pronounced peaks in the frequency-baroclinic mode space found in the moored observations. The simulations with the reduced gravity model in different configurations and the TRATL01 model confirm the result obtained by Han et al. (2011) and others, that the resonant equatorial basin modes are robust features, only weakly dependent on the structure of the equatorial basin and the wind forcing. Thierry et al. (2004) specifically analyzed the role of the Mid-Atlantic Ridge and found a negligible effect of this pronounced bathymetric feature, suggesting that a simple reduced-gravity model might be well suited for the simulation of equatorial basin modes. While the resonance of the semi-annual cycle in the Atlantic (as well as Indian) Ocean requires a phase speed close to the phase speed of the 2^{nd} baroclinic mode (Thierry et al. 2004; Ding et al. 2009), the resonance of the annual cycle is associated with a slower internal wave speed, which is achieved in the equatorial Atlantic by the 4^{th} baroclinic mode. The higher baroclinic mode has a first zero-crossing of the associated vertical structure function (derived from observations) at about 65 m depth (Table 1.1) suggesting an opposing effect of the annual basin mode on the zonal flow above and below the mean EUC core, as seen in the observations (Fig.1. 4a). The seasonal cycle of the EUC reveals strong deviations from a simple local response to the wind forcing. Such deviation can be seen for example by the following: i) the basin-wide vertical migration of the EUC within the seasonal cycle cannot be in balance at the same time with the differing wind stress forcing in the eastern (predominantly semi-annual forcing) and western (predominantly annual forcing) basin and ii) the velocity maximum within the EUC core during boreal spring is found during the period of weakest wind forcing (Johns et al. 2014). Using the reduced-gravity model simulations, we show that the superposition of the two dominant basin modes, i.e. the 2^{nd} baroclinic mode semi-annual cycle and the 4^{th} baroclinic mode annual cycle, provide a simple explanation for a substantial part of the seasonal EUC variability. Particularly, the seasonal cycles of the EUC transport, core depth and core velocity in the central equatorial Atlantic are well captured by the reconstructed velocity fields. However, the superposition of the two basin mode solutions cannot account for the downward phase propagation of the annual cycle found below the EUC core (Fig. 1.4), which must involve other baroclinic modes (Brandt and Eden 2005). This discrepancy between the simulations and observations is probably responsible for the deviations in the transport profiles derived from the reconstructions (Fig. 1.12) and observations (Johns et al. 2014). It might also be the reason that, although the amplitudes of the two basin modes are adjusted in comparison to the 23°W velocity data, the reconstructed and observed EUC transport at 23°W does not agree perfectly (Fig. 1.11a). There is general disagreement between observations and the linear reduced-gravity model simulations as well as GCM simulations of the EUC in the eastern equatorial Atlantic, e.g. at 0°E. Philander and Chao (1991) suggested that in the eastern equatorial Atlantic, the EUC acts as an inertial jet decelerated by lateral dissipation. As shown in satellite (Athie and Marin 2008) and in-situ observations (Jouanno et al. 2013), there is a strong seasonal cycle in the amplitude of intraseasonal waves. Model simulations indicate that these waves, which are mainly wind-generated by the high-frequency wind forcing, impact the seasonal cycle of turbulent mixing in the eastern equatorial Atlantic (Jouanno et al. 2013). Through their effects on lateral dissipation and vertical mixing, the intraseasonal variability might influence the seasonal cycle of the zonal velocity in the eastern equatorial Atlantic. However, such effects might also play a role in the central equatorial Atlantic, which is also characterized by substantial seasonal cycles in the strengths of tropical instability waves (Athie and Marin 2008) and vertical mixing (Jouanno et al. 2011; Hummels et al. 2014). These effects are not captured in the reduced-gravity model simulations. Besides the gravest equatorial basin

modes discussed so far, we want to mention also a possible role of the 2nd basin modes for the zonal velocity variability in the far eastern equatorial Atlantic. In the case of the 4th baroclinic mode semi-annual oscillations, this mode has substantial oscillation energy (Fig. 1.7). The 2nd basin mode likely has a stronger impact on the zonal velocity seasonal cycle east and west of the central equatorial Atlantic, which is dominated by the gravest basin mode. As the 2nd basin mode typically has reduced amplitude in the central equatorial Atlantic and is thus not well constrained by our observations on the equator at 23°W, it is not included here, but it clearly deserves further study. To correctly represent the seasonal variability of zonal velocity in GCMs, basin mode resonance must be captured. As suggested by Philander and Pacanowski (1981), the evaluation of the seasonal cycle provides a sensitive test of the different mixing parameterizations used in models. However, the response of the reduced-gravity model to varying frequency of the wind forcing (Fig. 1.7) indicates that the amplitude of the annual and semi-annual oscillations crucially depends on the proximity of the resonance peaks to the annual and semi-annual periods. The resonance periods for the 2nd and 4th baroclinic mode as calculated using the mean Brunt–Väisälä frequency profile from TRATL01 are 185 days and 339 days and as such, are about 20 days shorter than the estimates obtained from observations (Tab. 1). In general, variations in the vertical density structure of GCMs compared to observations could enhance or reduce the wave speeds of the specific baroclinic modes and thus modify the amplitude of the corresponding basin modes by shifting the period of the resonance peaks. Particularly for coarse resolution models, the vertical density structure could differ substantially from reality. The resulting alteration of the EUC transport seasonal cycle and its associated supply to the equatorial upwelling in turn has great potential to impact simulated sea surface temperature variability.

The analyzed simulation with the TRATL01 model show a deeper EUC (at 23°W: 85 m in TRATL versus 70 m in the observations) and a deeper first zero-crossing of the 4th baroclinic mode when using the mean Brunt–Väisälä frequency profile from the model instead from the observations (77 m versus 65 m). We also note a shift of the annual cycle to lower modes in the TRATL01 simulation compared to observations (Fig. 1.5). A similar result can be conjectured from the GCM simulation studied by Ding et al. (2009), where it was found that the model solution is determined by the four gravest baroclinic modes with the second and third being dominant. Simulation of the seasonal cycle of equatorial zonal velocity thus requires, besides valid mixing parameterizations, a realistic representation of the vertical density structure and the mean flow field, both affecting the amplitudes of the annual and semi-annual oscillations associated with the resonant basin modes.

1.6 References

- Ascani, F., E. Firing, J. P. McCreary, P. Brandt, and R. J. Greatbatch, 2015: The Deep Equatorial Ocean Circulation in Wind-Forced Numerical Solutions. *J Phys Oceanogr*, **45,** 1709-1734, doi:10.1175/JPO-D-14-0171.1.
- Athie, G., and F. Marin, 2008: Cross-equatorial structure and temporal modulation of intraseasonal variability at the surface of the Tropical Atlantic Ocean. *J Geophys Res-Oceans*, **113,** C08020, doi:10.1029/2007jc004332.
- Boyd, J. P., 1980: Equatorial Solitary Waves. Part I: Rossby Solitons. *J Phys Oceanogr*, **10,** 1699-1717, doi:10.1175/1520-0485(1980)010<1699:Eswpir>2.0.Co;2.
- Brandt, P., and C. Eden, 2005: Annual cycle and interannual variability of the mid-depth tropical Atlantic Ocean. *Deep-Sea Res Pt I*, **52,** 199-219, doi:10.1016/J.Dsr.2004.03.011.

- Brandt, P., A. Funk, A. Tantet, W. Johns, and J. Fischer, 2014: The Equatorial Undercurrent in the central Atlantic and its relation to tropical Atlantic variability. *Clim Dynam*, **43,** 2985-2997, doi:10.1007/s00382-014-2061-4.
- Brandt, P., A. Funk, V. Hormann, M. Dengler, R. J. Greatbatch, and J. M. Toole, 2011: Interannual atmospheric variability forced by the deep equatorial Atlantic Ocean. *Nature*, **473,** 497-500, doi:10.1038/Nature10013.
- Brandt, P., F. A. Schott, C. Provost, A. Kartavtseff, V. Hormann, B. Bourles, and J. Fischer, 2006: Circulation in the central equatorial Atlantic: Mean and intraseasonal to seasonal variability. *Geophys Res Lett*, **33,** L07609, doi:10.1029/2005gl025498.
- Brandt, P., and Coauthors, 2012: Ventilation of the equatorial Atlantic by the equatorial deep jets. *J Geophys Res-Oceans*, **117,** C12015, doi:10.1029/2012jc008118.
- Cane, M. A., and D. W. Moore, 1981: A Note on Low-Frequency Equatorial Basin Modes. *J Phys Oceanogr*, **11,** 1578-1584, doi:10.1175/1520-0485(1981)011<1578:Anolfe>2.0.Co;2.
- Cane, M. A., and P. R. Gent, 1984: Reflection of Low-Frequency Equatorial Waves at Arbitrary Western Boundaries. *J Mar Res*, **42,** 487-502
- Charney, J. G., 1960: Non-Linear Theory of a Wind-Driven Homogeneous Layer near the Equator. *Deep-Sea Res*, **6,** 303-310
- Claus, M., R. J. Greatbatch, and P. Brandt, 2014: Influence of the Barotropic Mean Flow on the Width and the Structure of the Atlantic Equatorial Deep Jets. *J Phys Oceanogr*, **44,** 2485-2497, doi:10.1175/JPO-D-14-0056.1.
- Debreu, L., and E. Blayo, 2008: Two-way embedding algorithms: a review. *Ocean Dynam*, **58,** 415-428, doi:10.1007/s10236-008-0150-9.
- Ding, H., N. S. Keenlyside, and M. Latif, 2009: Seasonal cycle in the upper equatorial Atlantic Ocean. *J Geophys Res-Oceans*, **114,** C09016, doi:10.1029/2009jc005418.
- Duteil, O., F. U. Schwarzkopf, C. W. Böning, and A. Oschlies, 2014: Major role of the equatorial current system in setting oxygen levels in the eastern tropical Atlantic Ocean: A high- resolution model study. *Geophys Res Lett*, **41,** 2033-2040, doi:10.1002/2013gl058888.
- Fu, L. L., 2007: Intraseasonal variability of the equatorial Indian Ocean observed from sea surface height, wind, and temperature data. *J Phys Oceanogr*, **37,** 188-202, doi:10.1175/JPO3006.1.
- Greatbatch, R. J., 1985: Kelvin Wave Fronts, Rossby Solitary Waves and the Nonlinear Spin-up of the Equatorial Oceans. *J Geophys Res-Oceans*, **90,** 9097-9107, doi:10.1029/JC090iC05p09097.
- Greatbatch, R. J., P. Brandt, M. Claus, S. H. Didwischus, and Y. Fu, 2012: On the width of the equatorial deep jets. *J Phys Oceanogr*, **42,** 1729-1740, doi:10.1175/Jpo-D-11-0238.1.
- Griffies, S. M., and Coauthors, 2009: Coordinated Ocean-ice Reference Experiments (COREs). *Ocean Model*, **26,** 1-46, doi:10.1016/j.ocemod.2008.08.007.
- Han, W. Q., J. P. McCreary, D. L. T. Anderson, and A. J. Mariano, 1999: Dynamics of the eastern surface jets in the equatorial Indian Ocean. *J Phys Oceanogr*, **29,** 2191-2209, doi:10.1175/1520-0485(1999)029<2191:Dotesj>2.0.Co;2.
- Han, W. Q., J. P. McCreary, Y. Masumoto, J. Vialard, and B. Duncan, 2011: Basin Resonances in the Equatorial Indian Ocean. *J Phys Oceanogr*, **41,** 1252-1270, doi:10.1175/2011JPO4591.1.
- Hazeleger, W., and P. de Vries, 2003: Fate of the Equatorial Undercurrent in the Atlantic. *Elsevier Oceanography Series*, G. J. Goni, and P. Malanotte-Rizzoli, Eds., Elsevier, 175-191.
- Hazeleger, W., P. de Vries, and Y. Friocourt, 2003: Sources of the Equatorial Undercurrent in the Atlantic in a high-resolution ocean model. *J Phys Oceanogr*, **33,** 677-693, doi:10.1175/1520-0485(2003)33<677:Soteui>2.0.Co;2.

- Hummels, R., M. Dengler, P. Brandt, and M. Schlundt, 2014: Diapycnal heat flux and mixed layer heat budget within the Atlantic Cold Tongue. *Clim Dynam*, **43,** 3179-3199, doi:10.1007/s00382-014-2339-6.
- Jensen, T. G., 1993: Equatorial Variability and Resonance in a Wind-Driven Indian-Ocean Model. *J Geophys Res-Oceans*, **98,** 22533-22552, doi:10.1029/93jc02565.
- Johns, W. E., P. Brandt, B. Bourlès, A. Tantet, A. Papapostolou, and A. Houk, 2014: Zonal structure and seasonal variability of the Atlantic Equatorial Undercurrent. *Clim Dynam*, **43,** 3047-3069, doi:10.1007/s00382-014-2136-2.
- Johnson, G. C., and D. X. Zhang, 2003: Structure of the Atlantic Ocean equatorial deep jets. *J Phys Oceanogr*, **33,** 600-609, doi:10.1175/1520-0485(2003)033<0600:Sotaoe>2.0.Co;2.
- Jouanno, J., F. Marin, Y. du Penhoat, and J. M. Molines, 2013: Intraseasonal Modulation of the Surface Cooling in the Gulf of Guinea. *J Phys Oceanogr*, **43,** 382-401, doi:10.1175/Jpo-D-12-053.1.
- Jouanno, J., F. Marin, Y. du Penhoat, J. Sheinbaum, and J. M. Molines, 2011: Seasonal heat balance in the upper 100 m of the equatorial Atlantic Ocean. *J Geophys Res-Oceans*, **116,** C09003, doi:10.1029/2010jc006912.
- Kanamitsu, M., W. Ebisuzaki, J. Woollen, S. K. Yang, J. J. Hnilo, M. Fiorino, and G. L. Potter, 2002: NCEP-DOE AMIP-II reanalysis (R-2). *B Am Meteorol Soc*, **83,** 1631-1643, doi:10.1175/Bams-83-11-1631.
- Lukas, R., and E. Firing, 1985: The Annual Rossby-Wave in the Central Equatorial Pacific-Ocean. *J Phys Oceanogr*, **15,** 55-67, doi:10.1175/1520-0485(1985)015<0055:Tarwit>2.0.Co;2.
- Madec, G., 2008: *NEMO ocean engine version 3.1.* Vol. 27, Institut Pierre-Simon Laplace, Paris, France.
- McCreary, J. P., 1981: A Linear Stratified Ocean Model of the Equatorial Undercurrent. *Philos T R Soc A*, **298,** 603-635
- ——, 1984: Equatorial Beams. *J Mar Res*, **42,** 395-430
- Philander, S. G. H., and R. C. Pacanowski, 1981: Response of Equatorial Oceans to Periodic Forcing. *J Geophys Res-Oc Atm*, **86,** 1903-1916, doi:10.1029/Jc086ic03p01903.
- ——, 1986: A Model of the Seasonal Cycle in the Tropical Atlantic-Ocean. *J Geophys Res-Oceans*, **91,** 14192-14206
- Philander, S. G. H., and Y. Chao, 1991: On the Contrast between the Seasonal Cycles of the Equatorial Atlantic and Pacific Oceans. *J Phys Oceanogr*, **21,** 1399-1406, doi:10.1175/1520-0485(1991)021<1399:Otcbts>2.0.Co;2.
- Qiao, L., and R. H. Weisberg, 1997: The zonal momentum balance of the equatorial undercurrent in the central Pacific. *J Phys Oceanogr*, **27,** 1094-1119
- Schott, F. A., J. P. McCreary, and G. C. Johnson, 2004: Shallow overturning circulations of the tropical-subtropical oceans. *Earth Climate: The Ocean-Atmosphere Interaction*, C. Wang, S.-P. Xie, and J. A. Carton, Eds., American Geophysical Union, 261-304.
- Schott, F. A., M. Dengler, R. Zantopp, L. Stramma, J. Fischer, and P. Brandt, 2005: The shallow and deep western boundary circulation of the South Atlantic at 5°-11°S. *J Phys Oceanogr*, **35,** 2031-2053, doi:10.1175/JPO2813.1.
- Shankar, D., J. P. McCreary, W. Han, and S. R. Shetye, 1996: Dynamics of the east India Coastal Current: 1. Analytic solutions forced by interior Ekman pumping and local alongshore winds. *J Geophys Res-Oceans*, **101,** 13975-13991, doi:10.1029/96JC00559.
- Stommel, H., 1960: Wind-Drift near the Equator. *Deep-Sea Res*, **6,** 298-302
- Thierry, V., A. M. Treguier, and H. Mercier, 2004: Numerical study of the annual and semi-annual fluctuations in the deep equatorial Atlantic Ocean. *Ocean Model*, **6,** 1-30

2. Intraseasonal to interannual variability of the eastern boundary circulation and hydrography off Angola inferred from moored and shipboard observations

Kopte R., Brandt, P., Dengler, M., Schlundt, M., Tchipalanga, P., Ostrowski, M., Coelho, P.

2.1 Introduction

The eastern boundary circulation off the coast of southwest Africa has been described only sparsely to date, although it is embedded in a very productive marine system that adjacent coastal countries strongly depend upon. These countries now face substantial challenges in terms of societal development, fisheries, and tourism associated with climate variability and global change. The boundary circulation itself can be regarded as key component for the southeastern Atlantic coastal upwelling region as the connecting element to the tropical Atlantic. As remote equatorial forcing is likely to play an important role for the variability observed in the upwelling system (e.g. *Lübbecke et al.* [2010]; *Rouault* [2012]), the region off Angola must be seen as the gateway for signals originating in the equatorial Atlantic and propagating to the upwelling region.One of the first descriptions of the Angola Current was published by *Moroshkin et al.* [1970], who reported subsurface southward geostrophic velocities exceeding 50 cm/s between 9°S and 16°S, based on a hydrographic survey in 1968. During the observational period, southward velocities extended from the surface down to 250-300 m depth. These observations are in agreement with the findings of *Dias* [1983a] and *Dias* [1983b], who measured current velocities at 12°S on four occasions between September 1970 and July 1971. In March 1971 southward flow was found to be stronger compared to July 1971: 50 cm/s vs. 42 cm/s at the surface, 70 cm/s vs. 33 cm/s at 100 m depth, respectively. Volume transport of the Angola Current was estimated relative to the 800 dbar-level across a section at 12°S for water depths greater than 500 m with the offshore limit at 9°E. Southward transports above 400 m depth were found to be 3.7 Sv / 2.0 / 2.6 Sv / 1.2 Sv in September 1970 / November 1970 / March 1971 / July 1971, respectively [*Dias*, 1983a]. Based on an extensive dataset of CTD and shipboard ADCP measurements from the EAF Nansen program introduced in section 2 we briefly describe the mean state of the alongshore flow across a number of monitoring lines along the path of the Angola Current, as well as the evolution of subsurface temperature anomalies from 1995 to 2015. Furthermore, moored long-term velocity observations, also described in section 2, for the first time give insight into the mean state, intra-seasonal to seasonal variability and transport of the Angola Current.

2.2 Data

Since 1983, an extensive oceanographic data set from repeated ship survey carried out in Angolan territorial waters is acquired within the EAF-Nansen program executed by the Food and Agricultural Organisation of the United Nations (FAO) and funded by Norwegian Agency for Development Cooperation (NORAD). Bi-annual cruises have been carried out by R/V Dr. Fridtjof Nansen on a regular basis since 1995 collecting data to estimate the abundance and map the distribution of the main commercially important fish species, perform biogeochemical measurements and to collect hydrographic and velocity data from shipboard acoustic Doppler current profiler. The bi-annual cruises are scheduled during austral summer (FMA) and winter (JJA). Between 1995 and 2015, a total of 8818 conductivity-temperature-depth (CTD) profiles were collected on the shelf and continental slope off spread along the entire coastline of Angola (Figure 2.1).

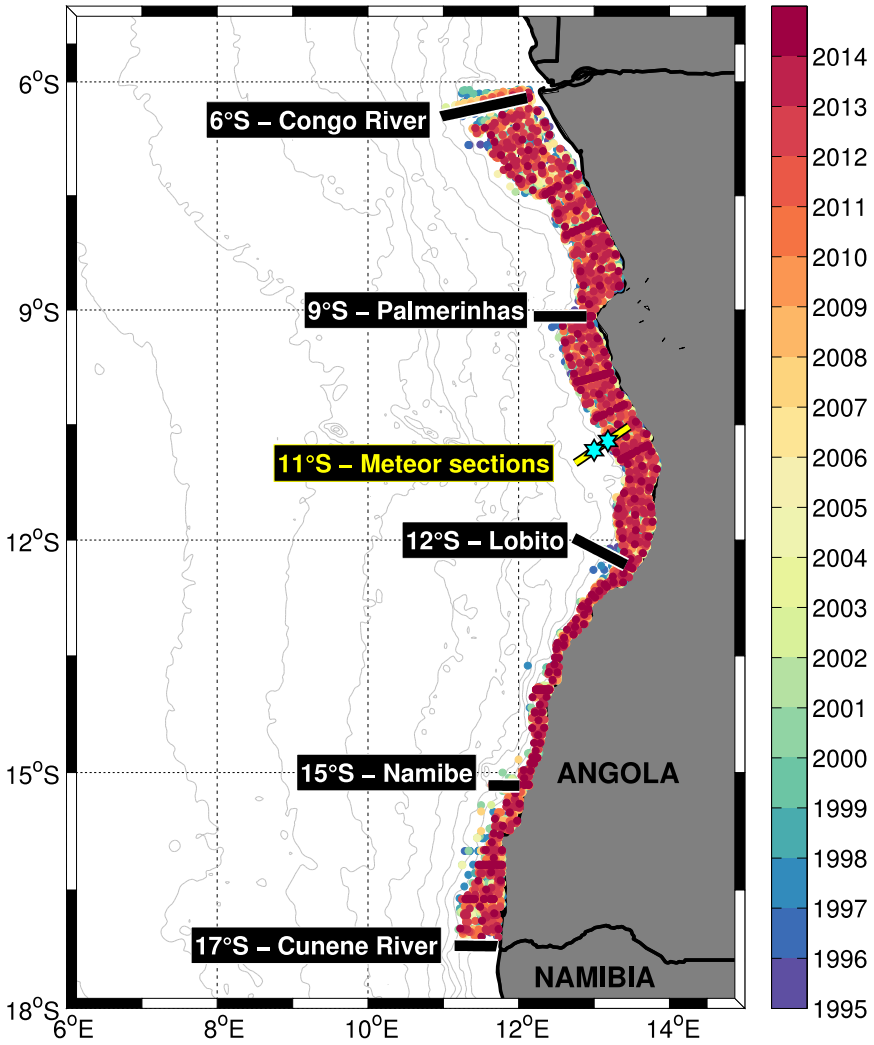

Figure 2.1: Map of the main survey area off Angola. CTD stations (total of 8818) on the shelf and continental slope that are used for the temperature analysis in Figure 2.2 are marked by colored dots with the color gives the year of measurements. Black lines show locations of monitoring lines repeatedly occupied within the EAF Nansen program. Yellow line represents the 11°S section visited by R.V. Meteor in July 2013 and October 2015 for mooring array installation/service. Cyan stars indicate mooring positions.

Furthermore, shipboard ADCP measurements from a 150 kHz Ocean Surveyor are available since 2005, and regularly repeated monitoring lines along 6°S, 9°S, 12°S, 15°S, and 17°S have been established. In cooperation between EU FP7 PREFACE and the SACUS project funded by the German Federal Ministry of Education and Research, a current meter mooring array was installed off the coast of Angola at 11°S in July 2013, recovered and redeployed in October 2015. The installed instrumentation provided the first long-term velocity observations of the Angola Current (see Fig. 2.1 for mooring positions). A bottom shield equipped with an ADCP had been deployed at 500 m water depth, accompanied by a mooring sitting on the 1200 m isobath with an ADCP being installed at 500 m depth. Both upward-looking instruments measured the current speed in the overlying water-column up to about 40 m below the sea surface.

2.3 Preliminary Results

The analysis of the CTD measurements obtained on the shelf and continental slope off Angola between 1995 and 2015 reveals a long term warming trend in the upper thermocline layer (26 kg m^{-3} ≤ σ_θ ≤ 26.5 kg m^{-3}) of 0.19°C/decade (Figure 2.2). Interannual temperature anomalies are in the range of ±0.6°C and can persist for several years, most likely associated with warmer/cooler South Atlantic central water (SACW) / Eastern SACW (ESACW) being advected into the region by the poleward Angola Current / equatorward Benguela Current during these periods. Furthermore, a comparison with interannual SST anomalies in the upwelling region indicates that thermocline heat anomalies might serve as a preconditioning for the occurrences of Benguela Niños/Niñas (not shown). The mean alongshore flow across the main monitoring lines of the EAF Nansen program is estimated using the individual snapshot sections acquired between 2005 and 2014, but also incorporating two sections recorded at 11°S by R.V. Meteor in July 2013 and October 2015 (Figure 2.3). Shipboard velocity data were used to construct the individual mean sections that are based at least on 13 individual sections for each monitoring line, except for 15°S where only 6 sections could be used. In general, the mean sections are characterised by southward flow on the shelf and at the continental slope in the range of 5-15 cm/s. However, due to the high temporal variability of the flow field (see also Figure 2.4) these mean sections need to be interpreted with caution, as single snapshots can dominate the mean substantially (not shown).

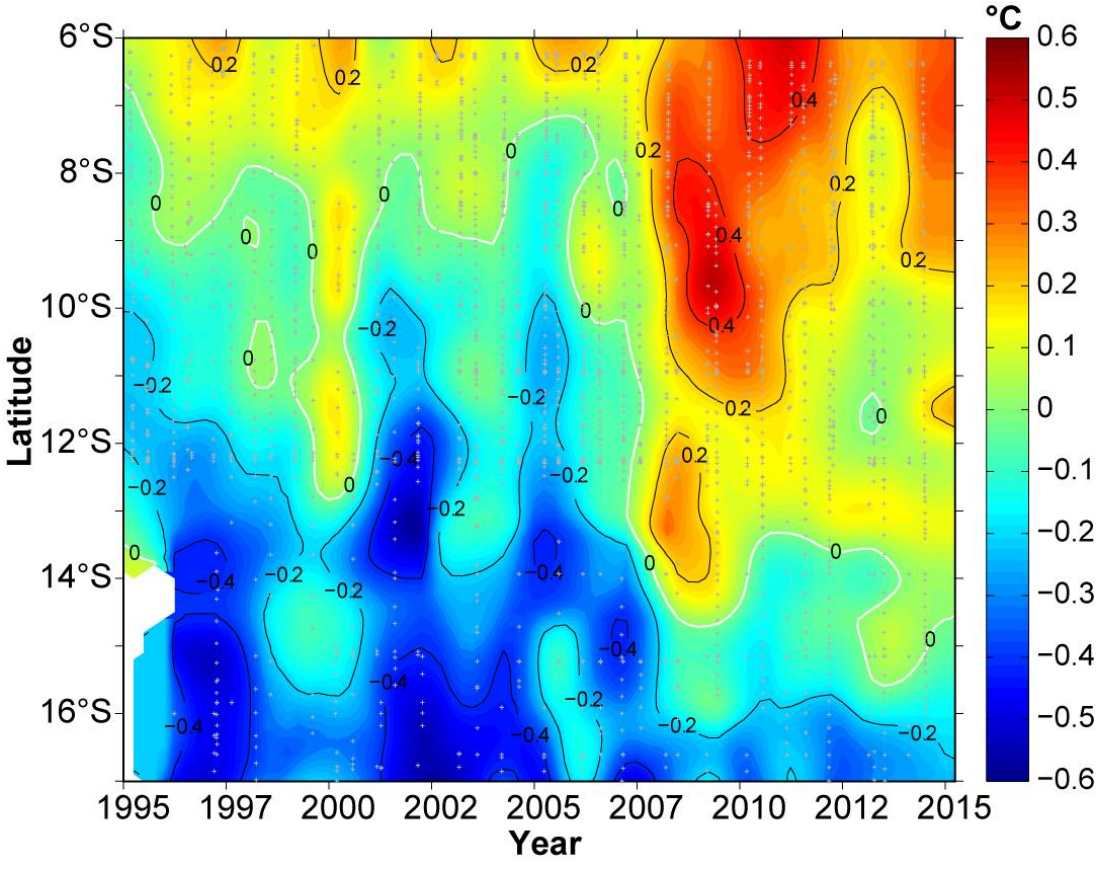

Figure 2.2: Evolution of temperature anomalies in the density layer 26 kg m^{-3} ≤ σ_θ ≤ 26.5 kg m^{-3} as function of latitude along the Angolan coast from CTD measurements obtained within the EAF-Nansen program. Grey dots mark individual CTD positions.

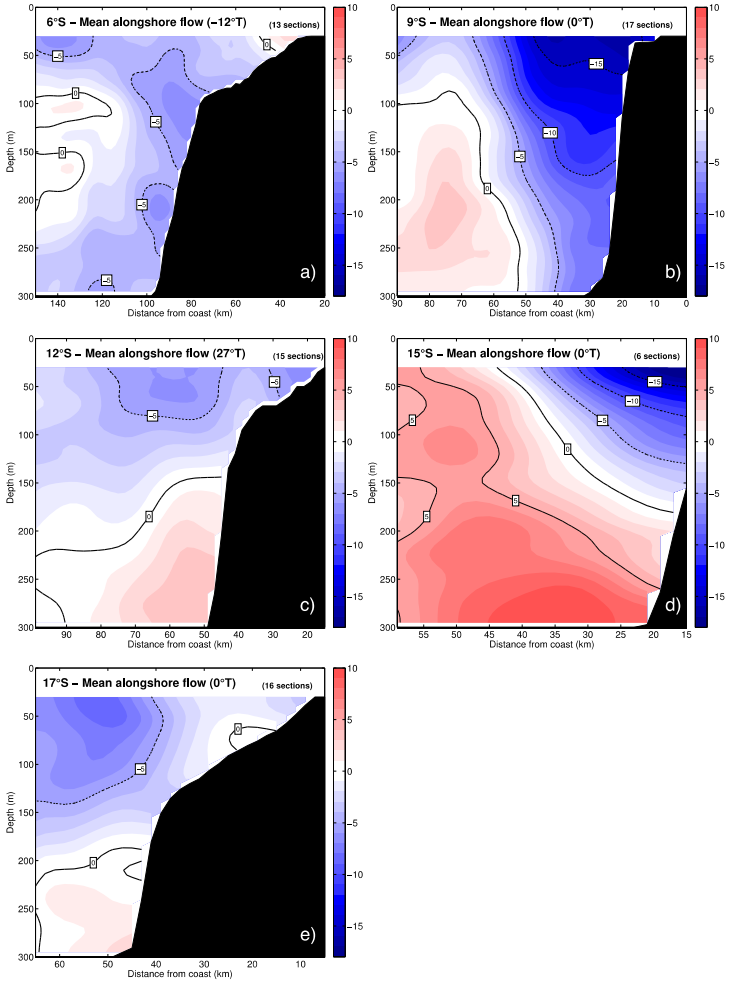

Figure 2.3: Mean sections of alongshore flow across Nansen monitoring lines. Angle of the alongshore current as well as number of sections used to calculate the mean sections are indicated in the upper part of the subplots. a) 6°S, b) 9°S, c) 12°S, d) 15°S, and e) 17°S. Note that two Meteor sections at 11°S are incorporated in the 12°S mean.

Contrary to the conclusion drawn from historical measurements, there is no steady southward flow at the continental slope off Angola at 11°S (Figure 2.4). Instead, the time series is dominated by alternating bands of southward and northward velocities that can last for a few months as well as higher frequency velocity pulses. Overall, the offshore ADCP recorded slightly more depth-independent current profiles than the inshore one. The mean current profiles reveal a weak southward flow of 5-8 cm/s at 50 m depth, slightly stronger on the inshore mooring, with the mean southward flow extending to depths of about 200 m (not shown). Another interesting parameter is the volume transport of the Angola Current. Based on two Meteor sections along 11°S and another eleven sections along 12°S recorded by R.V. Nansen, the first four complex patterns of variability of the boundary current are derived and regressed on the two moored time series of alongshore flow. For comparison, the procedure is repeated using the output of the high-resolution OGCM INALT01 [*Durgadoo et al.*, 2013] for deriving the variability patterns. The volume transport is then constructed by integrating the 3d flow field in the limits of the mean Angola Current from 30-300 m depth and between 15-90 km offshore (Figure 2.5). The Angola Current transport during the observational

period ranges from 2 Sv southward to 1.2 Sv northward, with a weak mean southward transport of about 0.3 Sv (with a standard deviation of 0.5 Sv). This is considerably less compared to the previous estimates by *Dias* [1983a].

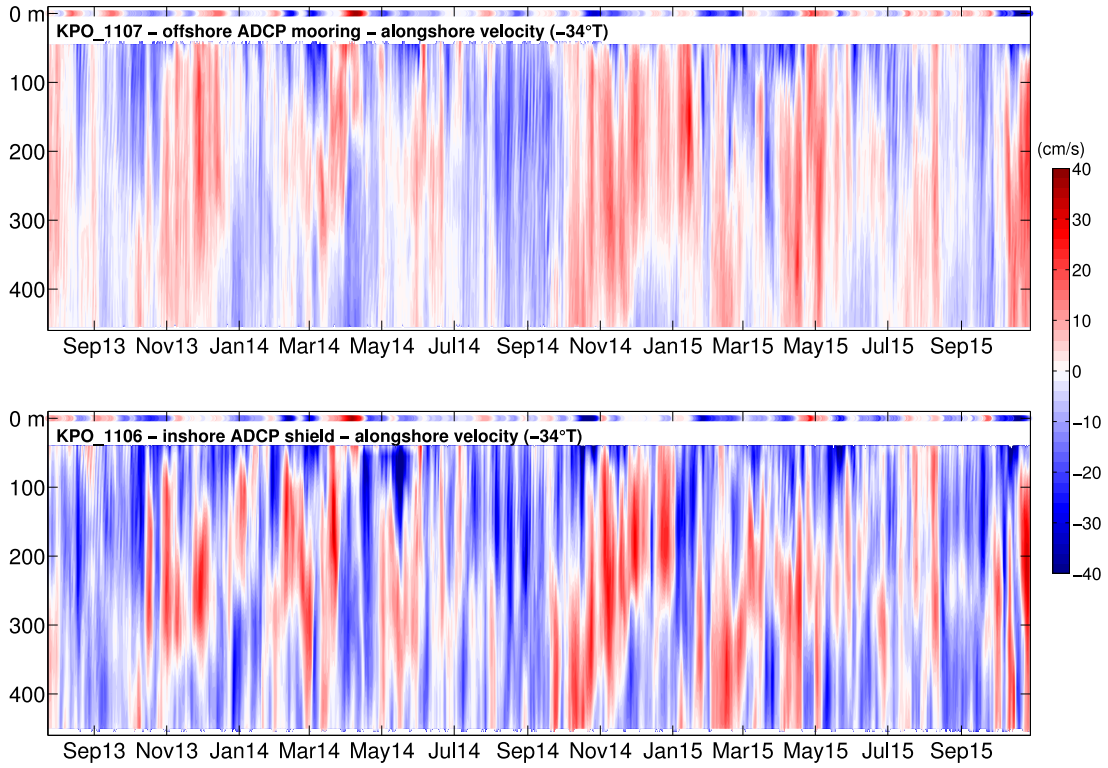

Figure 2.4: Moored time series of alongshore velocity (-34°T) at 11°S. *top*: offshore ADCP mooring (1200m water depth), *bottom*: inshore ADCP shield (500m water depth). At the surface alongshore geostrophic velocities derived from AVISO dynamic heights at the mooring position are plotted.

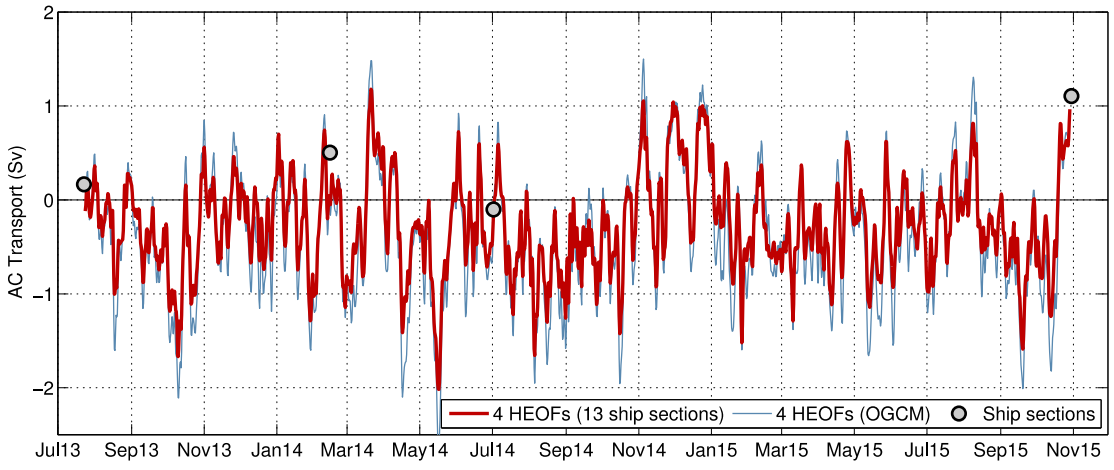

Figure 2.5: Angola Current transport as calculated by regressing the first four complex patterns of variability derived from *(i)* 13 ship sections (red), and *(ii)* high-resolution OGCM INALT01 (light blue) on the moored time series of alongshore flow. The integration is done from 30-200m depth, and 15-90km offshore. Also included are the Angola Current transport values calculated from the four ship sections within the observational period (grey dots).

2.4 References

- Dias, C. A. (1983a), Note on the evidence of a permanent southward flow of the upper oceanic tropospheric waters off Angola at 12°S, *Collection of Scientific Papers International Commission for the Southeast Atlantic Fisheries*, *10*, 99-102.
- Dias, C. A. (1983b), Preliminary report on the physical oceanography off southern Angola, March and July 1971, *Collection of Scientific Papers International Commission for the Southeast Atlantic Fisheries*, *10*, 103-116.
- Durgadoo, J. V., B. R. Loveday, C. J. C. Reason, P. Penven, and A. Biastoch (2013), Agulhas Leakage Predominantly Responds to the Southern Hemisphere Westerlies, *J Phys Oceanogr*, *43*(10), 2113-2131, doi:10.1175/JPO-D-13-047.1.
- Lübbecke, J. F., C. W. Böning, N. S. Keenlyside, and S.-P. Xie (2010), On the connection between Benguela and equatorial Atlantic Niños and the role of the South Atlantic Anticyclone, *Journal of Geophysical Research: Oceans*, *115*(C9), doi:10.1029/2009JC005964.
- Moroshkin, K. V., V. A. Bunov, and R. P. Bulatov (1970), Water circulation in the eastern South Atlantic Ocean, *Oceanology*, *10*, 27-34.
- Rouault, M. (2012), Bi-annual intrusion of tropical water in the northern Benguela upwelling, *Geophys Res Lett*, *39*(12), doi:10.1029/2012GL052099.

3. Role of Interannual Kelvin wave propagations in the equatorial Atlantic on the Angola Benguela current system.

Imbol Koungue R. A., Rouault M and Illig S. Manuscript to be submitted to Geophys Res Lett

3.1. Introduction

In the tropical Atlantic, the annual cycle is the most dominant driver, when compared to interannual variability [*Xie et Carton,* 2004]. At interannual timescales, the tropical Atlantic upper ocean temperature, especially along the equator and at its eastern border, is primarily controlled by equatorial wave dynamics [*Illig et al.,* 2004]. Indeed, the sudden relaxation or intensification of easterly Tradewinds in the western equatorial Atlantic leads respectively to the generation of downwelling or upwelling Interannual Equatorial Kelvin Waves (IEKW) which propagate eastward up to the African coast. Part of the IEKW energy bounces back westwards as equatorial Rossby waves, while a substantial amount of their energy is transmitted poleward along the coast of Africa as coastal trapped waves [*Bachèlery et al.,* 2016]. In the Pacific, along their poleward propagation, associated with anomalous alongshore currents, IEKW deepen or raise the thermocline and ultimately trigger coastal Sea Surface Temperature (SST) interannual anomalies. Such wave dynamics is thought to be at the origin of major warm and cold events in the Angola-Benguela current system also called Benguela Niños and Niñas [*Florenchie et al.,* 2004*; Lübbecke et al.,* 2010*; Ostrowski et al*., 2009; *Rouault et al.,* 2007*, Rouault,* 2012] but this hypothesis has not been yet properly demonstrated to our knowledge. IEKW change the thermocline depth and can be identified through their signature in Sea Surface Height (SSH) using altimetry or moorings data. They can be modelled with Ocean Linear Model (OLM) forced only by wind stress. In order to monitor Kelvin and Rossby waves along the equator in the Tropical Atlantic, the Prediction and Research Moored Array in the Tropical Atlantic (PIRATA) program has been established since 1997 [*Bourlès et al.,* 2008]. But no systematic study of equatorial Kelvin and Rossby waves has been conducted in the equatorial Atlantic. Such study, conducted here, provide an opportunity to link equatorial wave dynamics to warm and cold upper ocean abnormal events along the Angolan and Namibian Atlantic coastline (from 10°S to 24°S).. The prediction of these coastal extreme events is important because of their significant impacts on the regional marine ecosystem [*Ostrowski et al.,* 2009, Blamey et al, 2015] and on the rainfall [*Rouault et al.,* 2003*,* 2009]. In this paper, using outputs from an Ocean Linear Model, altimetry and PIRATA array *in situ* measurements, we demonstrate that major IEKW propagations along the equator are indeed linked to major warm and cold events in the Angola Benguela Current system. We show that IEKW signature leads the development of coastal events by about one month.

3.2 Data and model

We use monthly fields of 1 degree horizontal resolution Reynolds SST (Reynolds et al, 2002) available since 1982. We also use monthly PIRATA dynamic height anomalies [*Bourlès et al.,* 2008] from 3 PIRATA's buoys located along the equator at 23°W, 10°W and 0°E over the 1998-2012 period. PIRATA Moorings record and sample the water column with five temperature/conductivity sensors deployed at depths of 1, 10, 20, 40 and 120m, five temperature sensors positioned at depths of 60, 80, 100, 140 and 180m and two temperature/pressure sensors at 300m and 500m along the equatorial Atlantic. They were established to detect and monitor the propagation of Kelvin and Rossby waves along the equator. These data are available on the website http://www.pmel.noaa.gov/tao/disdel/. In addition, we used the reference SSH gridded product

distributed by AVISO, that combines data from TOPEX/POSEIDON and JASON-1 altimeters. Data are distributed by CLS with a 7-day temporal resolution and 1/3° spatial resolution. We first detrend the data because of a significant positive trend in temperature and SSH in the region and then we calculate monthly means. Interannual monthly anomalies of parameters presented below are estimated as the departure from the monthly climatology. In order to extract the IEKW amplitude along the equator, we carry out simulation with the equatorial Atlantic Ocean Linear Model (OLM) developed by *Illig et al.,* [2004] and used in *Rouault et al.,* [2007].The linear model domain extends from 50°W to 10°E and from 28.875°S to 28.875°N, with an horizontal resolution of 2° in longitude and 0.25° in latitude. It includes 6 baroclinic modes with phase speed, projection coefficient and friction derived from a high-resolution OGCM. The OLM is forced by wind stress fields provided by DRAKKAR Forcing Set (DFS) version 5. DFS5.2 is similar to ERA-Interim reanalysis with 3h outputs at a horizontal resolution of 0.75 degree. Forcing is first detrended and interannual anomalies are calculated over the 1980-2012 period. The model is forced with 2 day wind stress averages obtained by cubic extrapolation of monthly means.

3.3 Results

3.3.1 Identification of abnormal SSH propagations along the equator

We present in **Fig. 3.1** the monthly detrended interannual anomalies of dynamic height from PIRATA (blue line), along with monthly altimetry derived and OLM derived SSH anomalies (black line and red line, respectively) from January 1998 to December 2012 at [0°E; 0°N], top, [10°W; 0°N], middle and [23°W; 0°N], bottom. The standard deviation of PIRATA derived dynamic height anomaly at [0°E; 0°N] is 2.83 cm , it is at [10°W; 0°N] and [23°W; 0°N] and is represented by the horizontal green lines over the three panels. We then define an abnormal positive and negative SSH event when detrended SSH anomalies at [0°E; 0°N] (**Fig. 3.1a**) exceed the standard deviation of a PIRATA time series for at least 2 months in a row. Abnormal positive and negative SSH anomalies events at the eastern equatorial Atlantic are represented by red and blue rectangles respectively and their width is function of the duration of the episode. These coloured rectangles will constitute our equatorial variability index; it will be used throughout this paper and reproduced in the subsequent figures.

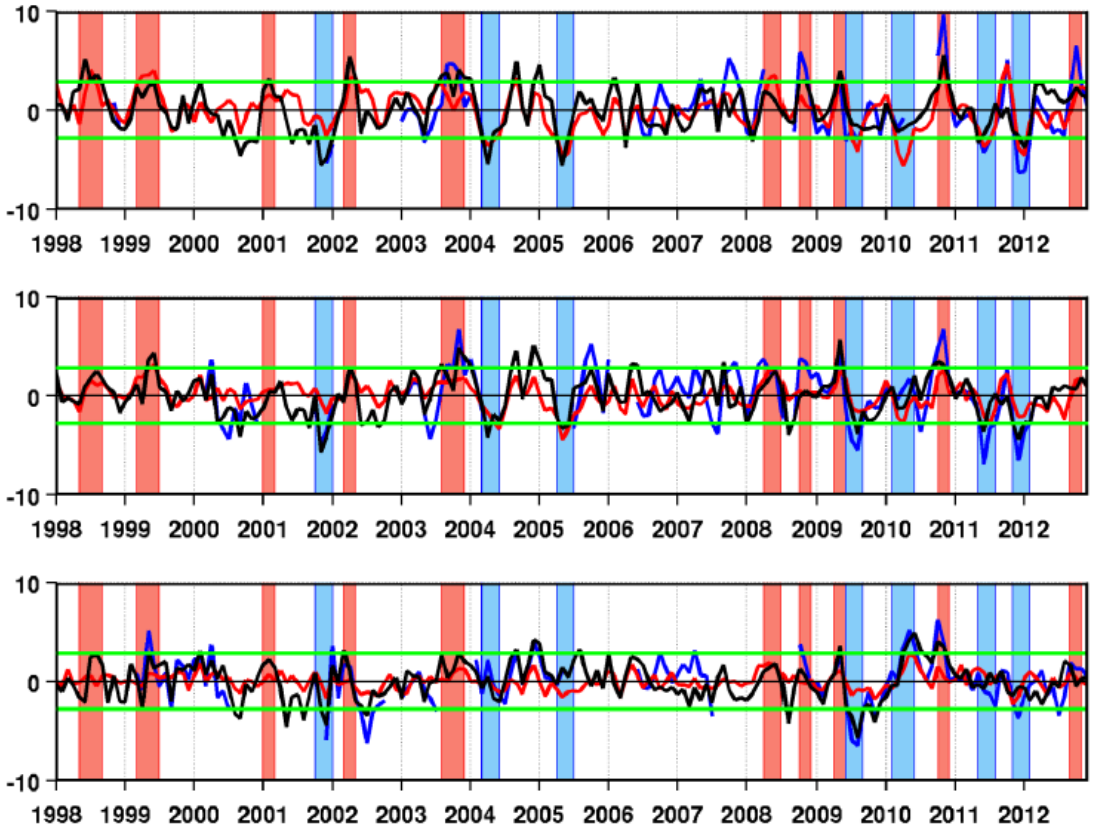

Figure 3.1: Monthly Detrended interannual anomalies of dynamic height (cm) from PIRATA in blue line, Aviso SSH monthly anomaly in black line and SSH monthly anomaly OLM in red line; top, at [0°E,0°N]; middle, at [10°W,0°N] and bottom, at [23°W,0°N]. The standard deviation derived from PIRATA is represented by the green horizontal line. Based on Figure 3.1 (top), abnormal positive and negative propagations of SLA are represented by red and blue rectangles respectively.

At the monthly scale, there is a 95% significant correlation of 0.68 between PIRATA dynamic height anomalies and altimetry derived SSH anomalies at [0°E; 0°N]. There is a significant correlation of 0.65 between the OLM SSHA and PIRATA dynamic height anomalies at the same location. Gaps occur occasionally in PIRATA at different location due to vandalism or data failure so we are using altimetry and OLM SSHA to fill up the gaps. A combined analysis of PIRATA, altimetry and OLM time series allows us to identify numerous significant upwelling and downwelling IEKW. According to our classification downwelling IEKW SSH signatures occurred in 1998 (May to September), 1999 (March to July), 2001 (January to March), 2002 (March to May), 2003 (August to December), 2008 (April to July), 2008 (October to December), 2009 (April to June), 2010 (October to December), 2012 (September to November). Negative SSH events occurred in 2001/2002 (October to January), 2004 (March to June), 2005 (April to July), 2009 (June to September), 2010 (February to June), 2011 (May to August) and 2011/2012 (November to February). Those events are clearly detected in the two other moorings (**Fig. 3.1**) at [10°W; 0°N] and [23°W; 0°N] confirming a propagation in SSH from west to east.

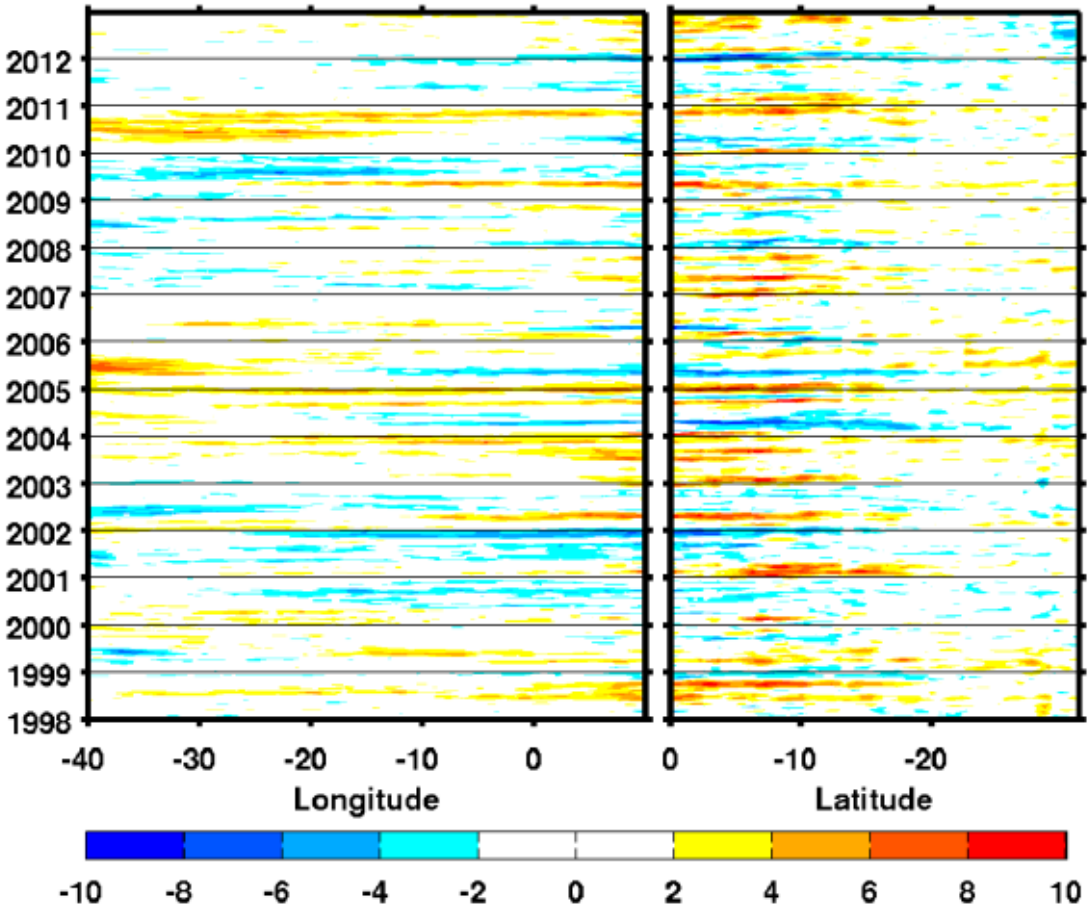

Figure 3.2 Longitude-time and latitude-time Hovmøller diagrams of weekly detrended SSH anomalies in cm, left panel averaged between 1°S and 1°N along the Equator and (right panel) along the African coast from 0°S to 30°S and averaged from the coast to 1° offshore

These abnormal propagations are also noticeable in the Hovmøller plot of altimetry derived SSH anomalies (**Fig. 3.2)** and in the Hovmøller plot of SST anomalies (**Fig. 3.3)** along the equator (averaged from 1°S to 1°N) and along the coast (averaged from the coast to 1° offshore for SST and from the coast to 2° offshore for Altimetry). The abnormal positive SSH propagation in 2001 was reported in [*Rouault et al.,* 2007] and linked to a warm event in the Angola-Benguela Current system while the start of the positive SSH 1999 event described here corresponds to a warm events at the Angola Benguela front reported by *Mohrholz et al*.[2001] and *Doi et al.*[2007]. The austral fall 2002 abnormal positive SSH event is described in the study of *Hoffman and Brandt* [2009] who mentioned strong downwelling Kelvin wave activities in 2002 along the Equator. Some abnormal negative SSH are occurring during the seasonal Atlantic cold tongue period (austral autumn and winter). For instance, during the negative SSH 2005 event, upwelling kelvin waves were identified along the Equator at the origin of that event [*Hoffman and Brandt.* 2009*; Marin et al.,* 2009].

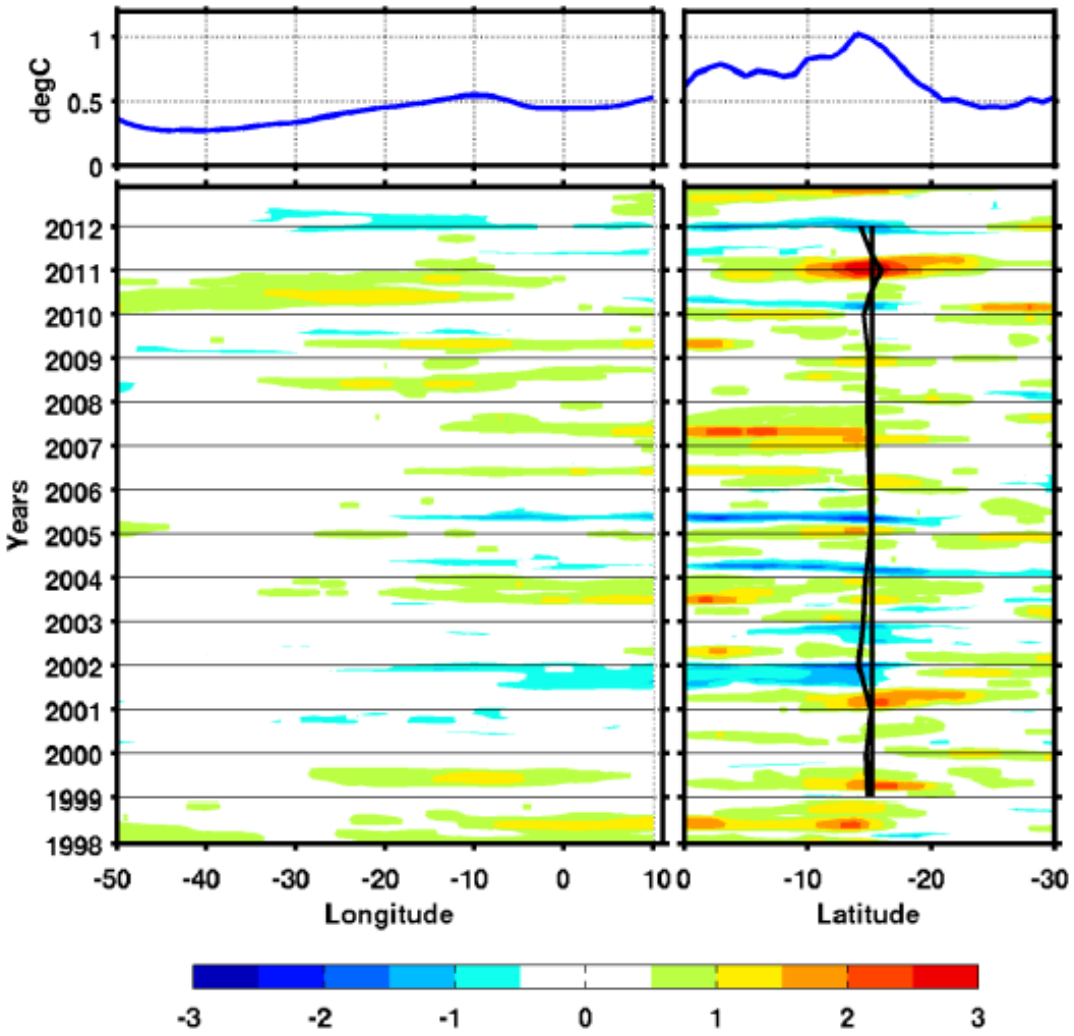

Figure 3.3: Left panel from top to bottom standard deviation and Hovmøller diagram of monthly detrended OI-SST anomalies in °C along the equator and averaged between 1°S and 1°N, and for the right panel from top to bottom standard deviation and Hovmøller latitude-time diagram of monthly detrended but along the African coast from 0°S to 30°S and averaged from the coast to 1°offshore. The mean latitude from 1998 to 2012 October to March fluctuations of the isotherm 22°C is represented by the black line and its averaged position by the straight line along the African coast.

3.3.2 Forcing and propagation of equatorial Kelvin waves from 1998 – 2012

Although some major Kelvin waves propagation were mentioned in the literature, they do not make the link with the Angola Benguela Current system (*Hoffman and Brandt.* 2009*; Marin et al.,* 2009). In order to document the link between Kelvin waves and the Angola-Benguela Current system, we have detrended and averaged the OLM key forcing parameter, *viz.* the zonal wind stress interannual anomalies (N/m^2) over the ATL4 domain (*i.e.* [50°W-25°W; 3°S-3°N], cf. *Illig and Dewitte*, 2006). This time series is displayed in **Fig. 3.3** (top). Most of the SSH positive and negative propagations described earlier are associated with weaker and stronger than normal easterlies wind stress anomalies respectively. 1998 exception will be discussed later. Following the decrease or the increase of the easterlies wind stress in the western equatorial Atlantic, positive or negative events

respectively propagate eastwards through the PIRATA array of moorings (**Fig.3.1**). There are also identified in the Hovmøller plot of altimetry derived SSH anomalies (**Fig. 3.2)**. Close inspection of lag correlation between zonal wind stress anomalies and OLM SSH anomalies (not shown) reveals a 0.6 correlation significant at 95% when the western equatorial zonal wind stress anomalies lead the OLM SSH anomalies at [0°E; 0°N] by a month. This lag of 1 month is consistent with the propagation of Kelvin wave mode 2 with an observed phase speed of 1.6 m/s, consistent with the study of *Illig et al.,* [2004]. This leads us to focus on IEKW and examine the output of the OLM in order to characterize the role of equatorial wave dynamics in the propagations of the events. **Fig. 3.4** (bottom) presents the first three gravest baroclinic modes of equatorial Kelvin wave contributions to sea level variation from 1998 to 2012.

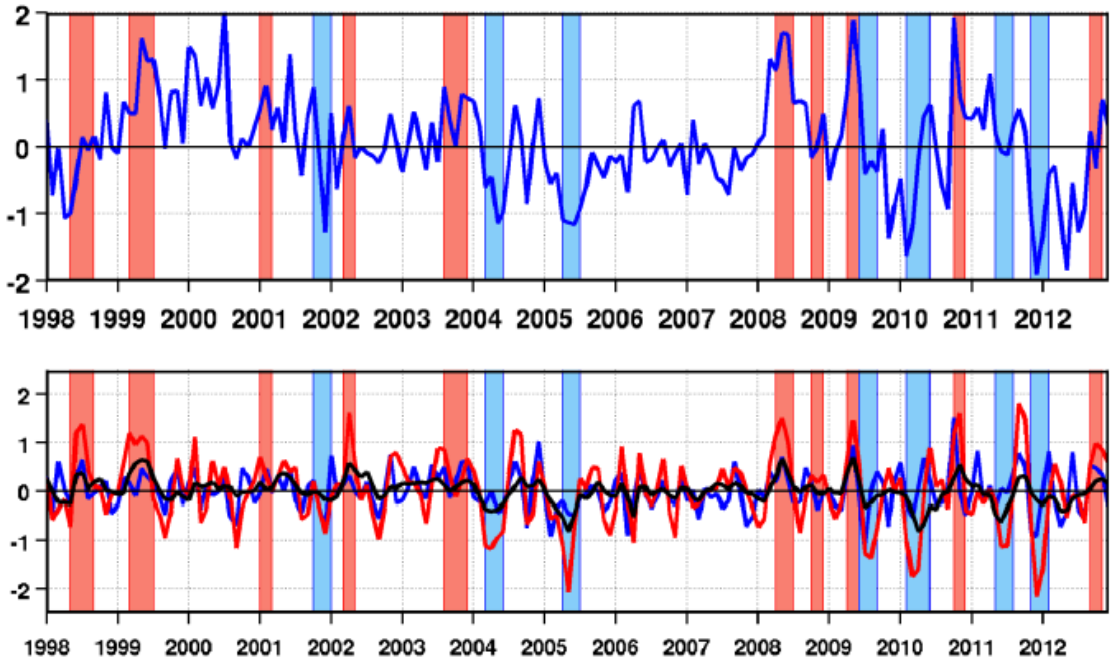

Figure 3.4: Top, Detrended monthly anomalies of zonal wind stress (N/m 2) averaged over ATL4 (50°W - 25°W, 3°S – 3°N); bottom, OLM detrended anomalies of Kelvin waves monthly contribution to sea level in cm: 1st baroclinic mode in blue line, 2nd baroclinic mode in red line, and 3rd baroclinic mode in black line, averaged over (20°W - 0°E, at 0°N). Based on Figure 3.1 (top), abnormal positive and negative propagations of SLA are represented by red and blue rectangles respectively.

These different contributions are averaged between 20°W and 0°E, at 0°N. Note that similar results are obtained when averaging these 3 different contributions from 20°W to 10°E, at 0°N (not shown). This suggests that the interannual signal of Kelvin waves do not vary considerably in the eastern equatorial Atlantic. The second baroclinic mode of IEKW is the most energetic mode, followed by the first one [*Illig et al.,* 2004; *Bachèlery et al.,* 2016].The linear model represents well the equatorial variability of IEKW propagations. The amplitude of IEKW averaged between 20°W and 0°E, at 0°N (**Fig. 3.4**, bottom) is compared with our equatorial index (**Fig. 3.1)** with good agreement. We observe that most of western zonal wind stress anomalies are related to propagation of downwelling or upwelling IEKW respectively. These waves propagate eastward and are observed through the positive or negative abnormal SSH at the eastern equatorial Atlantic (**Fig. 3.1(top)** and

Fig. 3.2 (left)). We note however that, according to what is expected from Kelvin wave dynamics and forcing, the modulation of zonal wind stress anomalies (**Fig. 3.4**) do not match the abnormal SSH propagations along the equator for some particular years, as in 1998, 2002 or 2009. In agreement with *Foltz and McPhaden,* [2010], the analysis of the wave sequence reveals that for some particular years (above mentioned), positive (negative) zonal wind stress interannual anomalies force preferentially westward downwelling (upwelling) Rossby waves, which in turn reflect at the Brazilian coast into Kelvin waves of opposite effect. Note that this is more likely due to the spatial pattern of the wind stress anomalies that is maximal off equator. This support our idea of defining an index based on the IEKW activity in the eastern Atlantic as monitored by PIRATA, rather than using the wind stress amplitude in the western Tropical Atlantic, in order to forecast SST anomalies along the coast of Angola and Namibia, which will be done in the following.

3.3.3 Link between equatorial variability and the Angola Benguela system

Most of the abnormal positive and negative propagation events described above are clearly observed in the Hovmøller diagram (**Fig. 3.2)** of monthly detrended altimetry derived SSH anomalies along the equator and along the African coast all the way to the Angola Benguela From (17^{o}S) or further south. Hovmøller diagram (**Fig. 3.3)** of monthly detrended SST somehow show the connection between between the equatorial domain and the African coastline but with less success. The main IEKW identified here propagate poleward when reaching the African coast. Recently, *Bachèlery* et al. [2016] demonstrated that the propagations along the coast were due to coastal trapped Kelvin waves, also mentioned in *Ostrowski et al.* [2009]. **Fig. 3.3** presents OI SST [*Reynold et al.,* 2002] detrended monthly anomalies from 1998 to 2012 along the Angola Benguela Current system. On top, we have the Southern Angola domain with data averaged from 10°S to 15°S and one degree from the coast; in the middle, the Angola Benguela Frontal zone with data averaged from 16.5°S to 17.5°S and one degree from the coast; at the bottom, the Northern Namibia upwelling domain with data averaged from 19°S to 24°S and one degree from the coast.

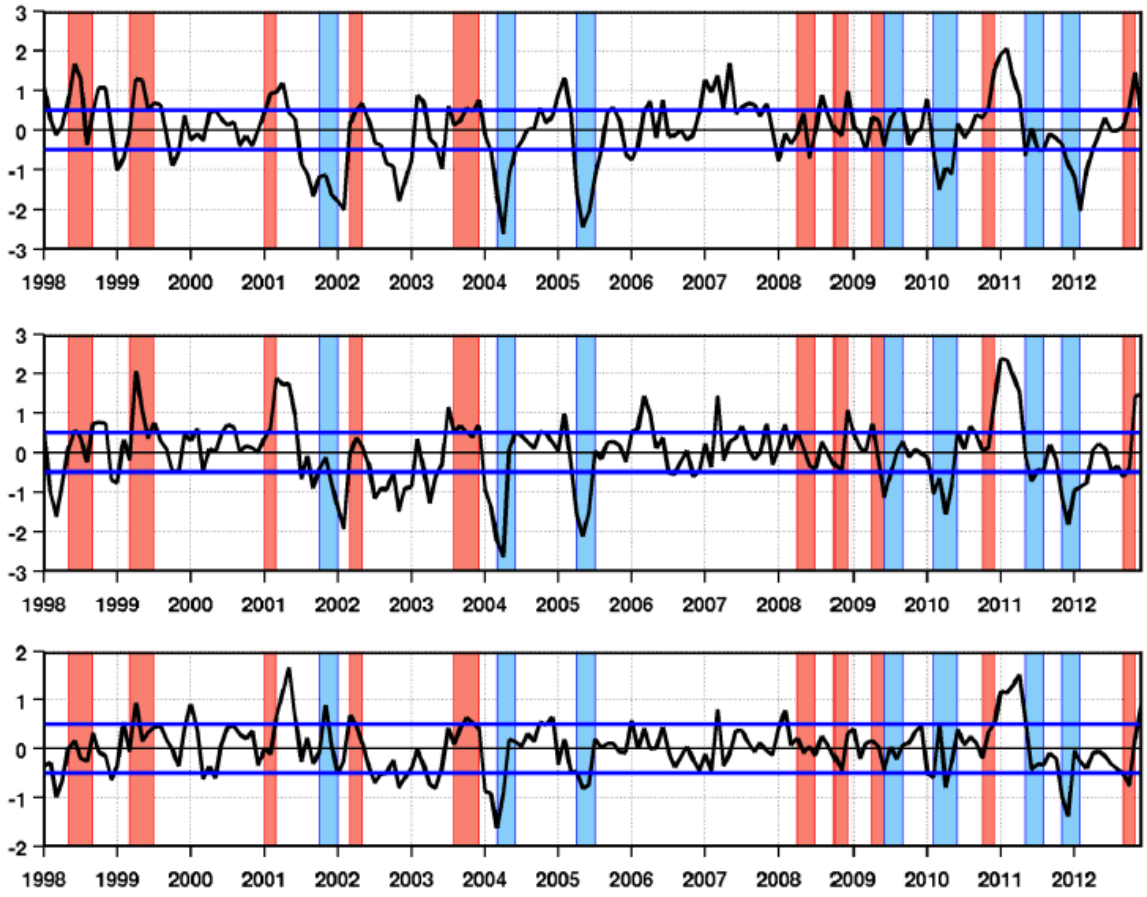

Figure 3.5: Monthly detrended anomalies of SST (°C) in (top) Southern Angola averaged from 10°S to 15°S and from the coast to 1° offshore, (middle) Angola Benguela Front averaged from 16.5°S to 17.5°S and from the coast to 1°offshore and (bottom) Northern Namibia averaged from 19°S to 24°S and from the coast to 1°offshore. The standard deviation is represented by the blue horizontal line. Based on Figure 1 (top), abnormal positive and negative propagations of SLA are represented by red and blue rectangles respectively.

After removing a significant warming trend in the region [*Blamey et al.,* 2015], monthly anomalies are calculated relative to the monthly climatology over the 1998-2012 period. A standard deviation of 0.5°C of the SST anomalies in the Angola Benguela Front domain is estimated. It is represented in **Fig. 1.5** by the horizontal blue lines over the three panels. Here we define a Benguela Niño or a Benguela Niña as a period in which the detrended SST anomalies in the 3 zones exceed the standard deviation for at least 3 months in a row in least 2 of the 3 domains. Most major warm and cold events along the African coast especially in Southern Angola and Northern Namibia domains are linked to the equatorial variability index, IEKW propagations and western zonal wind stress anomalies. Based on our criteria, we have selected 5 extreme warm events: in 1999 (March to August), 2001 (January to May), 2008 (November to December), 2010/2011 (November to April), 2012 (October to December) and 5 cold events in 2001/2002 (December to February), 2004 (January to April), 2005 (April to June), 2010 (February to May), 2011/2012 (November to March). Most of these Benguela Niños were already identified previously [*Rouault et al.,* 2007; *Ostrowski et al.*, 2009, *Lübbecke et al.,* 2010; *Rouault* 2012;] except for the Benguela Niño 2008, 2011/2012 and 2012/2013. There is little in the literature concerning Benguela Niña after 2002. The 1999 Benguela Niño at the

Angola Benguela Front was described by *Doi et al.,* [2007] and *Mohrholz et al.,* [2001]. A 0.4 lag correlation statically significant at 95% is found, when IEKW mode 2 averaged between 20°W-0°E at 0°N leads SST anomalies in the Southern Angola domain by 1 month. There is no significant correlation with the ABF and Northern Namibia domains. We observe in **Fig. 3.5**, slow propagations of SST anomalies as we move from Southern Angola to Northern Namibia. The persistence and slow propagations of SST anomalies from Southern Angola to Northern Namibia in those domains were already mentioned in *Rouault.* [2012] were attributed to advection of warm tropical water in the Northern Benguela upwelling domain. He found significant lag correlations between the two domains when Southern Angola SST anomalies lead Northern Namibia SST anomalies by one to four months. Also local effect could modulate the SST of those events south of the ABF.

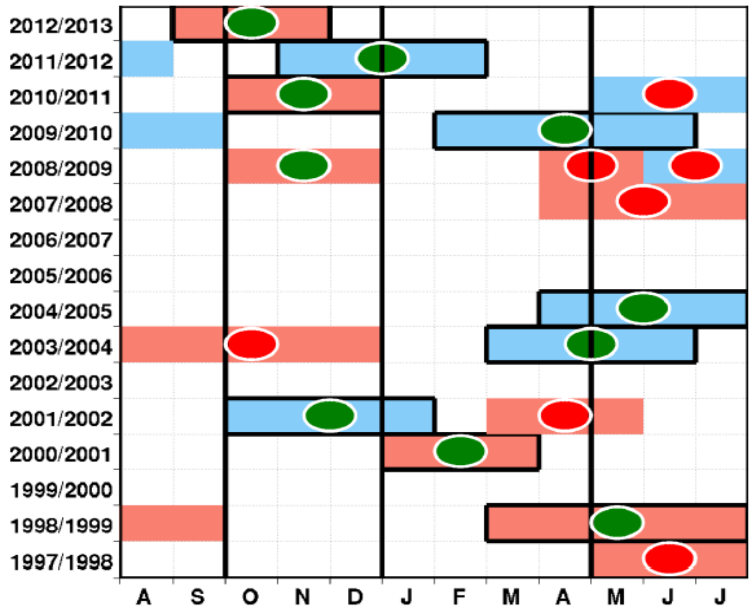

Figure 3.6: Score of prediction of coastal warm and cold events using the equatorial variability index from 1998 to 2012. Red rectangles with green circle inside and bold contours represent extreme coastal warm events which match abnormal equatorial SSH propagations. Red rectangles with red circle inside represent coastal warm events which do not match abnormal equatorial SSH propagations. Red rectangles with green circle inside represent coastal warm events which match with abnormal equatorial SSH propagations. Blue rectangles with green circle inside and bold contours represent extreme coastal cold events which match with abnormal equatorial SSH propagations. Blue rectangles with red circle inside represent coastal cold events which do not match with abnormal equatorial SSH propagations.

We summarize our equatorial variability index in relation with Benguela Niños and Niñas in **Fig. 3.6**. The red rectangles describe the positive propagation and their duration while the blue rectangles describe the negative events. Red circles inside a rectangle mean no match between equatorial propagations and warm or cold events in the Angola-Benguela Current system. Green circle mean good match between equatorial propagations and extreme warm or cold. The circle location is placed in the middle of the rectangle arbitrarily. From October to April nine out of twelve events matches. There is more of a mismatch from May to June. In general, From **Fig. 3.5** and **Fig. 3.6,** we observed a good score without including the local wind stress forcing and stratification effects. The 1998 mismatch is explained by *Foltz and McPhaden.* [2010] who highlighted the retroflection at the

Brazilian coast of a Rossby waves forced by stronger Tradewinds into a downwelling Kelvin waves that lead to the 1998 positive propagation along the equator. In general, October to April seems the best time for the successful prediction of the warm and cold events in the Angola Benguela current system. Our study is consistent with the modeling study of *Bachèlery et al.* [2016] who observed that at interannual timescales, remote equatorial forcing is more efficient than local forcing along the Angola Benguela coast. But the effects of the local forcing, unfavorable or favorable local upwelling wind and stratification are not negligible since they could modulate the signature of an equatorial propagation. Also *Polo et al.* [2008a] studied the intraseasonal EKW and found 2 dominant periods for the appearance of KW: Austral Spring (September-December) for downwelling KW and Austral summer (November-January) for upwelling KW. The favorable season where a potential propagation of the 2nd baroclinic mode of Kelvin waves could create a Benguela Niño or Niña one month later is mostly between October and April.

3.4 Conclusion

We demonstrate here that warm and cold events in the Angola Benguela Current system, also called Benguela Niño and Niñas, are remotely forced by Kelvin waves propagation in the tropical Atlantic, especially the the 2nd baroclinic mode. This confirms the hypotheses emitted by several authors. Major variations in thermocline depth at the origin of those events are observed by PIRATA and altimetry and simulated by an Ocean Linear Model forced by wind stress only. An Ocean Linear Model can be easily implemented in real time using satellite estimate or model output and easily implemented. PIRATA data and altimetry data are also available in real time and can be used in an early warning system. An Index based on PIRATA data at [0 S, 0 N] seems to work better than an index based on Wind stress anomalies in the Western Tropical Atlantic along the equator. Altimetry derived SSH link the equatorial propagation to the coastal region. It seems that local forcing has little to do with the generation of most of major cold and warm events although they could modulate their intensity. The PIRATA array of mooring is crucial to the observation of those Kelvin waves and must be maintained. At last, the study opens the possibility to forecast Benguela Niños and Niñas, especially from October to April, using an Ocean Linear Model forced by wind speed, altimetry and PIRATA data. Tide gauge and currentmeter available in real time in Angola and Namibia would complete the system. Further work will involve study the reason why some events did not fit our scenario although some answer can already be found in the literature and also better ascertain the relation between the Southern Angola and Northern Namibia domains.

3.5 References

- Bachèlery, M.-L., S. Illig, and I. Dadou (2016), Interannual variability in the South-East Atlantic Ocean, focusing on the Benguela Upwelling System: Remote versus local forcing, J.Geophys. Res. Oceans, 120, doi:10.1002/2015JC011168.
- Blamey, L. K., L. J. Shannon, J. J. Bolton, R. J. M. Crawford, F. Dufois, H. EversKing, C. L. Griffiths, L. Hutchings, A. Jarre, M. Rouault, K. Watermeyer, H. Winker (2015) Ecosystem change in the southern Benguela and the underlying processes. Journal of Marine Systems.
- Bourlès, Bernard, Rick Lumpkin, Michael J. McPhaden, Fabrice Hernandez, Paulo Nobre, Edmo Campos, Lisan Yu et al. "THE PIRATA PROGRAM." *Bulletin of the American Meteorological Society* 89, no. 8 (2008): 1111.
- Doi T, Tozuka T, Sasaki H, Masumoto Y, Yamagata T (2007). Seasonal and interannual variations of oceanic conditions in the Angola Dome.*J PhysOceanogr*, 37, 2698-2713.
- Florenchie, P., C. J. C. Reason, J. R. E. Lutjeharms, and M. Rouault (2004), Evolution of

interannual warm and cold events in the southeast Atlantic Ocean, J. Clim., 17, 2318–2334.
- Foltz, G. R., and M. J. McPhaden (2010), Interaction between the Atlantic meridional and Niño modes, *Geophys. Res. Lett.*, **37**, L18604, doi:10.1029/2010GL044001.
- Illig, S., Dewitte, B., Ayoub, N., du Penhoat, Y., Reverdin, G., De Mey,P., Bonjean, F., Lagerloef, G.S.E., 2004. Interannual long equatorial waves in the Tropical Atlantic from a high resolution OGCM experiment in 1981–2000. J. Geophys. Res. 109 (C2),C02022. doi:10.1029/2003JC001771.
- Illig, S., and B. Dewitte (2006), Local coupled equatorial variability versus remote ENSO forcing in an intermediate coupled model of the tropical Atlantic, J. Clim., 19(20), 5227–5252.
- Lübbecke, J. F., C. W. Böning, N. S. Keenlyside, and S.-P. Xie (2010), On the connection between Benguela and equatorial Atlantic Niños and the role of the South Atlantic Anticyclone, J. Geophy. Res., 115, C09015, doi:10.1029/2009JC005964.
- Marin, F., G. Caniaux, H. Giordani, B. Bourle` s, Y. Gouriou, and E. Key (2009), Why were sea surface temperatures so different in the eastern equatorial Atlantic in June 2005 and 2006?, J. Phys. Oceanogr., 39(6), 1416–1431, doi:10.1175/2008JPO4030.1.
- Mohrholz, V., Schmidt, M., Lutjeharms, J.R.E., 2001. The hydrography and dynamics of the Angola–Benguela frontal zone and environment in April 1999. South Afr. J. Sci. 97, 199–208.
- Polo, I., A. Lazar, B. Rodriguez-Fonseca, and S. Arnault (2008), Oceanic Kelvin waves and tropical Atlantic intraseasonal variability: 1. Kelvin wave characterization, *J. Geophys. Res*., 113, C07009, doi:10.1029/2007JC004495
- Ostrowski, M., J. C. B. da Silva, and B. Bazik-Sangolay (2009), The response of sound scatterers to El Niño- and La Niña-like oceanographicregimes in the southeastern Atlantic, ICES J. Mar. Sci., 66(6), 1063–1072,doi:10.1093/icesjms/fsp102.
- Rouault, M., P. Florenchie, N. Fauchereau, and C. J. C. Reason (2003) South East tropical Atlantic warm events and southern African rainfall,Geophys. Res. Lett., 30(5), 8009, doi:10.1029/2002GL014840
- Rouault, M., S. Illig, C. Bartholomae, C. J. C. Reason, and A. Bentamy (2007), Propagation and origin of warm anomalies in the Angola Benguela upwelling system in 2001, J. Mar. Syst., 68, 473–488.
- Rouault, M., J. Servain, C. J. C. Reason, B. Bourlès, M. J. Rouault, and N. Fauchereau (2009), Extension of PIRATA in the tropical South-East Atlantic: An initial one-year experiment, Afr. J. Mar. Sci., 31(1), 63–71, doi:10.2989/AJMS.2009.31.1.5.776.
- Rouault, M. (2012), Bi-annual intrusion of tropical water in the northern Benguela upwelling, Geophys. Res. Lett., 39, L12606, doi: 10.1029/2012GL052099.
- Schouten, M. W., R. P. Matano, and T. P. Strub (2005), A description of theseasonal cycle of the equatorial Atlantic from altimeter data, Deep SeaRes., Part I, 52, 477–493, doi:10.1016/j.dsr.2004.10.007.
- Xie, S.-P., and J. A. Carton (2004), Tropical Atlantic variability: Patterns,mechanisms, and impacts, in Earth Climate: The Ocean-AtmosphereInteraction, Geophys. Monogr. Ser., vol. 147, edited by C. Wang, S.-P.Xie, and J. A. Carton, pp. 121–142, AGU, Washington, D. C.

4. Origin, development and demise of the 2010-2011 Benguela Niño

Rouault M, Imbol Koungue R. A., Lübbecke J., Illig S. and Ostrowski M. Origin, development and demise of the 2010-2011 Benguela Niño. To be submitted to J Marine Syst.

4.1. Introduction

Ocean temperatures off the South-western African coast are characterized by a strong gradient between the warm tropical Atlantic and the cold Benguela current. This region is called the Angola Benguela Front and is on average located at about 17ºS (Veitch et al., 2006). Every few years, Sea Surface Temperature (SST) off the coast of Angola and Namibia reach values of up to 5ºC higher than seasonally normal. These warm events have been named Benguela Niños (Shannon et al., 1986) by analogy to their Pacific counterpart. They tend to peak in March/April (Florenchie et al., 2003, 2004; Rouault et al., 2007: Lübbecke et al., 2010). These warm events have large impacts on local fisheries (Boyer and Hampton, 2001) and on rainfall variability over south-western Africa (Rouault et al., 2003; Lutz et al, 2015). Understanding and potentially forecasting their development is thus of high socio-economic importance and the couple of months lead time between the decrease in winds along the Equator and the development of SST anomalies along the Angolan and Namibian coastline offer some predictability. While local wind forcing might play a role in the development of some of the Benguela Niño events, especially in the Benguela upwelling region (Richter et al., 2010, Junker et al, 2015), it has been shown that they are mainly generated by wind stress changes in the western equatorial Atlantic (Florenchie et al., 2003, 2004; Rouault et al., 2007; Lübbecke et al., 2010; Bachèlery et al. 2014). The hypothesis put forward is that wind stress variations in the western equatorial Atlantic generate equatorial and subsequent coastal Kelvin waves along the African coast. These waves are associated with thermocline deepening and thus subsurface temperature anomalies. They propagate along the African west coast up to the Angolan coast and generate strong SST anomalies due to a shallow thermocline there. The warm anomaly associated with Benguela Niño events is, however, not restricted to the region off Angola and down to the location of the Angola Benguela Front at 17ºS where the thermocline outcrops. Warm anomalies are observed as far south as 25ºS. Based on a regional ocean model study, Bachèlery et al. (2015) showed that at interannual time scales, remotely forced coastal trapped waves propagate poleward along the African southwest coast up to the northern part of the Benguela upwelling system. Based on model outputs, Rouault et al. (2012) attribute the warming off Namibia to southward advection of subsurface warm water. The latest strong Benguela Niños and other warm events occurred in Austral summer 1984 and 1995 (Shannon et al, 1986, Gammelsrød et al., 1998, Florenchie et al., 2003, 2004, Rouault, 2012). While they could be traced back to the equatorial Atlantic, information about the propagation of the anomaly in the subsurface ocean, i.e. subsurface temperatures and thermocline depth, had to be mostly inferred from model simulations. The focus of this study is the latest warm anomaly off the southwest African coast that occurred in early 2011. This event was also special in that it started already in Austral fall 2010. It is the strongest event since 1995 and it was observed by the PIRATA array of mooring as early as October 2010. In this study, we will analyse the evolution of the 2010/2011 Benguela Niño event from its origin to its demise using direct observations from the PIRATA array, satellite estimate of SST and SSH, as well as wind stress from ERA Interim atmospheric Reanalysis. Observation will be interpreted in the light of experimentation with an Ocean Linear Model and analysis of the GODAS ocean reanalysis product. In section 2, the observational data sets and the reanalysis product are described. In section 3, we describe the evolution of the event,

analyse its characteristics at its peak phase, and estimate the southward advection of temperature anomalies. The results are summarized and discussed in section 4.

4.2 Data, methods and models

We are using monthly fields of 1º horizontal resolution Reynolds SST (Reynolds et al, 2002) available from 1982 to 2013 and weekly and monthly TRMM TMI SST. TMI measures the microwave energy emitted by the earth and its atmosphere over a wide swath width of 760 km and can estimate SST measured through clouds. Weekly and monthly TMI SST is available in near real time from December 1997 to December 2013 at a 1/3° resolution. There are no data within 35 km from the coast. We further use weekly 1993-2013 1/3º horizontal resolution of AVISO merged altimetry SSH. We use the "reference product" that uses only two altimeters in order to have some homogeneity in the calculation of monthly anomaly from climatology. Wind stress estimates are provides by the ERA Interim atmospheric reanalysis (Uppala et al., 2005). We also make use of the PIRATA mooring array (Bourles et al.,2008). PIRATA has recorded subsurface temperature since 2000, providing a climatology upon which the anomalies are calculated online with the NOAA PIRATA data delivery and display web site Java toolsat (http://www.pmel.noaa.gov/tao/disdel/). There are 13 temperature sensors deployed at depths of 1, 10, 13, 20, 40, 60, 80, 100,120, 140, 180, 300 and 500 m (Rouault et al., 2009). There are two pressure sensors at 300 and 500 m depth. We are using here PIRATA monthly anomalies of the 20 ^{o}C isotherm as a proxy for thermocline depth anomalies and measured dynamic height from 0 to 500 Db. In order to investigate equatorial wave propagations, we use the Equatorial Atlantic Ocean Linear Model (OLM) developed by Illig et al. (2004). The linear model domain extends from 50°W to 10°E and from 28.875°S to 28.875°N, with an horizontal resolution of 2° in longitude and 0.25° in latitude. The model time-step is 2 days. It includes 6 baroclinic modes with phase speed, wind stress projection coefficient and friction derived from a high-resolution OGCM. In the present study, the model is forced by detrended ERA-Interim wind stress interannual anomalies relative to the 1980-2013 monthly climatology. We focus on the OLM Sea Level Anomaly (SLA) signal along the equator and in particular on the gravest baroclinic mode (1 and 2) long equatorial Kelvin wave contribution. In addition to the OLM Control Run (OLM-CR) simulation, a sensitivity experiment is carried out with the OLM in which no reflection of Kelvin and Rossby waves are allowed at the western and eastern boundaries. Comparing these paired experiments allows to highlight and calculate the contribution of reflected Rossby and Kelvin waves to overall signal.In addition, monthly ocean velocity and temperature fields for the time period 1980 to 2013 are taken from the National Centers for Environmental Prediction (NCEP) Global Ocean Data Assimilation System (GODAS) from the NOAA/NWS/CPC (Behringer and Xue 2004). They are available at a horizontal resolution of 1/3º latitude and 1º longitude, and the model has 40 vertical levels.

4.3. Results

4.3.1 Origin, development and demise of the warm event

In October 2010, weaker than normal easterly wind occurred in most of the Tropical Atlantic sector from 5°N to 10°S and from 50°W to 0°E (**Fig. 4.1** and **Fig. 4.2**).

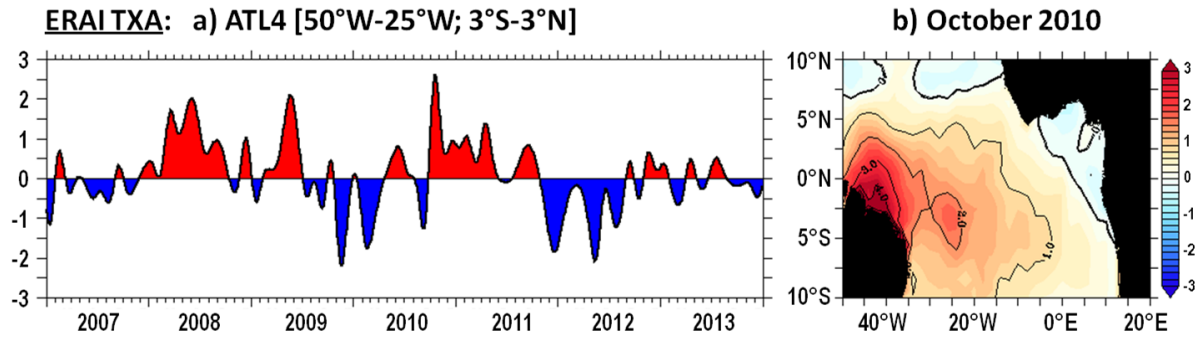

Figure 4.1: Left: Time series of monthly anomalies of zonal component of wind stress in the Western Equatorial Atlantic (WEA, averaged over [40°W-10°W; 2°S-2°N]). Right: map of monthly anomalies of zonal wind stress component in October 2010. Anomalies are computed as the departure from the 1980-2013 monthly climatology.

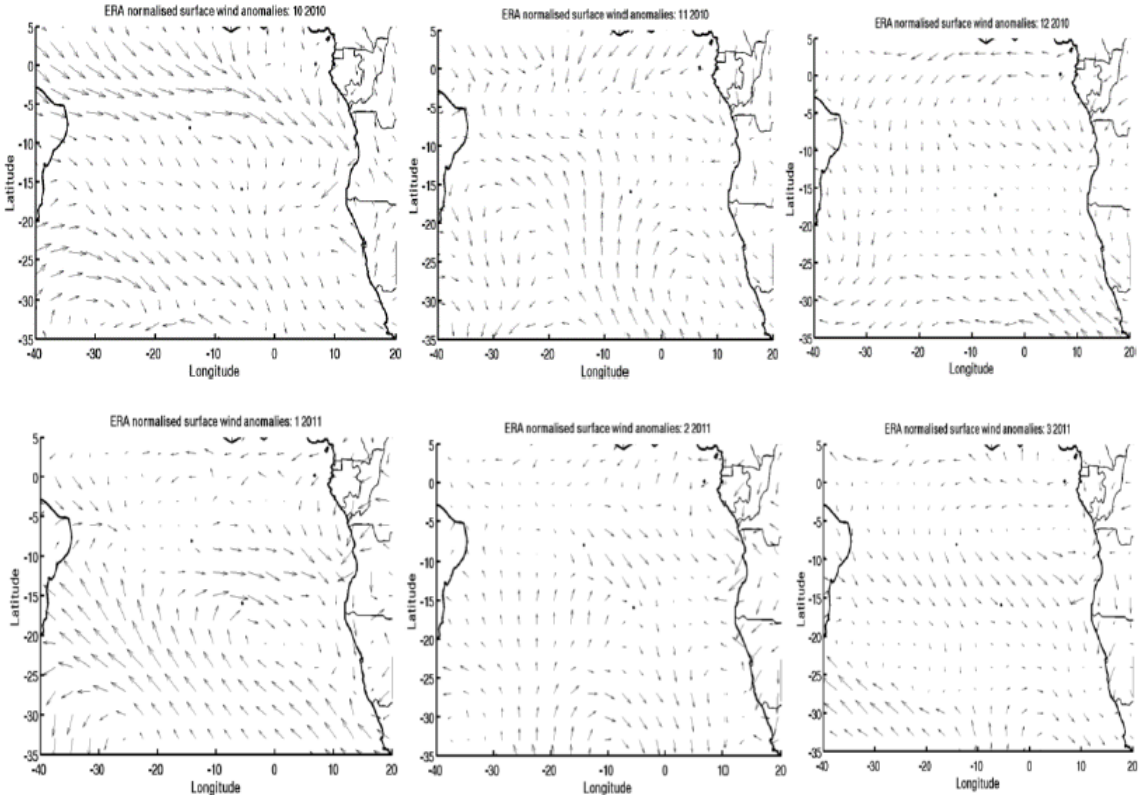

Figure 4.2: ERA Interim monthly mean anomaly divided by standard deviation from October 2010 to March 2011 (left to right and top to bottom).

According to ERA Interim reanalysis data, it was the largest decrease at the monthly scale in zonal wind speed since at least 1982 along the equator when averaged from 40 ^{o}W to the African Coastline and from 2 ^{o}N to 2 ^{o}S with positive anomaly above 2 standard deviation (not shown). Hovmøller diagram of FLK Atlas satellite (not shown) derived zonal wind speed along the Equator confirms the results inferred from ERA Interim reanalysis. Following the decrease in equatorial easterly winds, a deepening of the thermocline larger than 30 m was observed by the PIRATA

mooring array, propagating from East to West in October 2010, taking a month to reach the African coastline (**Fig. 4.3** and **Fig. 4.4**). Moorings are located at 35°W, 27°W 10°W and 0°W. Data shown in **Fig. 4.3** and **Fig. 4.4** are interpolated between moorings and between depths where subsurface temperature is measured. The actual positions of the sensors are indicated by a cross on **Fig 4.3**.

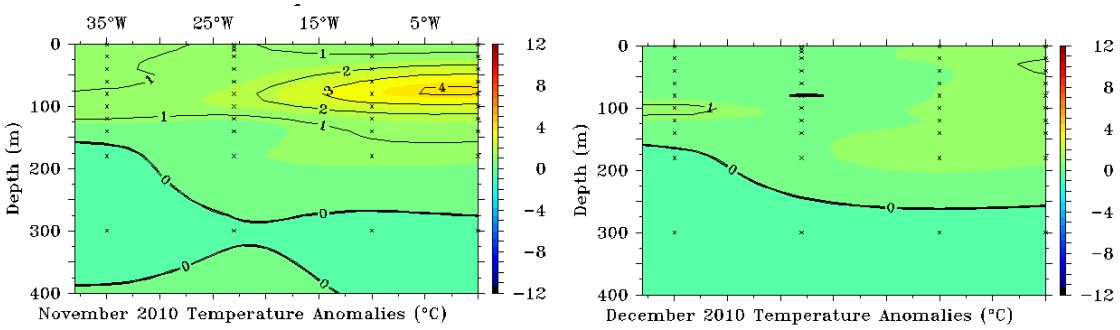

Figure 4.3: PIRATA observed subsurface temperature monthly anomaly interpolated between 4 mooring location and at depth indicated by a cross from September to December 2010 from 40 W to 0 W and from 0 to 400 m.

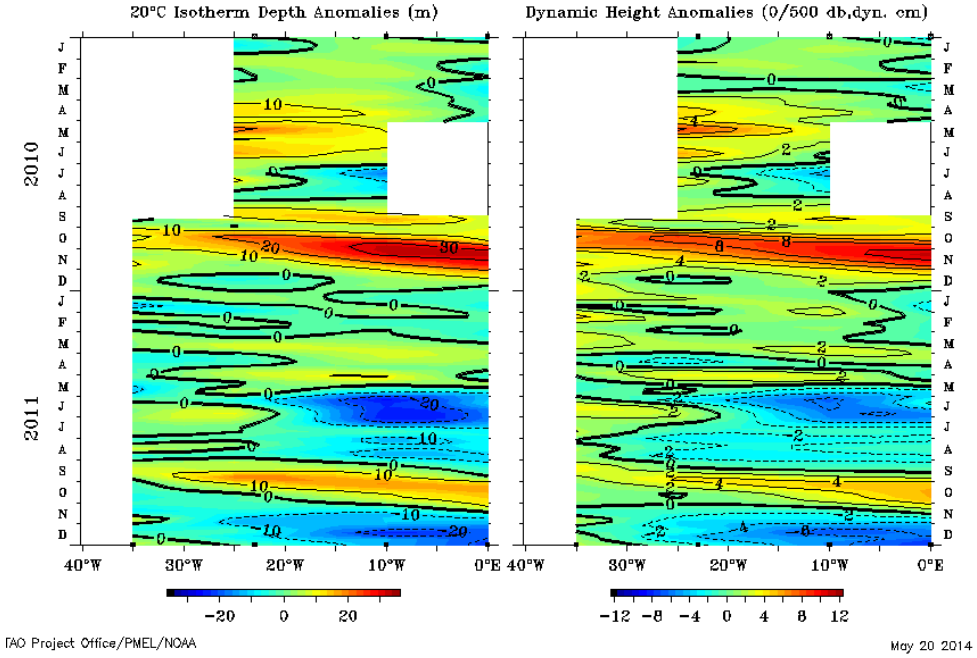

Figure 4.4: left Hovmøller diagram of 20 °C isotherm depth anomaly (m) and dynamic height anomaly from 2010 (top) to 2011(bottom) inferred from PIRATA moorings and interpolated between mooring location.

Maximum subsurface temperature anomalies of up to 3ºC are observed by the PIRATA mooring in October 2010 from 80 m to 130 m depth at 35°W, from 70 m to 120 m at 27°W ,from 50 m to 90 m at 10°W and from 50m to 80 m at 0°W. In the following month, November 2010, subsurface anomalies of 2°C to 4°C are observed only in the East of 20°W (**Fig. 4.3a**) suggesting an eastward propagation. A maximum anomaly of 4°C is observed at 0°W at 60 m in November. In December the subsurface anomaly has vanished.PIRATA derived monthly anomalies of the 20°C

isotherm depth and dynamic height monthly anomalies from 0 to 500dB (**Fig. 4.4**) as well as altimetry derived detrended monthly interannual anomaly of sea surface height (**Fig. 5**) confirm the propagation of subsurface temperature anomalies across the basin, the deepening of the thermocline and the duration of the event that lasted for two months along the Equator in October/November 2010. **Fig. 4.5** presents the Hovmøller diagram of monthly anomalies of SSH along the equator (left panel) from 40°W to the African coast and from 0°S to 30°S along the coast (right panel). Data is averaged between 1°S to 1°N along the equator and from the coast to 2º offshore along Southern Africa from January 2010 (bottom) to December 2011 (top). Data is detrended to remove a strong positive trend in SSH in the basin since 1993. We note that October corresponds to the maximum of climatological SSH in the Tropical Atlantic and one of the two maxima of SSH along the African coastline from 0°S to the Angola Benguela Front situated around 17°S. Climatological easterly winds also start to decrease at that time of the year in the western tropic Atlantic. In that respect, the event can be seen as an exaggeration of the annual cycle, but with important consequence further south as we will see later.

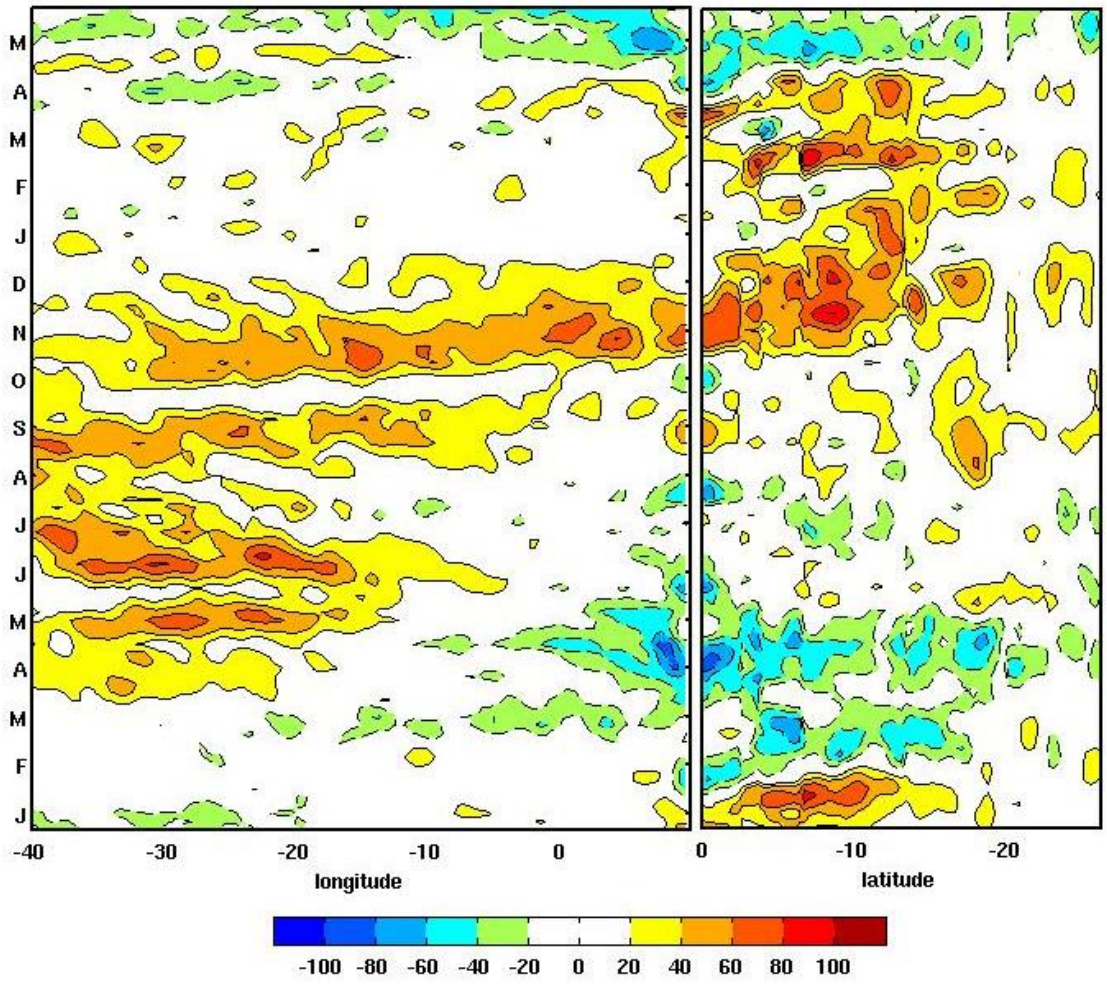

Figure 4.5: Hovmøller diagram of altimetry derived SLA anomalies from monthly climatology along the equator (averaged over 1ºS to 1ºN, left) from 40 ^{o}W to the African coastline and along the Southern African coast (averaged from coast to 2º offshore, right) from O to 25 ^{o}S from January 2010 (bottom) to May 2011 (top).

The propagation of above normal SSH along the Equator is followed by a poleward propagation of positive SSH anomalies along the African coastline from 0°S to 20°S, i.e. 3 degrees further south than the Angola Benguela Front. In contrast to the equatorial region, the SSH anomalies are observed to last from November 2010 to April 2011. In May 2011 abnormal negative anomaly of SSH are detected along the eastern equator and along the African coastline, putting an abrupt end to the positive SSH anomalies along the African coast. Shoaling of the thermocline along the equator of up to 20 m propagating from west to east and concomitant negative anomalies of dynamic height are measured by the PIRATA mooring array (**Fig. 4.4**) from 20°W to 0°W in agreement with the altimetry derived SSH anomalies (**Fig. 4.5**). We note that ERA Interim zonal wind stress anomaly was also negative in April and May 2011 from 30°W to the African coast, indicative of stronger than normal easterly wind stress. The results obtained from the Ocean Linear Model forced by ERA Interim wind stress emphasize the role of long equatorial Kelvin and Rossby waves in the origin of this Benguela Niño event (**Fig. 4.6** and **Fig. 4.7**).

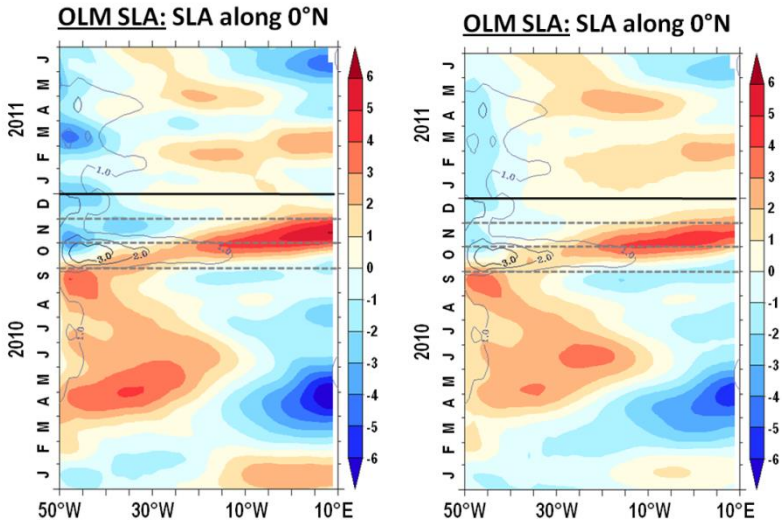

Figure 4.6: Longitude–time Hovmøller diagrams along the equator of monthly Ocean Linear Model SLA from January 2010 to June 2011. Left (right) panel: with (without) wave reflection at the meridional boundaries of the basin. Unit is cm. Contour lines highlight the ERA Interim zonal wind stress anomalies along the equator (averaged between 2°S to 2°N). Unit is in cm.

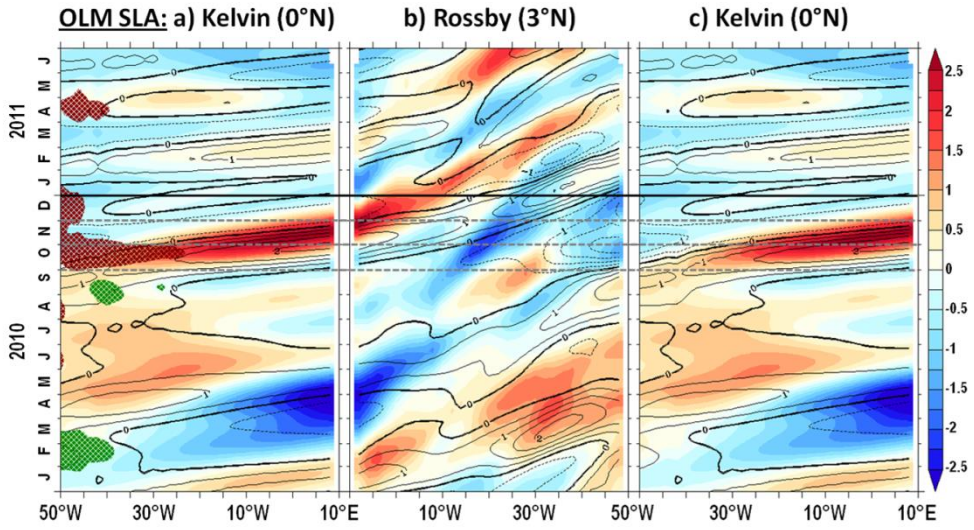

Figure 4.7: Panel a (b): Longitude–time Hovmøller diagrams of the eastward (westward) propagating Kelvin (Rossby) wave contribution to the monthly SLA along the equator (at 3°N) from the Ocean Linear Model from January 2010 to June 2011. The second baroclinic Kelvin wave contribution (dominant mode) is in colour, while contours denote the first baroclinic Kelvin wave contribution (fastest mode). Unit is cm. Note that Kelvin is repeated in panel c and the longitude axis in the Rossby is reversed in order to appreciate the reflexion at the meridional boundaries of the basin. In panel a, orange (green) shadings corresponds to zonal wind stress anomalies along the equator (averaged between 2°S-2°N) . Unit is in cm.

It confirms that anomalies of zonal wind stress in October 2010 are the main forcing of the thermocline anomaly along the Equator, in agreement with the PIRATA observations and altimetry results. Moreover, the wind forced Kelvin wave signature in October 2010 coincides with reflected Rossby waves at the Brazilian border in the Western part of the basin. The latter were forced by Kelvin waves reflected into Rossby waves at the African border in April 2010 for Kelvin wave mode 1, while the mode 2 Rossby wave appears to be forced by positive anomalies of meridional wind stress in austral winter 2010. There is a lag of one month between the arrival of Kelvin wave mode 1 and Kelvin wave mode 2 at the African border. Kelvin wave mode 1 arrived at the end of October 2010 while Kelvin wave mode 2 arrived at the end of November 2010. Together with the reflected Rossby wave, this could explain the anomaly in thermocline depth and subsurface anomaly in November 2010 observed with PIRATA. Reflections at the meridional boundaries explain 20% of the SSH anomaly along the Equator in November/December 2010. This results is obtained by calculated the ratio of SLA calculated with OLM with reflection allowed at the border and without reflection at the border (not shown). There is a small amplitude Kelvin wave along the Equator associated with a positive anomaly of zonal wind stress at that time (**Fig. 1**)..

4.3.2 The 2010/2011 Benguela Niño

Fig. 4.8 shows a Hovmøller diagram similar to **Fig. 4.5** but for TRMM TMI SST monthly anomalies. Along the Equator, a moderate increase in SST is visible from October to December along the equator with SST anomalies reaching +1.5°C, while along the coast of Africa and especially at the Angola Benguela Frontal zone the increase is more substantial. It reaches values of up to 4ºC, lasts for five months and extends as far south as 25°S in the Northern Benguela upwelling. An SST anomaly larger than 1 ^{o}C is first observed at the Angola Benguela front in November 2010 and appears to

spread southward and northward until May 2011, when the warm event suddenly ceases. We note that, off Namibia, the upwelling favourable wind decreased in November, December 2010, and March 2011 (**Fig. 4.2**) and this can partially explain the warming south of the Angola Benguela Front in the Northern Benguela upwelling. Wind was normal in February but failed to cool the event. In fact, there is a secondary maximum of positive SST anomaly in February corresponding to the maximum of positive SSH anomaly along the African coast at that time (**Fig. 4.5**) which is not observed along the Equator.**Fig. 4.8** shows maps of monthly TRMM TMI SST anomaly from November 2010 to April 2011 in the Tropical and South Atlantic. Highest positive SST anomalies are clearly seen of Angola and Namibia. In April, lower than normal SST starts to appear north the Angola Benguela Front marking the start of the demise of the warm event.

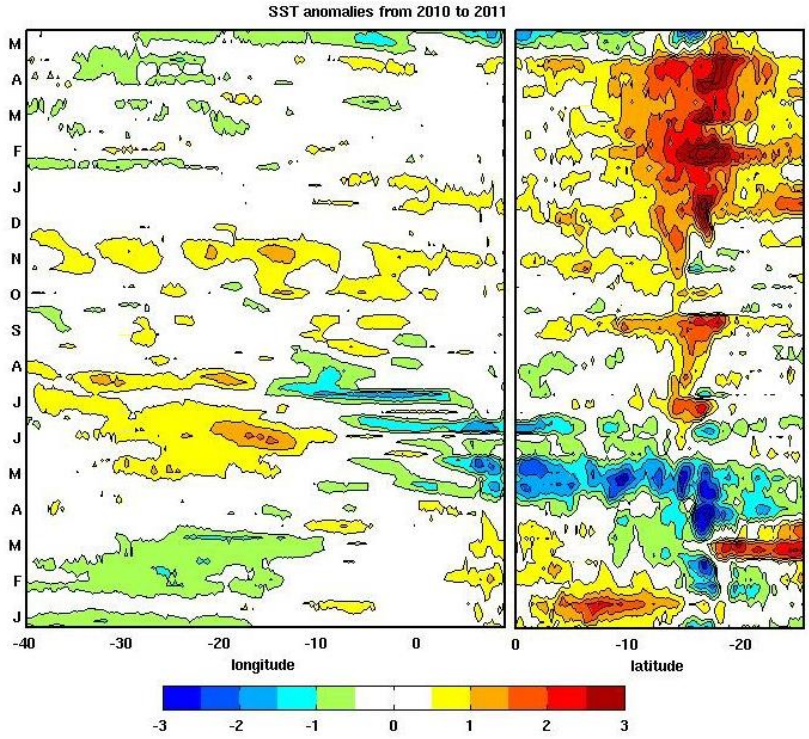

Figure 4.8: Hovmøller diagram of TRMM TMI SST anomaly from January 2010 (bottom) to May 2011 (top) along the equator (left) and along the South West African coast.

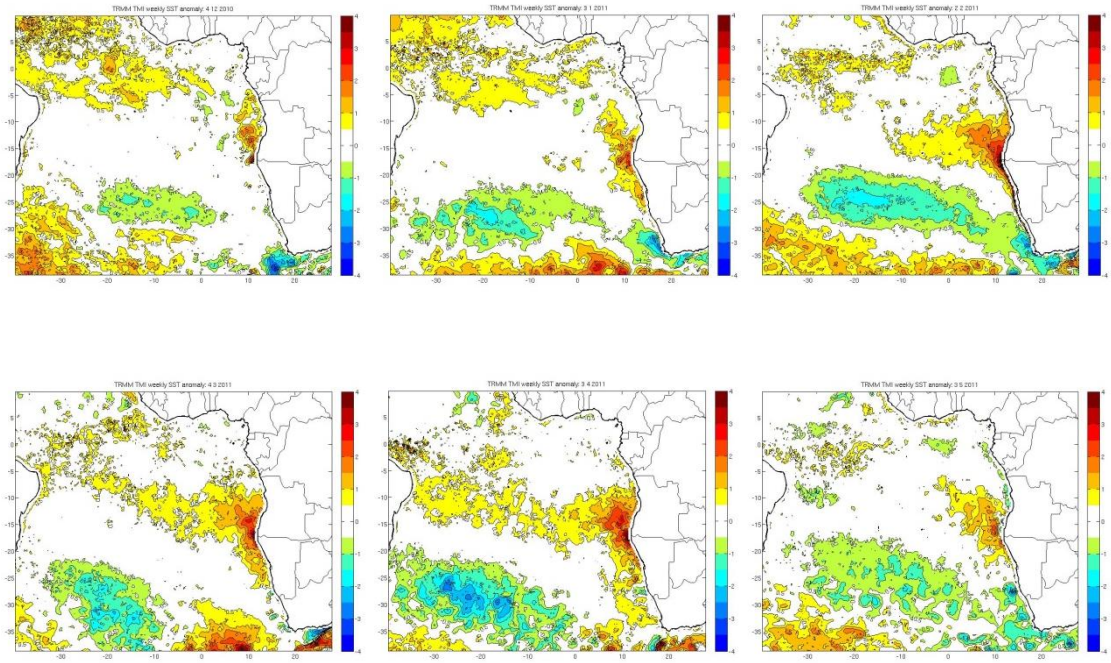

Figure 4.9: From top to bottom and left to right TRM TMI SST anomaly from monthly climatology from December 2010 to May 2011.

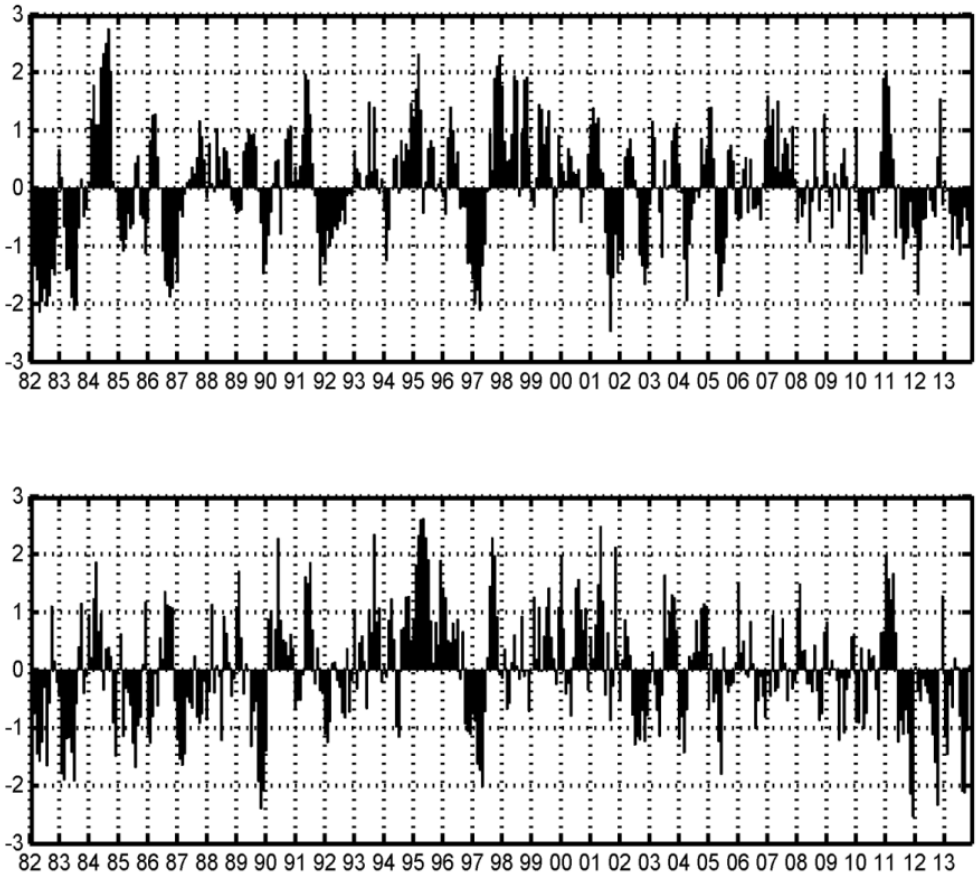

Figure 4.10: Time series of monthly detrended Reynolds SST anomalies f divided by standard deviation in Southern Angola averaged from 10 ^{o}S to 15S and from the coast to 1 degree offshore (top) and Northern Namibia averaged from 19 ^{o}S to 24 ^{o}S and from the coast to 1 degree offshore(bottom) from 1982 to 2013.

Additionally, basin wide cooling in the subtropics all the way to the South African coastline is observed in Austral summer 2010/2011. This is consistent with the effect of the Pacific Ocean La Niña event on the South Atlantic and the South West African coastline (Colberg et al, 2004, Blamey et al, 2015). During La Niña events, a poleward shift of the Santa Helena High pressure system displaces the easterly wind poleward and leads to an intensification of upwelling favourable South-Easterly wind in South Africa (and a weakening of upwelling favourable in Namibia (Blamey et al, 2015) concurrent to the appearance of below normal SST anomalies in South Africa south of 30°S. In Namibia, the shift in high pressure triggered lower than normal South-easterly upwelling favourable South-Easterly wind in 2010/2011 and above normal SST temperature in Namibia. This mechanism has been documented by Rouault et al (2010), Dufois and Rouault (2012) and Blamey et al (2015). Those basin wide shifts in the high pressure system and shifts in associated wind stress involving the Tropical and South Atlantic are at the origin of Benguela Niño and Atlantic Niño events as also document by Lübbecke et al. (2010, 2014) and can happen independently of Pacific La Niña conditions.The decrease in upwelling favourable winds off Namibia indicates that part of the warming in 2010/2011 might also have been locally driven, at least for the Northern Benguela. However,this warm event was the strongest austral summer warm event in Angola and Northern Namibia and also the longest since the 1995 Benguela Niño (**Fig. 4.10**). It was also the warmest event

at the Angola Benguela Front since 1982, with positive SST anomaly exceeding 3 standard deviations, as illustrated in **Fig. 4.10** which shows the magnitude of the Benguela Niño events in term of standard deviation and thus allows us to compare the 2010/2011 event with other warm event. **Fig. 4.10** presents the detrended monthly SST anomaly estimated from Reynolds data (Reynolds et al, 2002), averaged within 1° coastal band, and normalised from 1982 to 2013 in three coastal domains. At the top, data is averaged from 10°S to 15°S, which represents South Angola area. In the middle panel, data is averaged from 16°S to 17°S and represent the Angola Benguela Front zone, while at the bottom, data is averaged from 19°S to 24°S and represent the Northern Namibian upwelling. Data is first detrended because of a significant warming trend in the region (Blamey et al, 2015). For each month, an anomaly from monthly climatology is calculated by subtracting the monthly mean climatology and then by dividing the result with the standard deviation of that month. The 2010/2011 warm event is clearly on par with major warm events that occurred in austral summer since 1982, such as 1984 (January to June) 1994/1995 (November to July), 1997/1998 (October to January) or 2001 (February to April). A peculiarity of the 2010/2011 warm event is that it started quite early in the austral summer season.

4.3.3 Southward advection of warm tropical water

As for previous Benguela Niños, the warming was not restricted to the Angola Benguela Frontal zone where the coastal tropical thermocline outcrops but was observed as far south as 25°S (**Fig. 4.8** and **Fig. 4.9**). Rouault (2012) argued that such a southward expansion is related to anomalous poleward advection of warm water in the Benguela upwelling. Looking at monthly anomalies of meridional volume transport at the Angola Benguela Front at 17ºS from 0 to 250 m depth and 8.75^{o}E to the coast at 11.5^{o}E from the NCEP/GODAS ocean reanalysis product, we find that there is indeed an enhanced southward transport across the section in late 2010 (**Fig. 4.11**). This anomalous transport corresponds to a strengthening of the seasonal cycle of modelled transport (Rouault et al, 2012). There is also a secondary anomalous poleward advection of warm water in February that can explain the secondary maximum in SST and SSH mentioned above. The equatorial subsurface warming is also well represented by GODAS, showing a strong thermocline anomaly along the equator in October to November 2010 (**Fig. 4.12**). In May 2011, i.e. at the time of the demise of the warm event, an anomalous equatorward transport occurs in the GODAS data at the Angola Benguela Front. This suggests that the propagation of shallow thermocline anomalies - caused by stronger zonal winds along the equator - all the way to the Angola Benguela front is a way to interrupt a warm event in Angola and Northern Namibia.

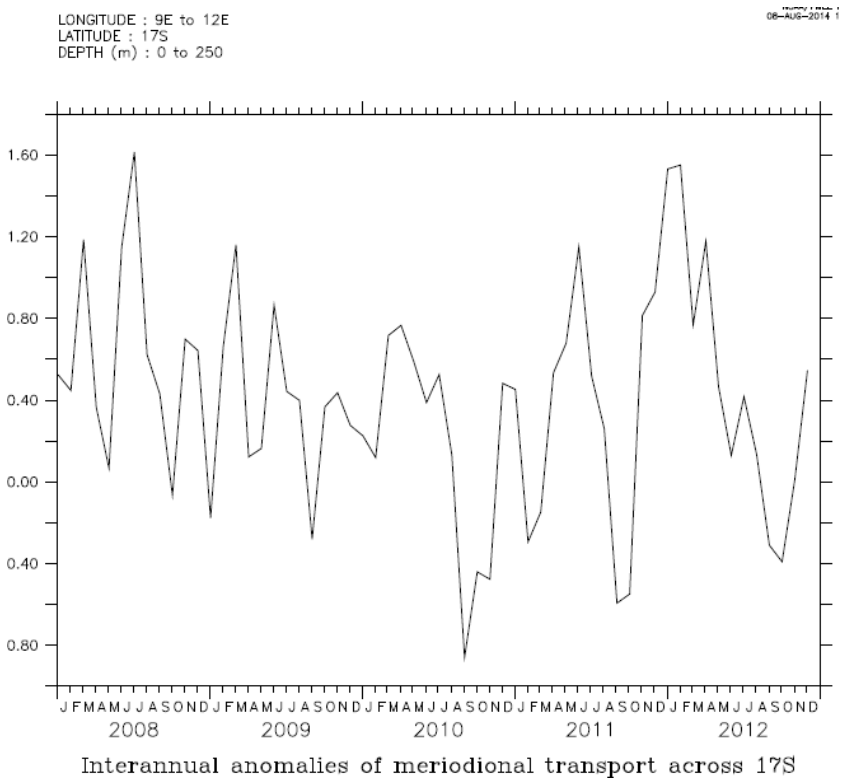

Figure 4.11: GODAS modelled transport monthly anomaly across the Angola Benguela Front at 17 ^{o}S anomalies from GODAS (positive values denote northward i.e. equatorward transport anomalies).

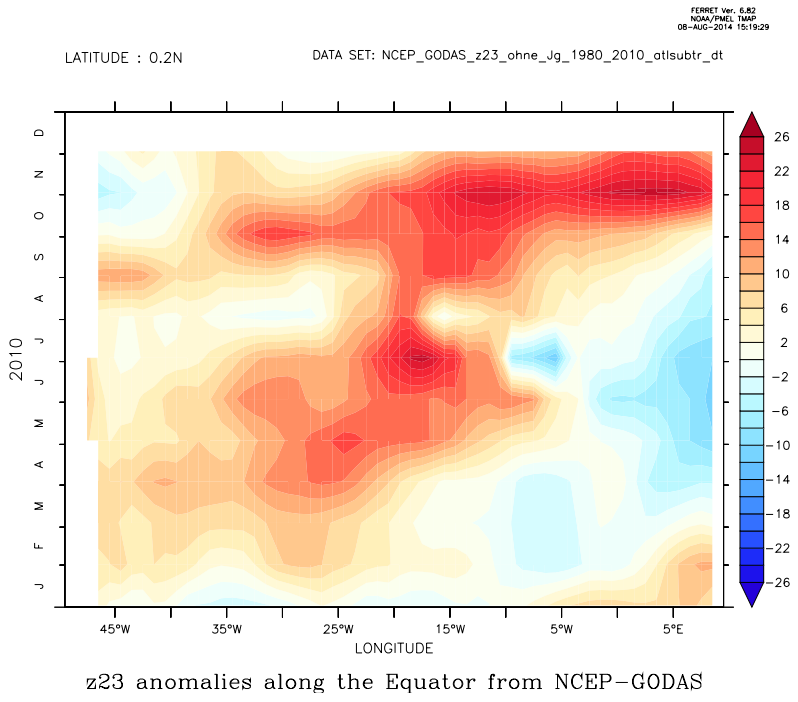

Figure 4.12: GODAS modeled 23 ^{o}C isotherm depth proxy for thermocline monthly anomalies in 2010.

4.4 References

- Bachèlery, M.-L., S. Illig, and I. Dadou (2015), Interannual variability in the South-East Atlantic Ocean, focusing on the Benguela Upwelling System: Remote versus local forcing, J. Geophys. Res. Oceans, 120, doi:10.1002/2015JC011168.
- Behringer, D., and Y. Xue (2004), Evaluation of the global ocean data assimilation system at NCEP: The Pacific Ocean. Preprints, Eighth Symp. on Integrated Observing and Assimilation Systems for Atmosphere, Oceans, and Land Surface, Seattle, WA, Amer. Meteor. Soc., 2.3. [Available online at https://ams.
- confex.com/ams/pdfpapers/70720.pdf.]
- Blamey, L. K., L. J. Shannon, J. J. Bolton, R. J. M. Crawford, F. Dufois, H. EversKing, C. L. Griffiths, L. Hutchings, A. Jarre, M. Rouault, K. Watermeyer, H. Winker (2015) Ecosystem change in the southern Benguela and the underlying processes. Journal of Marine Systems.
- Bourlès, Bernard, Rick Lumpkin, Michael J. McPhaden, Fabrice Hernandez, Paulo Nobre, Edmo Campos, Lisan Yu et al. "THE PIRATA PROGRAM." *Bulletin of the American Meteorological Society* 89, no. 8 (2008): 1111.
- Boyer, D. C. and I. Hampton (2001), An overview of the living marine resources of Namibia, South Afr. J. Mar. Sci., 23, 1, 5-35.
- Colberg, F., Reason, C. J. C., & Rodgers, K. (2004). South Atlantic response to El Niño–Southern Oscillation induced climate variability in an ocean general circulation model. *Journal of Geophysical Research: Oceans (1978–2012)*, *109*(C12).
- Dufois, F., Rouault, M., (2012) Sea surface temperature in False Bay (South Africa): Towards a better understanding of its seasonal and interannual variability. Continental Shelf Research, 43, 24–35, http://dx.doi.org/10.1016/j.csr.2012.04.009
- Florenchie, P., J. R. E. Lutjeharms, C. J. C. Reason, S. Masson, and M. Rouault (2003), The source of Benguela Niños in the South Atlantic Ocean, Geophys. Res. Lett., 30(10), 1505, doi: 10.1029/2003GL017172.
- Florenchie, P., C. J. C. Reason, J. R. E. Lutjeharms, and M. Rouault (2004), Evolution of interannual warm and cold events in the southeast Atlantic Ocean, J. Clim., 17, 2318–2334.
- Illig, S., Dewitte, B., Ayoub, N., du Penhoat, Y., Reverdin, G., De Mey,P., Bonjean, F., Lagerloef, G.S.E., 2004. Interannual longequatorial waves in the Tropical Atlantic from a high resolutionOGCM experiment in 1981–2000. J. Geophys. Res. 109 (C2),
- C02022. doi:10.1029/2003JC001771.
- Junker, T., Schmidt, M., &Mohrholz, V. (2015). The relation of wind stress curl and meridional transport in the Benguela upwelling system. *Journal of Marine Systems*, *143*, 1-6.
- Lübbecke, J. F., C. W. Böning, N. S. Keenlyside, and S.-P. Xie (2010), On the connection between Benguela and equatorial Atlantic Niños and the role of the South Atlantic Anticyclone, J. Geophy. Res., 115, C09015, doi:10.1029/2009JC005964.
- Lübbecke, J. F., N. J. Burls, C. J. C. Reason, and M. J. McPhaden (2014), Variability in the South Atlantic Anticyclone and the Atlantic Niño Mode. J. Climate, 27, (21), 8135-8150, doi: 10.1175/JCLI-D-14-00202.1
- Richter, I., S. Behera, Y. Masumoto, B. Taguchi, N. Komori, and T. Yamagata (2010), On the triggering of Benguela Niños - remote equatorial vs. local influences, Geophys. Res. Lett., 37, L20604, doi: 10.1029/2010GL0444461.
- Rouault, M., P. Florenchie, N. Fauchereau, and C. J. C. Reason (2003), South East tropical Atlantic warm events and southern African rainfall, Geophys. Res. Lett., 30, doi:10.1029/2003GL014840.
- Rouault, M., S. Illig, C. Bartholomae, C. J. C. Reason, and A. Bentamy (2007), Propagation and origin of warm anomalies in the Angola Benguela upwelling system in 2001, J. Mar. Syst., 68, 473–488.

- Rouault, M., B. Pohl and P. Penven, (2010) Coastal Oceanic climate change and variability from 1982 to 2009 around South Africa, African Journal of Marine Science 32(2): 237–246
- Rouault, M. (2012), Bi-annual intrusion of tropical water in the northern Benguela upwelling, Geophys. Res. Lett., 39, L12606, doi: 10.1029/2012GL052099.
- Shannon, L. V., A. J. Boyd, G. B. Brundrit, and J. Taunton-Clark (1986), On the existence of an El Niño–type phenomenon in the Benguela system, J. Mar. Sci., 44, 495–520.
- Uppala, S. M. et al., 2005: The ERA-40 re-analysis. Q. J. R. Meteorol. Soc. **131** 2961–3012.
- Veitch, J. A., P. Florenchie, and F. A. Shillington (2006), Seasonal and interannual fluctuations of the Angola-Benguela Frontal Zone (ABFZ) using 4.5 km resolution satellite imagery from 1982 to 1999, Int. J. Rem. Sens., 27, 5-6, 987-998, doi: 10.1080/01431160500127914.

5. Seasonal to interannual variability of water mass characteristics and currents on the Namibian shelf

Junker T, Mohrholz V, Siegfried L and v. d. Plas A. (2016) Seasonal to interannual variability of water mass characteristics and currents on the Namibian shelf. Submitted to J Marine Syst

5. 1. Introduction

Hydrographic long-term observations are one of the keys to assess the inter- annual to decadal variability of the world oceans and hence the earth's climate. They allow a robust estimation of the system's mean state and its anomalies as well as to discover possible trends in the climate. Eastern boundary regions such as the Benguela upwelling system are hereby of particular interest due to their important role in the oceans carbon and nutrient cycles and their impact on economic welfare. Within the South Atlantic the Benguela upwelling system is a well observed and investigated area. First observations of the sea surface temperature (SST) in the Benguela system were already made in the very beginning of the 20th century; see Taunton-Clark and Shannon (1988). A regularly monitoring of various environmental parameters including the subsurface started in the early 1950s off Namibia, Stander and De Decker (1969). From then on, standard depth resolved ship-born temperature measurements in the area off central Namibia have been continued during various campaigns and monitoring programs, Bartholomae and van der Plas (2007). Based on these measurements and remotely sensed data, the seasonal to interannual variations of temperature and salinity in the Benguela system has been described by several studies, e.g. Shannon (1985), Cole and Villacastin (2000), Hardman-Mountford et al. (2003), and references therein. A well-known feature contributing to seasonal changes of temperature and salinity is the periodical intrusion of tropical waters into the Benguela upwelling system, e.g. Boyd et al. (1987) and Lass and Mohrholz (2008). This water is present on the shelf in late austral summer and early fall and may reach as far south as 27° S, Gordon et al. (1995), Duncombe Rae (2005), and Fennel et al. (2012). The advection of this warm and oxygen poor water impacts the environmental conditions on the shelf heavily as it causes hypoxic-anoxic conditions and may support sulphur outbreaks, Copenhagen (1934), Monteiro et al. (2006), Mohrholz et al. (2008), and Ohde and Mohrholz (2011). The advection of tropical water and therefore the distribution of oxygen, temperature and salinity are subject to interannual variations as well, Walker (1987). The occurrence of warm events is intensively described in the literature, e.g. for 1963 (Stander and De Decker (1969)), 1984 (Shannon et al. (1986) and Taunton- Clark and Shannon (1988)), 1995 (Gammelsrød et al. (1998)), and 2001 (Rouault et al. (2007)). These events that are often referred to as Benguela Niños are the lowest frequency and largest-scale instance of variability in the Benguela region, Shillington et al. (2006). The mechanisms driving this variability are discussed extensively in the scientific community, e.g. Florenchie et al. (2003), Rouault et al. (2007), Richter et al. (2010). Although there is quite a huge amount of temperature and salinity data for the Benguela system available in the recent decades and many studies de- scribing the seasonal to interannual variability based on those data exist, the Benguela system lacks *robust* long-term observations. Remotely sensed data near the coast is influenced by clouds and land contamination and do not allow conclusions about the conditions in the water column. Sporadic ship-born measurements may be disturbed by non-linear internal waves affecting the

vertical structure of the water body on short time scales and thus biasing the results. However, long-term high resolution mooring data overcomes these drawbacks and therefore allows a much more robust estimation of seasonal changes, inter- annual variability and possible trends of the hydrographic conditions in general. Added to this is the fact that current observations were not part of the long lasting monitoring off central Namibia at all. Continuous current observations commenced south of about 27° S in the early 1980s, but coherent records cover time scales of only a few months, Nelson and Polito (1987), Holden (1987), and Nelson (1989). Long-term current meter records, however, together with robust salinity and temperature measurements presented in this study allow an observation of the advection across and along the Namibian shelf and its relation to the water mass characteristics on a seasonal time scale and beyond.

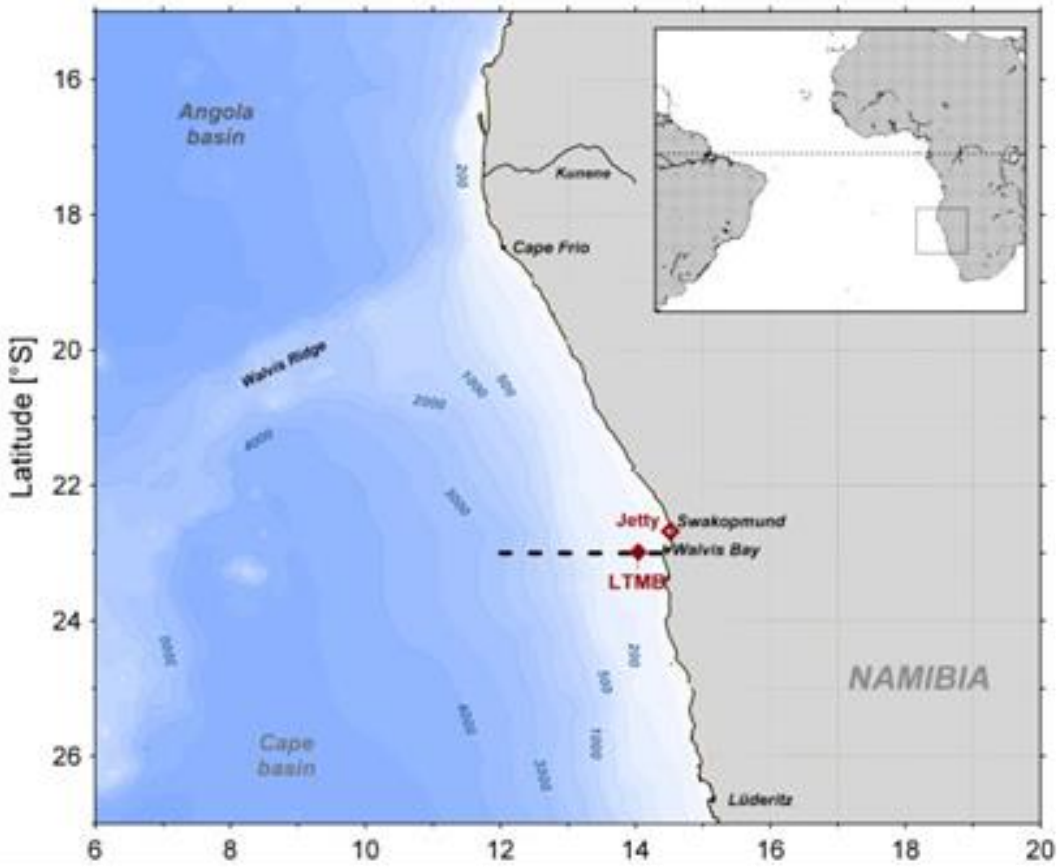

Figure 5.1: Map showing the location of the mooring (LTMB, red), the location of the coastal temperature sensor at the Swakopmund Jetty and the monitoring transect (black dashed line).

5.2. Data and methods

5.2.1. Mooring data

5.2.1.1. Mooring set up

Temperature, salinity, and currents were measured with an oceanographic mooring on the Namibian shelf at about 14°E and 23°S, see fig. 5.1. The mooring has been operating since December 2002 throughout 19 deployment periods. The data set we present comprises data until November 2015 and faces two major periods when the mooring was not deployed: from September 2006 to November 2007 and July 2008 to October 2009. Thus, the mooring was deployed 2907 days (about 95 months) stretching across 156 months. Figure 5.2 gives an overview of the deployment periods and the availability of data.

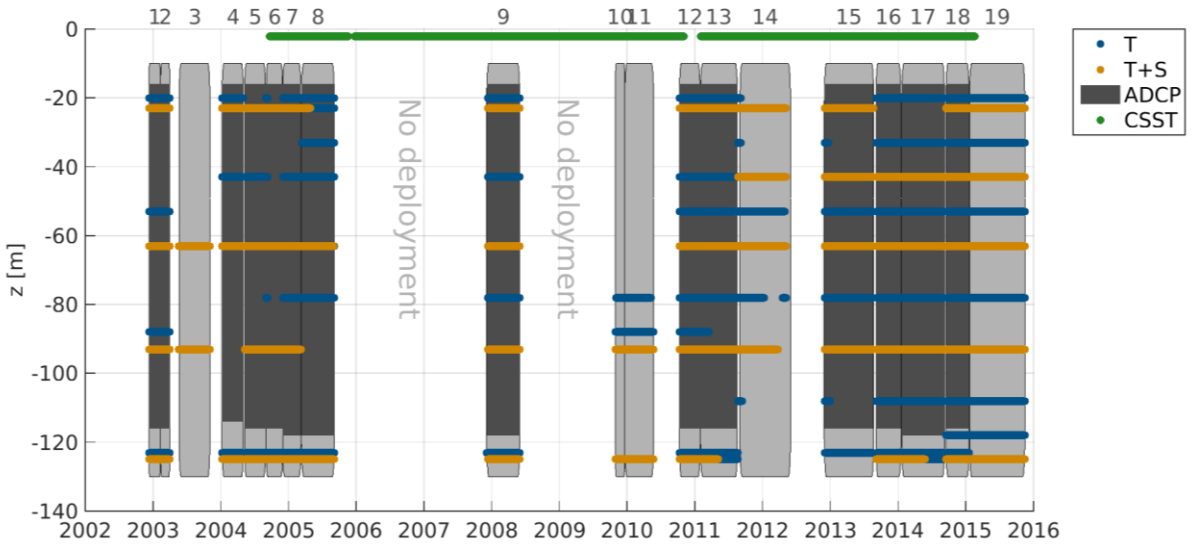

Figure 5.2: Timeline of the mooring deployment periods and the availability of temperature (T), salinity (S), and current meter (ADCP) data after validation. Data gained by the oxygen, pressure, and turbidity sensors is not indicated in this figure. Besides, the availability of coastal sea surface temperature (CSST) data from the Swakopmund Jetty is shown.

The number and depths of the mounted instruments vary slightly with the different deployment periods due to logistical constraints, technical reasons, and loss of instruments or scientific needs. The mooring has been equipped with up to five SBE 16 SeaCAT (or SBE 37 MicroCAT) sensors (located at a water depth of about 23 m, 43 m, 63 m, 93 m, 125 m) measuring conductivity and temperature, five RBR temperature loggers (33 m, 53 m, 105 m, 118 m, 125m), two RBR pressure and temperature loggers (20 m, 78 m), three PME miniDOT oxygen sensors (63 m, 93 m, 125 m), and one turbidity sensor (125 m). Moreover, an upward looking ADCP (RDI-Workhorse 300 kHz) is mounted at 120 m depth measuring the current profile between about 115 and 16 m water depth with a vertical resolution (bin size) of 4 m. Mayor changes in the design of the mooring throughout the different deployment periods were the mounting of an additional SeaCAT sensor at 43 m and a RBR temperature logger at about 30 m depth from period #14 onwards to better resolve the vertical structure near the thermocline. Instruments mounted below 120 m water depth including the ADCP were lost near the end of period 14 (09/2011-05/2012). During the recovery of the mooring at the end of period eleven (11/2009-05/2010) devices mounted

above 60 m water depth were lost. As a result, no temperature and salinity data can be presented for that period and depth range. The temporal resolution of the temperature and salinity data varies between two seconds and ten minutes depending on the device and deployment period. The accuracy of the instruments could be kept within a range of ±0.01 K for temperature and ±0.01 for salinity due to the use of anti-fouling tubes, Mohrholz et al. (2008). The ADCP has been measuring every hour, and the depth averaged error of the horizontal current velocities is typically about 1 cm s^{-1}.

5.2.1.2. Data validation

If possible, all instruments were calibrated in the laboratory before being deployed. After recovery, the data from each deployment period was truncated at the actual deployment and recovery time. Each sensors time series was then inspected for sensor drifts by comparing the data with the CTD measurements from the monthly monitoring program of the National Marine Information and Research Centre (NatMIRC) and suspicious data was discarded. Data from salinity sensors that showed a constant offset from the CTD data throughout their deployment period were corrected by linear regression. The ADCP data was compensated for magnetic declination after each recovery. Moreover, the heading bias of the compass was estimated by calculating the mean orientation of the M2 tidal ellipse (about 174°) throughout all deployments using the Matlab Toolbox T TIDE, Pawlowicz et al. (2002). This analysis delivered a mean heading bias of the ADCPs compass of about 5°. Unfortunately, we have to acknowledge that the ADCP data from the deployment periods ten, eleven (11/2009-05/2010), and nineteen (01/2015 - 11/2015) had to be discarded since a malfunctioning of the instruments compass is likely for these periods.

5.2.1.3. Water mass definition

The fraction of a sub-type of South Atlantic Central Water at the mooring site is calculated from the high resolution and validated temperature and salinity data. The definition of the water mass used in this study is based on CTD samples from the Angola Gyre and is referred to as Angolan Gyre Central Water (AGCW). It is defined by a straight line in the Θ-SP diagram between points with a potential temperature of 16°C and practical salinity 35.6366 and a potential temperature of 8° C and practical salinity 34.7201, see Mohrholz et al. (2008).

5.2.1.4. Data processing

In order to derive the alongshore and cross-shore current components, the coordinate system was rotated anti-clockwise by 17° according to the approximate orientation of the coastline and the bathymetry near the mooring position. Then, monthly values were calculated from the data whereby only those months were assumed to be significant that were covered by at least two-thirds. From the monthly data, climatology of temperature,

salinity, water mass fraction and cross-shore and alongshore velocity was derived. In the climatology, only those depth levels were included that is covered by at least three years for the particular month. Temperature data of eight depth levels (20 m, 23 m, 43 m, 63 m, 78 m, 93 m, 123 m, 125 m) and salinity data of four levels (23 m, 63 m, 93 m, 125 m) satisfy this requirement. The months December, January, February, and March are represented most of all in the current meter climatology (seven years each). For August and September, only three monthly values were available to enter the climatology.

5.2.2. Monthly monitoring data

In addition to the mooring measurements, we make use of temperature and salinity data sampled along a cross-shore transect at 23°S. The measurements are performed in the frame of a quasi-monthly monitoring program (Monthly Oceanographic Monitoring, MOM) run by the Namibian Ministry of Fisheries and Marine Resources, e.g. Monteiro et al. (2008). The data was sampled along nine stations with a Seabird 911plus or Seabird 19plus CTD-O with rosette between January 2003 and October 2013. A comprehensive analysis of the CTD data at the 10 n.m. station of this transect was presented by Bartholomae and van der Plas (2007). In this study, we use only data sampled at the mooring location (40 n.m. offshore).

5.2.3. Coastal sea surface temperature data

Since the mooring observations do not cover the surface, we additionally include coastal sea surface temperature (CSST) data sampled at the Jetty of Swakopmund (14.52° E, 22.63° S) in about 1.5 m water depth. The distance between the Jetty and the mooring is about 35 nautical miles and the CSST data is assumed to mimic the large scale variability of the sea surface temperature at the mooring position. The data was recorded with a StarMon mini temperature sensor using a temporal resolution between 5 and 10 minutes. The data set comprises temperature records from September 2004 to January 2015, see fig. 5.1. A monthly climatology is calculated from the data following the procedure described above.

5.2.4. Sea level data

Besides the in-situ data, Delayed Time Maps of Sea Level Anomalies (DT- MSLA) merged from all satellites were downloaded from AVISO. The daily data is on a 1/4° by 1/4° Cartesian grid. A monthly climatology based on the years 1993 to 2012 was calculated from the dataset.

5.3. Seasonal variability

5.3.1. Temperature and salinity

A monthly climatology including mean values of temperature and salinity as well as their standard deviation is presented in Fig. 5.3 and 5.4, respectively. For clarity, temperature data from only six (1.5 m , 20 m, 43 m, 63 m, 93 m, 125 m) of the possible nine depth levels is shown including CSST.

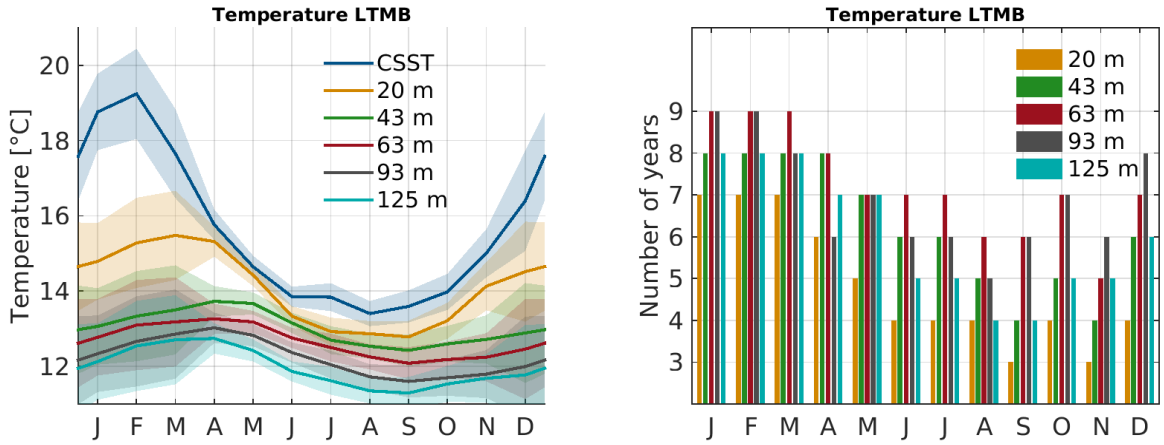

Figure 5.3: (a) Monthly climatology of the temperature including the mean values (lines) and the standard deviation (shadings) and (b) number of years included in the climatological data for each month. For clarity, only six (of the possible nine) depth levels of the temperature data are presented.

There is an apparent seasonal cycle in temperature in all depth layers. Maximum temperatures were reached in February to April (19.2°C, 15.5°C, 13.7°C, 13.3°C, 13° C, and 12.7°C) and minimum temperatures are observed in August to September (13.4°C, 12.8°C, 12.4°C, 12.1°C, 11.6°C, and 11.3°C) during the main upwelling season in the northern Benguela system. Obviously, there is downward phase propagation in the seasonal cycle of the temperature. The temperature at the surface peaks about one month prior to the temperature at 20 m water depth, which in turn leads the temperatures in the layers below by about the same time span. The temperature difference between the sea surface and the lowermost of the presented layers is largest in February (about 6.7 K) and smallest in June (2 K). This is associated with a mean vertical temperature gradient of 0.14 K m^{-1} across the thermocline (0 m to 43 m) and about 0.01 K m^{-1} below for February. In June, the vertical temperature gradient is quite constant (about 0.015 K m^{-1}) throughout the water column as no thermocline is pronounced. The climatological standard deviation of the temperature is highest in summer since the interannual variability is strongest in that season. However, to some extent, this finding may also result from the seasonal differences of the data availability, see fig. 5.3. In September, only three to six years (depending on the depth level) were included in the calculation of the climatology, whereas the most data was available for January, February, and March (seven to nine years).

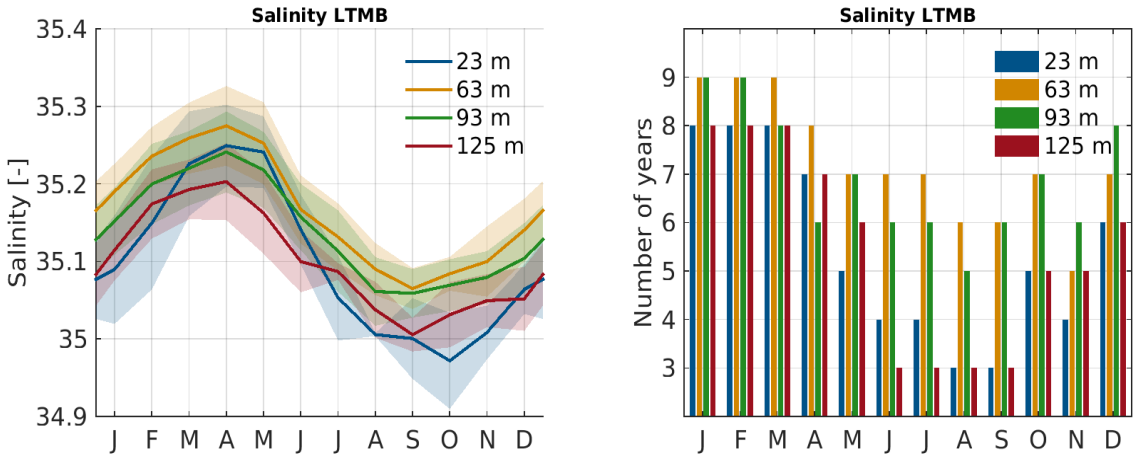

Figure 5.4: (a) Monthly climatology of the salinity including the mean values (lines) and the standard deviation (shadings) and (b) number of years included in the climatological data for each month.

The salinity in all four layers (23 m, 63 m, 93 m, 125 m) follows basically the seasonality of the temperature, see Fig. 5.4. The salinity is highest at all levels in April (35.25, 35.27, 35.24, and 35.2) and lowest during September to October (35, 35.07, 35.06, and 35.01) with a maximum near 60 m year round. The amplitude of the seasonal cycle is most pronounced in the top layer (23 m) where the salinity is lower than in 63 m depth in summer but exhibits about the same salinity as in the bottom layer in September. Moreover, the amplitude in the 63 m layer is higher than at 93 m depth. Consequently, the salinity is more or less equal in both levels in September and October but differs by about 0.03 in April. Thus, the vertical salinity gradient is most (less) pronounced in the lower (upper) half of the water column in late winter. In summer, the situation is vice versa. The climatological standard deviation of the salinity is slightly higher in summer than in winter at all depth levels.

5.3.2. Currents

A monthly climatology of the horizontal velocity components (cross-shore, alongshore) is presented in Figs. 5.5 and 5.6.

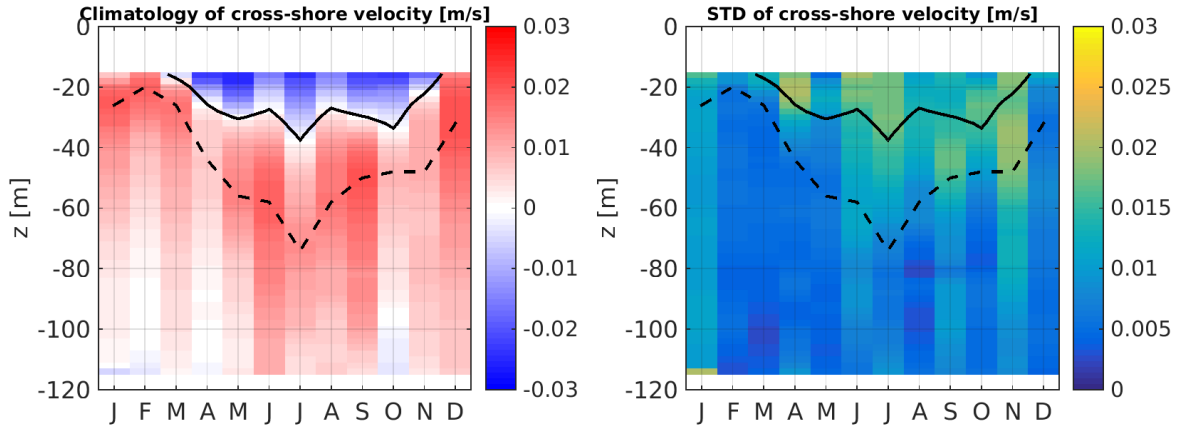

Figure 5.5: (a) Monthly climatological mean and (b) standard deviation of the cross-shore velocity [m s^{-1}]. The solid line shows the depth of the Ekman layer. The dashed line depicts the depth where the Ekman compensation flow is at its maximum.

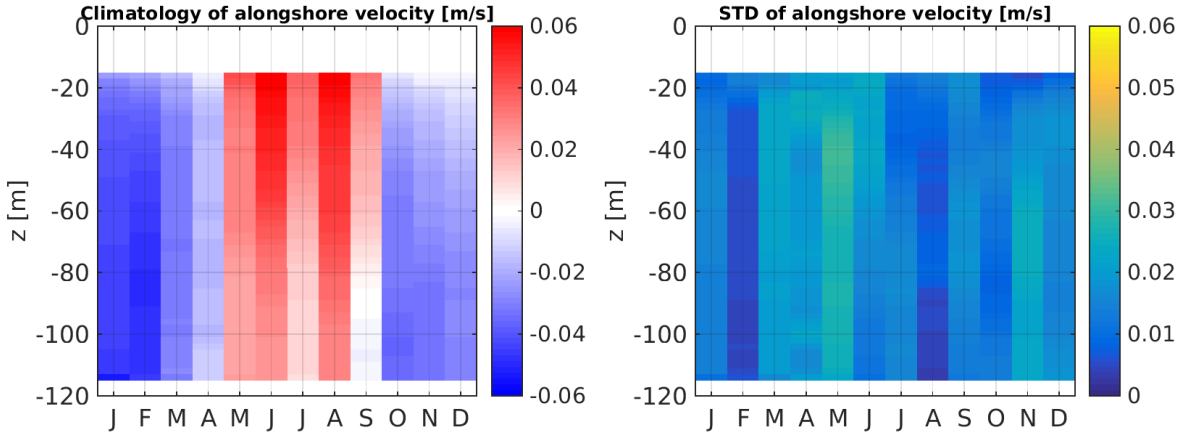

Figure 5.6: (a) Monthly climatological mean and (b) standard deviation of the alongshore velocity [m s^{-1}].

The mean cross-shore velocity corresponds with the basic pattern well known from eastern boundary upwelling systems, e.g. Lentz (2001). In the top layer, the currents are directed offshore (Ekman transport). Below the Ekman depth, the onshore compensation flow is observed. Both, the Ekman depth and the depth of the maximum Ekman rectification flow vary seasonally. The maximum of the onshore flow is shallowest in February (about 20 m) and deepest in July (about 70 m) when also the Ekman depth reaches its maximum (40 m). For the months of January, February, and December, the mean Ekman depth is shallower than 16 m which is the depth of the upper most bins detected by the ADCP. The standard deviation is highest around the Ekman depth from April to November indicating strong interannual variations in the Ekman layer. In terms of direction, the alongshore velocity is divided into two seasons, see Fig. 5.6. From May to September, the alongshore currents are directed northwards in the entire water column covered by the mooring (except for depths greater than 90 m in September). In the summer period (October to April), the alongshore currents are negative, and hence directed southward throughout the sampled water column. The

alongshore flow exhibits a local minimum in July, when the mean currents are weaker than in June and August (when the northward flow is strongest) but still directed equator ward. In February, the poleward flow is most intense throughout the water column. The alongshore velocity seems to be highly dominated by the barotropic mode since the vertical variability in the water column is very low. The standard deviation is lowest in February although for that month most data was available for the climatology. This leads to the conclusion, that the interannual variability in the alongshore flow is very low in general in February. In May, shortly after the alongshore velocity direction switches, the standard deviation is highest. This might be explained by interannual variations in the timing of the flow reversal from poleward to equatorward. However, in September and October, when the flow reverses again from equatorward to poleward, the standard deviation is not that exposed. The vertically integrated alongshore velocity is presented in Fig. 5.7.

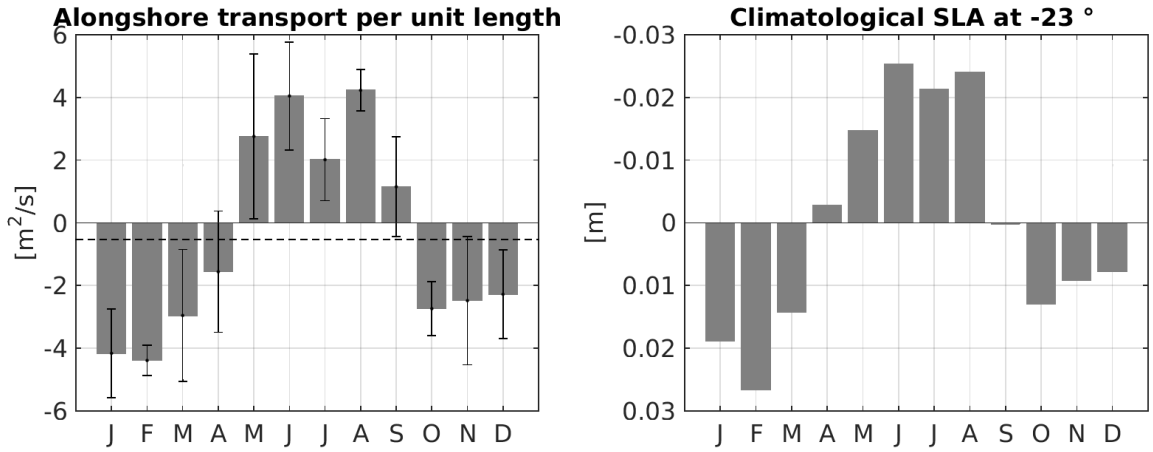

Figure 5.7: (a) Alongshore transport per unit length [$m^2\ s^{-1}$] and (b) anomaly of the sea level [m] derived from AVISO. The dashed black line in (a) depicts the overall mean of the alongshore transport. Note that the axis of ordinate is reversed in figure (b) for comparability.

Together with the AVISO climatological sea surface height (SSH) anomaly at 23° S at the nearest point to the coast. A harmonic analysis of the alongshore trans- port signal reveals that the seasonal cycle is most dominant explaining about 84 % of the variance (not shown). The semi-annual cycle and a cycle with a period of about 120 days are explaining 3 to 4 % of the variance. The alongshore transport is most negative (southward) during February and a second minimum is observed in October. In June and August, the equatorward transport is at its maximum. The SSH anomaly reflects well the annual and semi-annual cycle of the alongshore transport. A negative (positive) sea level anomaly corresponds to equatorward (poleward) transport. Differences between both data sets are seen most clearly in the months around the time when the direction of the flow reverses (April and September). The overall (annually averaged) transport is directed southward and amounts to $-0.5\ m^2\ s^{-1}$. Of course, this estimate might be slightly biased since the upper 16 m of the water column are not included. Nevertheless, data from a regional ocean general

circulation model of the South- East Atlantic corroborates the finding of an overall southward transport at 23°S see Muller et al. (2014).

5.3.3 Water masses

The climatological mean of the AGCW mass fraction is presented in Fig. 5.8 for two depth levels. Besides, we compare this data to the temporally integrated alongshore velocity in the same figure. The fraction of water masses from the Angolan Gyre is generally higher in 93 m than in 63 m (except for April). Around April, tropical waters account for 64 % (93 m) to 67 % (64 m) of the water mass content on the shelf, and from August to September the portion of these waters is about 16 % (63 m) and 43% (93 m). Thus, the AGCW fraction is comparable in both layers in summer, whereas a strong difference in the water column is evident in winter. The difference between both layers hereby originates from the vertical structure of the alongshore velocity of which the seasonal amplitude is more pronounced in 63 m depth than in 93 m. In both layers, the seasonality of water mass fraction agrees well with the temporally integrated alongshore velocity. When the cumulated alongshore velocity reaches its minimum (maximum), i.e. at the end of the southward (northward) flow phase in April (September), the AGCW content exhibits a maximum (minimum).

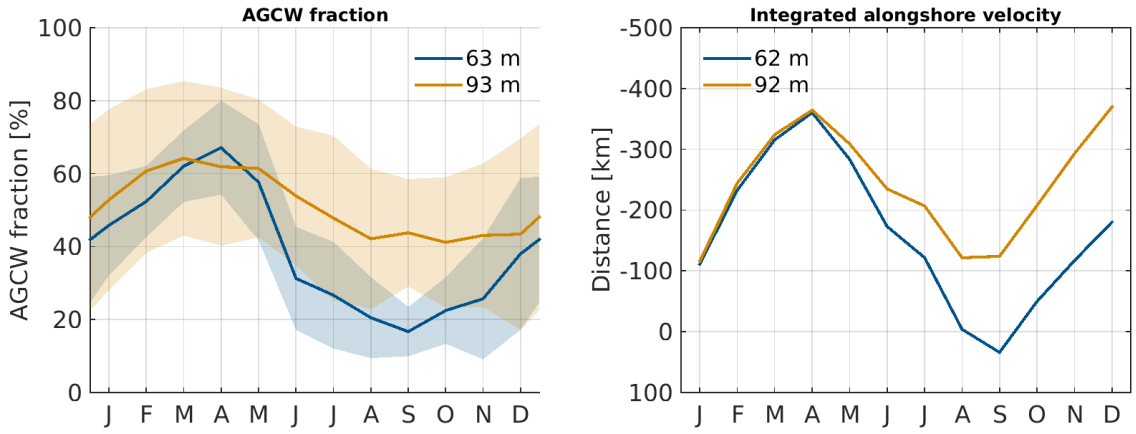

Figure 5.8: (a) Monthly climatological mean of the AGCW fraction in 63 m and 93 m depth and (b) temporally integrated alongshore velocity in the same layers. Note that the axis of ordinate is reversed in figure (b) for comparability.

5.4. Interannual variability

5.4.1. Temperature

Since the mooring data shows some data gaps for various reasons we constructed a monthly temperature time series combining the mooring measurements and the CTD observations in order to discuss the interannual variability of the temperature at the mooring position. Hereby, the CTD data was interpolated linearly on the regular grid of the monthly mooring data. Having combined both data sets, we subtracted the climatological values presented in section 3 from the data. The resulting monthly residuals at selected depth levels are presented in Fig. 5.9.

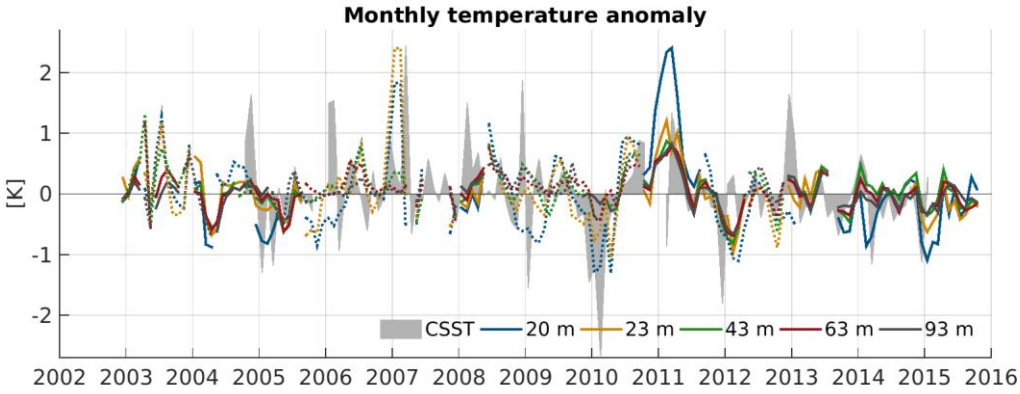

Figure 5.9: Time evolution of the monthly temperature residuals from selected depth levels between 2002 and 2015. Lines depict data sampled with the mooring. Dotted data originates from the ship-born monthly monitoring. On top, the monthly coastal SST anomaly is presented.

Together with the monthly CSST anomaly (based on the period 10/2004 to 01/2015). Based on the data derived at the mooring position, there is evidence for three anomalous temperature events lasting for at least two months during the observed period: Two warm events in the years 2007 and 2011, and one cold event in 2012. In January and February 2007, the monthly mean temperature was about 1.8 to 2.4 K warmer than on average in the top layers (20 m, 23 m) while below no pronounced anomaly was observed. The CSST anomaly is comparable but peaks in March 2007 and thus one month later. During late summer 2010, the observed water temperature is much colder than usual. Peak values of the monthly anomalies reach 1.3 K in 20 m depth, while the CSST residuals are about twice as large for February 2010. In March 2011, the temperature is about 2.4 K warmer than on average in 20 m depth and thus compares to the values reached during the 2007 event. However, contrary to 2007, the temperature in the lower half of the water column shows also a strong anomaly of about 0.8 K. Moreover, this event lasted much longer as the temperature anomaly in 20 m depth exceeded 1 K for five consecutive months. The CSST anomaly peaks as well in March (1.3 K), but there is no data available for the months November 2010 to January 2011. Although the presented time series is rather short to estimate a robust long- term temperature trend, it is of interest that the mooring data, as well as the CSST exhibit a cooling trend. The temperature decreases by about 0.12 K in 13 years (0.09 K dec^{-1}) in the water column (43 m) while at the surface near the coast the trend is rather strong (0.38 K dec^{-1}) (not shown). A possible cause for this temperature trend (that is stronger near shore) may be the intensification of upwelling as proposed by Bakun (1990).

5.4.2. Currents

Since the interannual temperature variability is highest during the summer months and these months are covered most often in the ADCP data (seven years) we chose the season January to March (JFM) to evaluate the interannual variability of the currents profiles. The averaged profiles are presented in Fig. 5.10. For seven years. Unfortunately, we

must acknowledge that there is no velocity data available for the year 2007 and 2012.

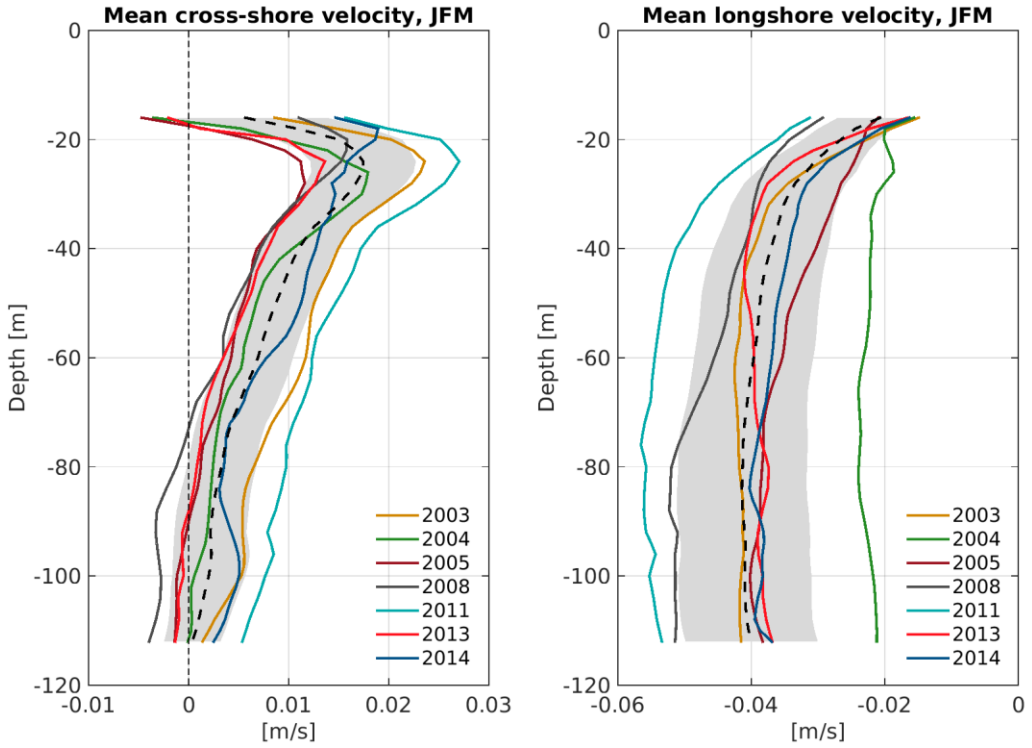

Figure 5.10: Interannual variability of the (a) cross-shore and (b) alongshore current profiles averaged from January to March (JFM) for seven different years. The black dashed line depicts the mean profile and the grey shading marks the standard deviation across all years.

The observations show that the general shape of the cross-shore velocity profiles is very constant. The minor differences between the years are mostly of barotropic nature and the standard deviation amounts to about 0.3 cm s^{-1} for this velocity component. The depth where the Ekman rectification flow becomes maximal is about 22 m in all years. The actual Ekman depth is always shallower than 20 m. In four (2003, 2008, 2011, 2014) of the seven years, the Ekman depth is even shallower than 16 m and therefore not captured by the measurements. The alongshore velocity is directed southward in the whole water column covered by the ADCP throughout all of the years. However, the data reveals large interannual variations regarding the strength of the poleward flow and the general shape of the profiles. The velocity is most negative during summer 2011 and less poleward during 2004. The difference between these extremes is in the order of 3 cm s^{-1} in the lower water column. The standard deviation regarding all the different years amounts up to 1 cm s^{-1} depending on the depth. The variability of the alongshore currents is hereby highest at about 100 m water depth and decreases when approaching the surface.

5.5. Summary and Discussion

In this study, data gained from a long-term mooring (2002 - 2015) on the Namibian shelf is presented. Monthly climatologist of temperature, salinity, water mass fraction, and currents are calculated. Consequently, the seasonal to interannual variability of these parameters is investigated. Temperature, salinity, and the water mass fraction show an apparent seasonal cycle that is associated with the meridional advection. We showed that the annual maxima (around April) and minima (around October) of these variables match the timing of the meridional flow reversals. This is in accordance with Shannon et al. (1986) who stated that the warming in late summer in the whole water column is linked to the intrusion of tropical waters. The differences in the seasonal amplitudes of temperature, salinity, and water mass fraction in different depth levels is hereby explained by the vertical structure of the along- shore velocity component. It is more barotropic in austral summer whereas the vertical velocity shear is more pronounced in austral winter. The nature of the seasonal flow reversal, however, is elusive. We showed that the direction and strength of the alongshore transport is well related to the sea surface height on a seasonal scale suggesting a geostrophic ally adjusted system in the vicinity of the coast. A Kelvin wave propagation apparent in the sea level along the South-West African coast (Schouten et al. (2005), Polo et al. (2008), Lass and Mohrholz (2008)) matches the timing of the seasonal flow reversals at the mooring site well. Although the coastal propagation is not as pronounced in austral spring than in austral fall (Lübbecke et al. (2010)), it seems likely that the flow reversals (and therefore the meridional advection in general) is controlled to a great extent by remote effects. The fact that the interannual variability of the alongshore velocity is much higher than the cross-shore flow (driven by local forcing only, e.g. Fennel (1999)) points in the same direction. However, there are also indications that the seasonal variability of the meridional transport may be forced locally as it corresponds well to the annual and semi-annual cycle of the wind stress curl, Junker et al. (2015). This study evinces that the alongshore advection seems to play a crucial role in the development of extreme temperature events in the Benguela system, such as in austral fall 2004 (cold) and 2011 (warm). These events were associated with the weakest (2004) and strongest (2011) poleward transport recorded by the current meter in the JFM season. AVISO data confirms that the sea level is elevated higher than usual along the south-west African coast in austral summer and fall 2011 (not shown). Based on these facts one would expect an increased proportion of waters of tropical origin on the Namibian shelf during that period. However, only about 71 % of waters in 63 m and 93 m depths stem from the Angolan Gyre in March 2011 (not shown). This fraction is only slightly above the mean value for that month. Therefore, other effects than the advection of warm waters such as a strong change in the vertical temperature gradients (as indicated in figure 5.9) are likely to contribute to the evolution of the 2011 warm event that was the strongest temperature anomaly observed by the mooring. The temperature in the surface layer (20 m) exceeded the monthly mean values by more than 1 K for about five months (December 2010 to April 2011) and the monthly peak temperature was 2.4 K in the surface layer (20 m) and about 0.8 K in the lower half of the water column in March. These warm temperature anomalies were reported recently by Louw et al. (2016) based on ship-born monitoring data. Lahajnar (2011) reported the presence of water masses from the Angola-Dome in the very northern Benguela system (off Kunene) accompanied by a shift of the

biological inventory during February 2011. The mooring data verifies that such warm or cold events are not a surface phenomenon but can be detected in the whole water column as already stressed by Shannon et al. (1986). Although the temporal evolution of the CSST is concurrent with the temperature in the water column in general, there are some periods when the CSST anomaly deviates drastically from the values in the top layer (20m) (e.g. November 2004, January to February 2006, and December 2012). Such deviations result probably from anomalous sea surface fluxes near the coast (due to cloud cover, etc.) that does not affect the water column below the mixed layer. Thus, if temperature anomalies are also seen in the deeper layers of the water column an adjective cause seems likely. Whereas we observe a slight cooling trend in the water column and at the surface, several studies based on remotely sensed SST products reported a warming trend in the northern Benguela based on different periods, e.g. 0.3 K dec^{-1} (Hutchings et al. (2009)), 0.35 K dec^{-1} (Monteiro et al. (2008)), or 0.62 K dec^{-1} Hardman-Mountford et al. (2003)). In contrast, Demarcq (2009) found a slight cooling of the northern Benguela upwelling system of about -0.12 K dec^{-1} to -0.20 K dec^{-1}. Likewise, results from Santos et al. (2012) suggest that there is a positive SST trend (0.06 K $dec^{-1)}$ at open sea locations but a negative one (-0.13 K $dec^{-1)}$ near shore. The authors attributed this finding to the general strengthening of upwelling. Although most of the data presented in this study is limited to the mooring position there are indications that most of the conclusions drawn here are representative for the entire inner shelf area of the northern Benguela upwelling system. Model results, for instance, integrated over the shelf reproduce the observed annual cycle of the meridional advection including the flow reversal around April and October, e.g. Junker et al. (2015). Nevertheless, we have to acknowledge that the winter months (JAS) are relatively underrepresented in the mooring data compared to the summer months. But since the standard deviation of the temperature is lowest in austral winter in the Benguela system in general (Shannon et al. (1986)) this should be only a minor shortcoming of the study. The mooring dataset may be used for the validation of ocean general circulation models that still have deficiencies in modeling adequately the eastern boundary region of the South Atlantic. As the mooring is still operating it may be possible to extend the already thirteen year long time series in the future. Such an extension will consolidate estimates of interannual variations and possible trends of the Benguela system.

5.6 References

- Bakun A. Global climate change and intensification of coastal ocean upwelling. Science, 1990; 247(4939):198–201.
- Bartholomae CH, van der Plas AK. Towards the development of environmental indices for the Namibian shelf, with particular reference to fisheries management. African Journal of Marine Science 2007; 29(1):25–35
- Boyd AJ, Salat J, Maso´M. The seasonal intrusion of relatively saline water on the shelf off northern and central Namibia. South African Journal of Marine Science 1987; 5(1):107–
- Cole J, Villacastin C. Sea surface temperature variability in the northern Benguela upwelling system, and implications for fisheries research. International Journal of Remote Sensing 2000 ;(January).

- Copenhagen WJ. Occurrence of sulphides in certain areas of the sea bottom on the South African coast. Fisheries and Marine Biological Survey Division Investigational Report 1934; 3:1–18.
- Demarcq H. Trends in primary production, sea surface temperature and wind in upwelling systems (1998? 2007). Progress in Oceanography 2009; 83(1-4):376–85
- Duncombe Rae CM. A demonstration of the hydrographic partition of the Benguela upwelling ecosystem at 2640 S. 2005
- Fennel W. Theory of the Benguela Upwelling System. Journal of Physical Oceanography 1999; 29(2):177–90
- Fennel W, Junker T, Schmidt M, Mohrholz V. Response of the Benguela upwelling systems to spatial variations in the wind stress. Continental Shelf Research 2012; 45:65–77. .
- Florenchie P, Lutjeharms JRE, Reason CJC, Masson S, Rouault M. The source of Benguela Niños in the South Atlantic Ocean. Geophysical Research Letters
- 2003; 30(10):1505–7.
- Gammelsrød T, Bartholomae CH, Boyer DC, Filipe VLL, O'Toole MJ. Intrusion of warm surface water along the Angolan-Namibian coast in February-March 1995: The 1995 Benguela Nino. South African Journal of Marine Science 1998; 19(1):41–56

- Gordon A, Bosley K, Aikman F. Tropical Atlantic water within the Benguela upwelling system at 27 S. Deep Sea Research Part I 1995; 42(1):1–12.
- Hardman-Mountford NJ, Richardson AJ, Agenbag JJ, Hagen E, Nykjaer L, Shillington FA, Villacastin C. Ocean climate of the South East Atlantic observed from satellite data and wind models. Progress in Oceanography 2003; 59(2-3):181–221.
- Holden CJ. Observations of low-frequency currents and continental shelf waves along the west coast of South Africa. South African Journal of Marine Science
- 1987; 5(February):197–208. Doi: 10.2989/025776187784522360.
- Hutchings L, van der Lingen C, Shannon L, Crawford R, Verheye H, Bartholomae C, van der Plas A, Louw D, Kreiner A, Ostrowski M, Fidel Q, Barlow R, Lamont T, Coetzee J, Shillington F, Veitch J, Currie J, Monteiro P. The Benguela Current: An ecosystem of four components. Progress in Oceanography 2009;83(1–4):15–32. doi:10.1016/j.pocean.2009.07.046.
- Junker T, Schmidt M, Mohrholz V. The relation of wind stress curl and meridional transport in the Benguela upwelling system. Journal of Marine Systems 2015; 143:1–6. doi:10.1016/j.jmarsys.2014.10.006.
- Lahajnar N. Cruise Report MSM 17-3. Technical Report; University of Hamburg; 2011.
- Lass HU, Mohrholz V. On the interaction between the subtropical gyre and the Subtropical Cell on the shelf of the SE Atlantic. Journal of Marine Systems 2008; 74(1-2):1–43doi:10.1016/j.jmarsys.2007.09.008.
- Louw DC, van der Plas AK, Mohrholz V, Wasmund N, Junker T, Eggert A. Seasonal and interannual phytoplankton dynamics and forcing mechanisms in the Northern Benguela upwelling system. Journal of Marine Systems 2016; 157:124–34. URL:
- Lübbecke JF, Boning CW, Keenlyside NS, Xie SP. On the connection between Benguela and equatorial Atlantic Niños and the role of the South Atlantic Anticyclone. Journal of Geophysical Research 2010; 115(C9):C09015.

- Mohrholz V, Bartholomae CH, van der Plas AK, Lass HU. The seasonal variability of the northern Benguela undercurrent and its relation to the oxygen budget on the shelf. Continental Shelf Research 2008; 28(3):424–41. URL:
- Monteiro PMS, van der Plas AK, Melice JL, Florenchie P. Interannual hypoxia variability in a coastal upwelling system: Ocean shelf exchange, climate and ecosystem-state implications. Deep Sea Research Part I: Oceanographic Research Papers 2008; 55(4):435–50. URL:
- Monteiro PMS, van der Plas AK, Mohrholz V, Mabille E, Pascall A, Joubert W. Variability of natural hypoxia and methane in a coastal upwelling system: Oceanic physics or shelf biology? Geophysical Research Letters
- 2006; 33(16):L16614.
- Muller AA, Reason CJC, Schmidt M, Mohrholz V, Eggert A. Computing transport budgets along the shelf and across the shelf edge in the northern Benguela during summer (DJF) and winter (JJA). Journal of Marine Systems 2014; 140:5-20
- Nelson G. Poleward Motion in the Benguela Area; Springer-Verlag. p. 110–30.
- Nelson G, Polito a. Information on currents in the Cape Peninsula area, South Africa. South African Journal of Marine Science 1987; 5(1):287–304.
- Ohde T, Mohrholz V. Interannual variability of sulphur plumes off the Namibian coast. International Journal of Remote Sensing 2011; 32(24):9327–42.
- Pawlowicz R, Beardsley B, Lentz S. Classical tidal harmonic analysis including error estimates in MATLAB using T TIDE. Computers & Geosciences 2002; 28(8):929–37.
- Polo I, Lāzar A, Rodriguez-Fonseca B, Arnault S. Oceanic Kelvin waves and tropical Atlantic intraseasonal variability: 1. Kelvin wave characterization. Journal of Geophysical Research 2008;113(C7):C07009.
- Richter I, Behera SK, Masumoto Y, Taguchi B, Komori N, Yamagata T. On the triggering of Benguela Niños: Remote equatorial versus local influences. Geophysical Research Letters 2010;37:L20604. doi:doi:10.1029/2010GL044461.
- Rouault M, Illig S, Bartholomae C, Reason C, Bentamy A. Propagation and origin of warm anomalies in the Angola Benguela upwelling sys- tem in 2001. Journal of Marine Systems 2007; 68(3-4):473–88.
- Santos F, Gomez-Gesteira M, DeCastro M, Alvarez I. Differences in coastal and oceanic SST trends due to the strengthening of coastal upwelling along the Benguela current system. Continental Shelf Research 2012; 34:79–86
- Schouten MW, Matano RP, Strub TP. A description of the seasonal cycle of the equatorial Atlantic from altimeter data. Deep Sea Research Part I: Oceanographic Research Papers 2005; 52(3):477–93
- Shannon LV. The Benguela ecosystem, Part I. Evolution of the Benguela, physical features and processes. Oceanography and marine biology, An annual review 1985; 23:105–82.
- Shannon LV, Boyd AJ, Brundrit GB, Taunton-Clark J. On the existence of an El Nino-type phenomenon in the Benguela System. Journal of Marine Research 1986; 44(3):495–520.
- Shillington FA, Reason CJC, Rae CMD, Florenchie P, Penven P. Large Scale Physical Variability of the Benguela Current Large Marine Ecosystem (BCLME). In: Large Marine Ecosystems. Elsevier; volume 14 of *Large Marine Ecosystems Series;* 2006. p. 47–68.
- Stander GH, De Decker AHB. Some physical and biological aspects of an oceanographic anomaly off South West Africa in 1963. 1969.

- Taunton-Clark J, Shannon LV. Annual and interannual variability in the South-East Atlantic during the 20th century. South African Journal of Marine Science 1988; 6(1):97–106.
- Walker ND. Interannual sea surface temperature variability and associated atmospheric forcing within the Benguela system. South African Journal of Marine Science 1987; 5(1):121–32.

6. Ecosystem change in the southern Benguela and the underlying processes

Adapted from Blamey, L. K., L. J. Shannon, J. J. Bolton, R. J. M. Crawford, F. Dufois, H. EversKing, C. L. Griffiths, L. Hutchings, A. Jarre, M. Rouault, K. Watermeyer, H. Winker (2015): Ecosystem change in the southern Benguela and the underlying processes. J Marine Syst. 144: 9-29.

6.1 Introduction

Over-exploitation of marine species, coupled with human-induced climate change, is putting severe pressure on marine ecosystems on a global scale. Even the most remote parts of the ocean are reported to have experienced some form of human impact, with fishing and anthropogenic climate change undoubtedly the major culprits. The ecosystem effects of overfishing have been well documented and there is compelling evidence for the impacts of climate change on marine systems. In the marine environment, most climate-related research focuses on temperature change and its impacts on species distribution, abundance patterns and community structure. In general, oceans across the globe are thought to be warming at a slow to rapid rate, particularly over the last 30 years (Belkin 2009). However, some major upwelling systems appear to show either opposite trends, or mixed signals (McGregor et al. 2007, Belkin 2009, Leduc et al. 2010, Gutiérrez et al. 2011). The Benguela ecosystem, located off the west coast of southern Africa, is one of four major eastern boundary upwelling systems and is divided into northern and southern sections (Shannon 1985). The northern Benguela ecosystem, situated off Angola/Namibia, is decidedly different, in terms of both physico-chemical characteristics and biota, to the southern Benguela, off the west and south coasts of South Africa. Only the latter is considered in this review. The cold, upwelled waters of the southern Benguela fuel most of South Africa's major commercial fisheries, including large-scale offshore pelagic and demersal fisheries, as well as the commercially valuable inshore linefish, rock lobster and abalone fisheries. Most of these fisheries have a long history, described, e.g., by Griffiths et al. (2004), and this, coupled with spatio-temporal changes in key species over the last three decades has severely impacted some of South Africa's fisheries and ecosystems (Cockcroft et al. 2008, Coetzee et al. 2008a, Plagányi and Butterworth 2010, Jarre et al. 2013, Blamey et al. 2014). Changes in marine ecosystems can be driven by natural and/or anthropogenic processes (deYoung et al. 2008) with key drivers including biotic processes, changes in structural habitat, climate change and fishing. In this section we provide a summary of spatial and temporal changes that have taken place in the southern Benguela ecosystem since the mid 20th century and we investigate potential climate drivers of these changes before discussing directions for future interdisciplinary research.

6.2. Spatio-temporal changes in the southern Benguela

A number of spatial and temporal changes have taken place in South Africa's marine ecosystems, particularly in the last 30-40 y. In this section we focus on changes that have taken place in some of the major species and/or ecosystems within the southern Benguela. For a comprehensive review of changes in all South Africa's coastal habitats see Mead et al. (2013) and for that in the offshore and Benguela system as a whole, see Griffiths et al. (2004), Hutchings et al. (2009, 2012), Moloney et al. (2013).

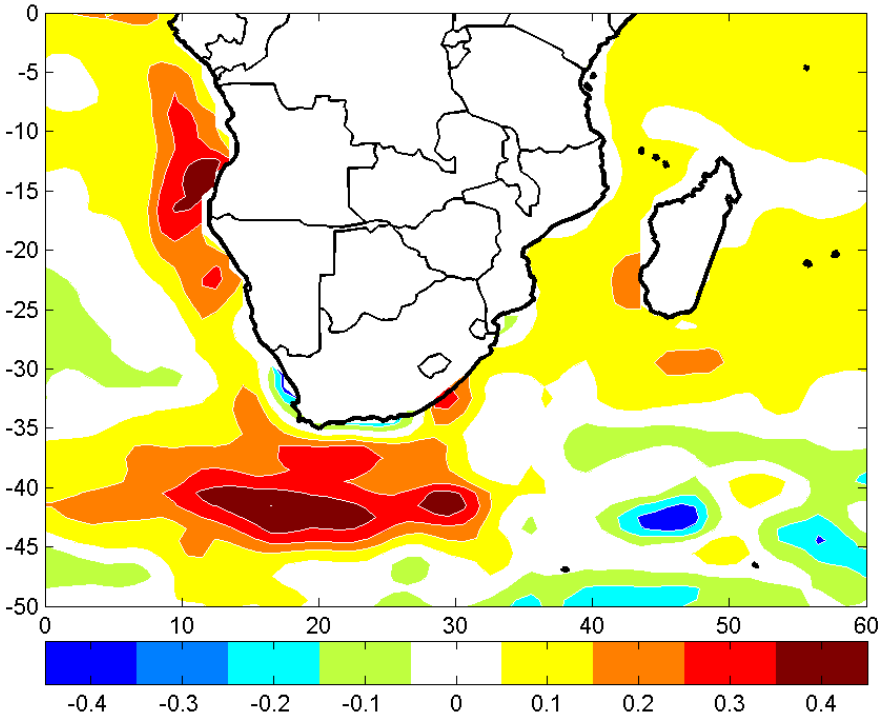

Figure 6.1: Linear trend of 1 × 1° resolution Reynolds SST in °C per decade from 1982 to 2014.

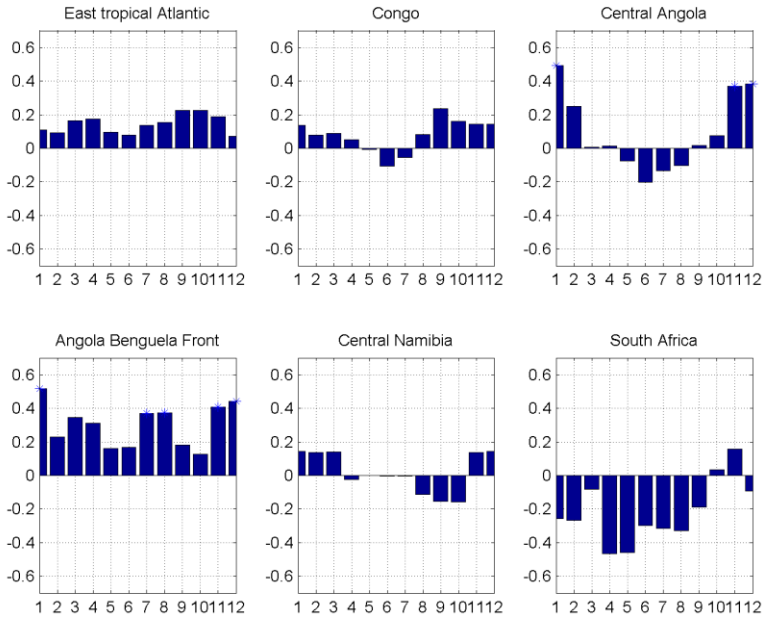

Figure 6.2: Linear trend of 1 × 1° resolution Reynolds SST in °C per decade from 1982 to 2014 at each month of the year for various region of the East Atlantic.

6.2.1. Phytoplankton

While shipboard sampling of phytoplankton for the entire Benguela ecosystem has been too irregular to derive changes over time, two time series of satellite observations of near-surface chlorophyll *a* have been analysed. The first, from Coastal Zone Colour Scanner series 1979-1986, shows marked interannual variability on the west coast (De Villiers 1998), attributed to changes in the quantity of Agulhas water advected from the south coast. The second series, derived from SEAWIFS 1997-2003 and MODIS 2003-2012, demonstrates distinct seasonal and interannual variability, but no clear trend over the 13 years of observations. In the productive St Helena Bay, an important nursery area for juvenile fish, *in situ* measurements of chlorophyll *a* (as a proxy indicator for phytoplankton biomass) indicate a rapid increase from the early-to mid-1990s, linked to increased availability of nutrients (Verheye 2000). Primary production estimates in St Helena Bay, calculated from nitrate deficits in the upper mixed layer for the period 1982-2007, showed an increase since 2000 (Hutchings et al. 2012) which, however, is not reflected in satellite-derived estimates of near-surface primary production along a cross-shelf transect in this area for the period 1998-2010 (Hutchings et al. 2012). Harmful Algal Blooms (HABs) occur as event scale phenomena in the southern Benguela (Pitcher and Calder 2000). Impacts from these phenomena are associated with toxicity from the presence of particular phytoplankton species and the decay of high biomass (where chlorophyll *a* concentrations can exceed 100 mg m^{-3}), which can lead to anoxia (Pitcher and Probyn 2011). The occurrence of blooms varies both temporally and spatially within the southern Benguela (Pitcher and Calder 2000). A distinct seasonality coincides with the wind-driven upwelling season and as such HABs have been shown to vary at the event, seasonal, and interannual scale with meteorological forcing (Pitcher et al. 1995). Blooms most frequently occur north of Cape Columbine and often affect Lamberts Bay and Elands Bay within the greater St Helena Bay region, with less frequent occurrence in False Bay (Pitcher and Calder 2000, Pitcher et al. 2008). Studies of reported incidence have suggested a six-fold increase in HABs per decade from the 1960s until 2005 with a concurrent increase in severity (Stephen and Hockey 2007). This study also suggested 'hotspots' in Elands Bay and False Bay. However, *in situ* data and reports are likely insufficient to fully resolve all occurrences and the severity of HABs. Satellite ocean colour offers suitable temporal and spatial resolution for routine monitoring (Bernard et al. 2006) but traditional chlorophyll *a* algorithms lack the dynamic range required to detect high biomass and further information on phytoplankton community composition is needed to indicate toxicity. New techniques are being developed to meet these challenges including indicators of cell size (Evers-King et al. 2014).

6.2.2. Zooplankton

Zooplankton abundance has been recorded for a majority of years in St Helena Bay during autumn (April-June) since 1951. Copepod densities, which dominate the meso-zooplankton community, increased by two orders of magnitude between 1950 and 1996 and declined by almost an order of magnitude between 1998 and 2007 (Verheye et al. 1998, Verheye 2000, Hutchings et al. 2009). Larger copepod species dominated during the 1950s-60s and smaller species in the 1990s (Verheye 2000). In addition to the long-term trends, monthly sampling in St Helena Bay between 2000 and 2011 showed strong seasonal and interannual variability of zooplankton biomass, which peaked during summer and decreased in austral autumn as pelagic fish recruits move through the inshore area and upwelling intensity declines (Hutchings et al. 2012). In contrast to the long-term autumn trends reported above, summer (peak) densities of dominant copepods remained roughly

the same during the 2000s, with no obvious decline (Hutchings et al. 2012). On the Agulhas Bank, a long-term decline in zooplankton was noted between 1988 and 2012, with a shift from larger to smaller copepods.

6.2.3. Small Pelagic Fish

Sardine *Sardinops sagax* and anchovy *Engraulis encrasicolus* are the greatest contributors to the South African small pelagic fishery and have shown alternating dominance in the catch since the fishery's inception (van der Lingen et al. 2006). Commercial fishing of sardine began in the 1940s along the west coast of South Africa and catches increased rapidly during the 1950s and peaked in the early 1960s, but then declined just as rapidly resulting in a stock collapse in the late 1960s. Sardine catches remained low during the 1970s and 1980s and instead anchovy dominated the pelagic fishery catch until the mid 1990s (van der Lingen et al. 2006). In the late 1990s and early 2000s, there was an unusual upsurge in abundance of both species, but South Africa's sardine stock collapsed for the second recorded time in the mid 2000s (Coetzee et al. 2008b). In addition to these temporal shifts in species dominance, which have been observed in a number of upwelling systems (e.g., Schwartzlose et al. 1999), spatial shifts in the distributions of small pelagic fish have occurred within the past two decades (van der Lingen et al. 2002, 2005). Changes in the distributions of both sardine and anchovy in the southern Benguela have been observed since the mid–to–late 1990s. From 1985, when November spawner biomass surveys were initiated, until 1996, the majority of the anchovy biomass was found to the west of Cape Agulhas (on the west coast) including over the Western Agulhas Bank. Since 1996, however, the bulk of anchovy spawner biomass has been located east of Cape Agulhas on the Central and Eastern Agulhas Bank. The same pattern was evident in anchovy egg abundance from as early as 1989 (van der Lingen et al. 2002). A more gradual, but similar, change was observed in sardine – with an increasing proportion of biomass found to the east of Cape Agulhas since 1995. Indeed, from 1999 the majority of spawner biomass has been located east of Cape Agulhas, with the exception of 2008-2010 and 2012. Other pelagic species such as redeye and chub mackerel have also shown similar increases in the proportion of biomass found east of Cape Agulhas over this period, although not to the same extent as the sardine and anchovy (Watermeyer 2014).

6.2.4. Seabirds

There have been long-term shifts in the distributions of several seabirds off southern Africa. Five species, which compete with commercial fisheries for prey, have undergone distributional shifts in a south-easterly direction around the southern African coast as summarized below (see also Crawford et al. 2008c). African Penguins *Spheniscus demersus*, Cape Gannets *Morus capensis*, Cape Cormorants *Phalacrocorax capensis* and the nominate race of Swift (Crested) Terns *Thalasseus bergii bergii* breed only in the Benguela upwelling ecosystem and feed mainly on anchovy and sardine. Since the late 1960s, the proportions of Cape Gannets breeding in Namibia have declined, while in South Africa they have increased. These trends closely match the proportions of the combined abundance of anchovy and sardine in the Benguela ecosystem occurring in Namibia and South Africa (Crawford et al. 2007a). In South Africa, the proportion of Cape Gannets breeding on the west coast has decreased, whereas the proportion breeding on the south eastern coast has increased (Crawford et al. 2007a). The proportion of African Penguins breeding in Namibia has also declined (Crawford et al. 2013). In South Africa the proportion of African Penguins breeding on the west coast has declined

since the mid 20th century, although it did increase in the 1990s when sardine in the region were abundant, but subsequently declined again in the 2000s, whereas the proportion breeding on the south eastern coast has increased. The shifts in gannets and penguins to the east have followed the shifts in distributions of their prey off South Africa. Almost all of South Africa's Cape Cormorants breed on the west and south-western coasts (Cooper et al. 1982, Crawford et al. 2007b) and the proportion breeding on the west coast decreased in a fluctuating manner after 1956. Comprehensive information on numbers of Swift Terns breeding on the west and south-western coasts is only available from 1984 (Cooper et al. 1990). Since then, the proportion of Swift Terns breeding on the northern west coast has decreased, although large numbers of Swift Terns bred here at the turn of the 21st century, when anchovy and sardine were abundant in the region (Crawford 2009). The Bank Cormorant *Phalacrocorax neglectus* is also endemic to the Benguela ecosystem. It is a benthic feeder that in South Africa feeds largely on the West Coast rock lobster (Hockey et al. 2005). Eleven localities on the west and south-western coasts have been reasonably well monitored and, of these, sites to the north have supported a decreasing proportion of breeding birds since. Populations in the south have either increased or remained stable (Crawford et al. 2008a). The breeding distributions of several other seabirds in the Benguela ecosystem, which do not feed primarily on prey that is harvested by fisheries, have also shifted south and east. These include Crowned *P. coronatus* and White-breasted *P. lucidus* Cormorants (Whittington 2004, Crawford et al. 2012, 2013), Hartlaub's *Larus hartlaubii* and Kelp *Larus dominicanus* Gulls (Whittington et al. 2006, Crawford et al. 2008c,2009a) and Damara Terns *Sterna balaenarum* (Crawford et al. 2009b).

6.2.5. Demersal fish

The South African demersal offshore trawl fishery, which began in the early 1900s, is based primarily on two species of hake – the shallow-water hake *Merluccius capensis* and deep-water hake *Merluccius paradoxus* (Payne and Crawford 1989). Initially, this fishery was centred around Cape Town, but it now extends from Port Nolloth on the northern west coast, to the south-eastern area of the Agulhas Bank. The fishery increased gradually, escalated after World War II and peaked in the early 1970s (Atkinson et al. 2011a). However, these catches were unsustainable and led to the implementation of a number of management plans in the mid-to-late 1970s, which reduced catches. Recently, the offshore trawl fishery has been certified by the Marine Stewardship Council and the two hake species are now assessed separately (Rademeyer et al. 2008). Biomasses are projected to increase with the OMP-2006, including a recovery plan for *M. paradoxus* from very low biomass. Field et al. (2013) present an overview of institutional arrangements and an analysis of recent structural changes in this fishery, respectively. Other fisheries targeting these two species of hake are the demersal longline fishery, the inshore trawl fishery and the commercial handline fishery. However, these three fisheries together are not allocated more than 15% of the total allowable catch. Research trawl surveys have been conducted since 1986 and, based on these data, spatial analyses showed that demersal fish assemblages were clearly influenced by depth and latitude (Atkinson et al. 2011a). Species diversity decreased with increasing depth and fish assemblages changed around the shelf break (ca. 300-400 m depth). Fish assemblages also indicated that trawl grounds can be broken into a southern and northern area, separated at approximately 33 ^{o}S (off Cape Columbine), with the northern area extending into Namibia to about 26 ^{o}S (Atkinson et al. 2011a). The southern region is dominated by (in addition to the hakes) Cape gurnard *Chelidonichthys capensis*, Bluntnose spiny dogfish *Squalus megalops* and Rattails *Caelorinchus* spp, and the northern

region by Cape dory *Zeus capensis*, Longnose spiny dogfish *Squalus mitsukurii*, Ribbon fish *Lepidopus caudatus*, Angelfish *Brama brama*, Rattail *Malacocephalus laevis* and Kingklip *Genypterus capensis* (Atkinson et al. 2011a). Multivariate analyses indicated temporal changes in the demersal fish assemblage in the early 1990s and mid-2000s and suggested there had been an increase in fast-growing, early-maturing species and a decline in slow-growing, long-lived species (Atkinson et al. 2011a). Temporal data on benthic invertebrate assemblages are not available, but experiments from heavily and lightly trawled areas showed differences in invertebrate assemblage, suggesting that trawling intensity has some impacts on invertebrate epifaunal and infaunal communities (Atkinson et al. 2011b).

6.2.6. Linefish

The South African term 'linefishery' denotes a multi-species, multi-sector, multi-area cluster of low to medium technology fisheries in which more than 200 fish species are caught by hand-line or rod and reel (long-line fisheries excluded) over a large geographical range (Solano-Fernàndez et al. 2012). Species are usually classified as warm-temperate reef fish, cool-temperate reef fish or pelagic nomads (Griffiths 2000). Within this cluster there are three recognized fishery sectors: commercial, recreational, and small-scale (formerly termed subsistence). Although the linefishery operates along the entire South African coast, here we focus on the Cape commercial linefishery, which extends from Port Nolloth to just east of East London. The boat-based commercial linefishery is a low-earning, labour-intensive sector that is very important from the perspective of human livelihoods. It is the oldest of South Africa's commercial fisheries dating back to the mid-1800s (Griffiths 2000) and concerns about the overfishing of some linefish species were voiced already in the 1940s (Griffiths 2000). However, regulation of the fishery did not occur until 1985. An increase in fishing effort, combined with technological advances in the second half of the 20th century, led to serial over-exploitation of most of the important linefish species and steady decreases in catches (Griffiths 2000). In the 1990s, spawner-biomass per recruit analyses and comparisons with historical catch data indicated alarming declines for many linefish stocks (Griffiths 1997a, b, 2000). This work led to the declaration of an emergency in the linefishery in 2000 and was followed by a mandatory reduction in effort. The total allowable effort (TAE) was reduced by 70% in 2000. However, fishing effort for some species e.g., hottentot *Pachymetopon blochii* on the west coast and reef fish on the south-west coast was already declining prior to the 2000s, suggesting that the abundance of some species was already low. Since 2006, the average total annual catch was just under 10000 t and mainly comprised pelagic shoaling species, such as snoek (*Thyrsites atun*) and yellowtail (*Seriola lalandi*); and demersal species, such as silver kob (*Argyrosomus inodorus*) and geelbek (*Atractoscion aequidens*). The availability of these wide-ranging, shoaling species can be erratic, and fishers therefore often switch fishing strategies to target other species, including a large variety of reef-associated seabreams such as carpenter (*Argyrozona argyrozona*), slinger (*Chrysoblephus puniceus*) and hottentot (*Pachymetopon blochii*), when the preferred species are unavailable (Griffiths 2000). However, the more resilient species are likely those with nomadic lifestyles and shorter lifespans, unlike the reef fish that are long-lived, slow growing, late-maturing and sometimes protogynous hermaphrodites (Penny et al. 1989). Most prominent examples of reef fish collapses include the large sparids seventy four *Polysteganus undulosus* and red steenbras *Petrus rupestris* (Attwood and Farquhar 1999, Griffiths 2000), which are now protected under a catch moratorium. In 2010, an initiative was set up to revise stock assessments for a number of important linefish species, many of

which had not been updated in over a decade. The extensive National Marine Linefish System (NMLS) database contains over 25 y of more than 2.5 million spatially-referenced catch and effort records, and was recognized by the 'Census of Marine Life' mega-project as the largest dataset of its kind (McIntyre 2010). Nevertheless, most linefishes remain in an unknown or collapsed state.

6.2.7. Rock Lobster

The South African commercial fishery for West Coast rock lobster *Jasus lalandii* is located along the west and south-west coasts, although the majority of catches have always been concentrated on the west coast. The fishery dates back to the late 19th century (Melville-Smith and van Sittert 2005) and catches peaked in 1950/51 and have steadily declined since then, largely due to overexploitation of the resource, particularly in the north, but also to changes in productivity and environmental conditions in more recent decades (Melville-Smith and van Sittert 2005). During the 1980s, rock lobster catches appeared to have stabilized and exploitation was regarded as sustainable. However, catches declined unexpectedly in the early 1990s and fishing effort shifted from the west coast to the south-western coast (Cockcroft et al. 2008). In recent years, catches have failed to recover significantly and the biomass of legal-sized male lobsters is currently estimated to be less than 3% of 'pristine' (Johnston 2013). The proportion of rock lobster caught on the west coast has also fallen from ~65-70% to under 10% in the last decade while in the south it has increased from 10- ~70%.

6.2.8. Abalone

The South African abalone *Haliotis midae* occurs from Cape Columbine on the west coast to just north of Port St Johns along the east coast, although the heart of the fishery has historically been located along the south-western coast, between Cape Hangklip and Quoin Point. Abalone have been fished commercially since ca. 1950 (Tarr 1992), but only in the last two to three decades have numbers declined substantially due to changes in the ecosystem and intense illegal fishing (Blamey et al. 2014). The recreational fishery was closed in 2003/2004 and a temporary ban on the commercial fishery was implemented in 2008/09 (van der Lingen et al. 2012). At this stage the resource was estimated to be less than 18% of its pre-exploitation spawning biomass, with one of the four major fishing zones sitting at about 4% (Plagányi and Butterworth 2010).

6.2.9. Kelp

Important recent changes in seaweed distribution concern the most abundant and economically important seaweed in the region, the large forest-forming kelp *Ecklonia maxima*. The eastern biogeographical limit of the species was static for at least 50 years at Suiderstrand (just west of Cape Agulhas) but moved more than 70km eastwards around Cape Agulhas in 2006-2007 (Bolton et al. 2012). A significant *E. maxima* bed now exists in De Hoop Nature Reserve (Bolton et al. 2012, Reimers 2012). Figure 6.1 and Bolton et al. (2012) suggest that coastal cooling may be implicated in this eastward shift, although the very small amount of previous coastal temperature data available for De Hoop (Bolton and Stegenga 1990) suggests that De Hoop was considerably warmer than west of Cape Agulhas. As well as this eastward range expansion, there is evidence that *Ecklonia maxima* is becoming more prevalent and abundant within its distribution range. Reimers (2012) used repeat photography to demonstrate this at a number of sites between False Bay and Hermanus while an increase in abundance of this species in subtidal fringe sites in False Bay between 1987 and 2008-9 was documented in detail by Mead (2011). Although kelp abundance has increased along the south-

west coast, in some areas the harvesting of kelp is approaching the prescribed limits (Troell et al. 2006).

6.2.10. Intertidal fauna

The most significant change in rocky intertidal biota in the southern Benguela has been the introduction of marine invasive species. The introduced marine species present in the region are documented by Mead et al. (2011a), and their distributions and impacts are discussed by Mead et al. (2011b). A total of 85 introduced, plus 39 suspected or 'cryptogenic'marine species are reported from South Africa. Distributional data could be established for 80 of these species of which the majority, 55, were reported from the west coast (Mead et al. 2011b). Many of these are inconspicuous forms, or are confined to one or a few harbours, estuaries and lagoons, but three abundant, bed-forming species have profoundly affected the rocky intertidal biota. On many west coast shores the upper shore is thus now dominated by an alien barnacle, the mid-shore by dense beds of *M. galloprovincialis* and the lowshore by a virtual monoculture of *S. algosus* (de Greef et al. 2013). Another temporal change in the intertidal fauna has been the progressive reduction in the warm-water brown mussel *Perna perna* along the west coast of False Bay. Although common all along the False Bay coastline in the 1980s and before, surveys undertaken in 2008-10 revealed only small relict populations of adult *P. perna* clinging to the warmest corner of the Bay at Bailey's Cottage, the main population having retreated eastwards as far as Arniston. This finding closely parallels the increased abundance of cold-water kelps in the same region (south-western coast), reported above.

6.3. Climate drivers of change

Spatial and temporal changes in the southern Benguela ecosystem can be attributed to a number of natural and anthropogenic drivers, however, in this paper we focus on two main drivers: fishing and climate. Other drivers are reviewed in Mead et al. (2013) and Moloney et al. (2013).

6.3.2. Wind

Wind data have been recorded at Cape Point since 1960 and mostly show decadal-scale variability, although a prominent decline in southerly winds occurred during the 1980s, lasting for over a decade, followed by a dominance of strong southerly winds for most of the 1990s.Using a sequential t-test algorithm for the detection of regime shifts (STARS), Blamey et al. (2012) detected significant shifts between northerly/southerly wind dominance in 1971, 1983, 1994 and 2007. Further analyses (results not shown) detected a significant shift from winter easterlies to westerlies also during the 1980s, and stronger summer south-easterly winds during the 1990s (see Blamey et al. 2012). Wind data from Cape Columbine lighthouse for 1957-1993 also show mostly decadal-scale changes, with no obvious trend (Hutchings et al. 2012). However, there was a pronounced decrease in southerly winds between 1983-1990 (Hutchings et al. 2012), consistent with the decline in southerly winds at Cape Point during the 1980s. Unfortunately data post-1993 were not available for Cape Columbine. The long-term wind data (particularly for Cape Point) are problematic because of changes in collection methods that occurred in the early-to-mid 1980s, and again in 1993. However, Blamey et al. (2012) argue that a shift in wind patterns did occur during the early 1980s, albeit exaggerated by the change in measurement method.

6.3.3. Ocean temperature and El Niño Southern Oscillation (ENSO)

We analysed monthly Reynolds Optimally Interpolated Sea Surface Temperature (OI SST) (Reynolds et al. 2002), a 1x1 degree resolution product based on satellite remote sensing (AVHRR) and *in situ* observations that are optimally interpolated when data are missing. (Fig 6.1). We found a positive trend (warming) in SST of up to 0.55°C per decade in the Agulhas Current system during most months of the year, except for KwaZulu–Natal, where the warming was only significant in January and February. The warming was attributed to an intensification of the Agulhas Current in response to increases of wind stress curl in the south Indian Ocean (Rouault et al. 2009, Backeberg et al. 2012). In the southern Benguela (west coast), we found a statistically significant cooling trend of up to 0.5°C per decade from January to August only, and along the south coast, a less pronounced cooling trend up to 0.4 °C per decade from May to August only (Fig. 6.2). This cooling is most likely due to an increase in upwelling-favourable south-easterly and easterly winds. Changes in the tropical Atlantic and adjacent upwellings are reflecting a variety of process and have a distinct seasonality. Some regions have warmed up and some regions have cooled down while some other regions have not significally changed. The tropical Atlantic experienced a slight warming of 0.1 to 0.2 ^{o}C per decade at all months of the year while the Angolan and North Namibian coastline displays also a warming at all month of the year but higher, from 0.2 C to 0.5 ^{o}C per decade. The central part of the Benguela upwelling has not changed while the South Benguela has cooled down mainly from April to August by 0.3 to 0.5 ^{o}C per decade which out of the upwelling season suggesting stronger unseasonal upwelling favourable winds (Fig. 6.2). Prior to the satellite era, 1980, it is difficult to ascertain coastal changes using gridded products that are based on a paucity of observations with gaps filled up with statistical technics. For instance Hadley SST version 1 (Rayner et al, 2003) uses satellite remote sensing estimate of SST from 1982 and sparse observation before and cannot be used for trends analysis in upwelling regions. Further work will look at the cause of those changes, namely change in wind speed and related latent and sensible heat fluxes, change in thermocline depths and changes in current system.

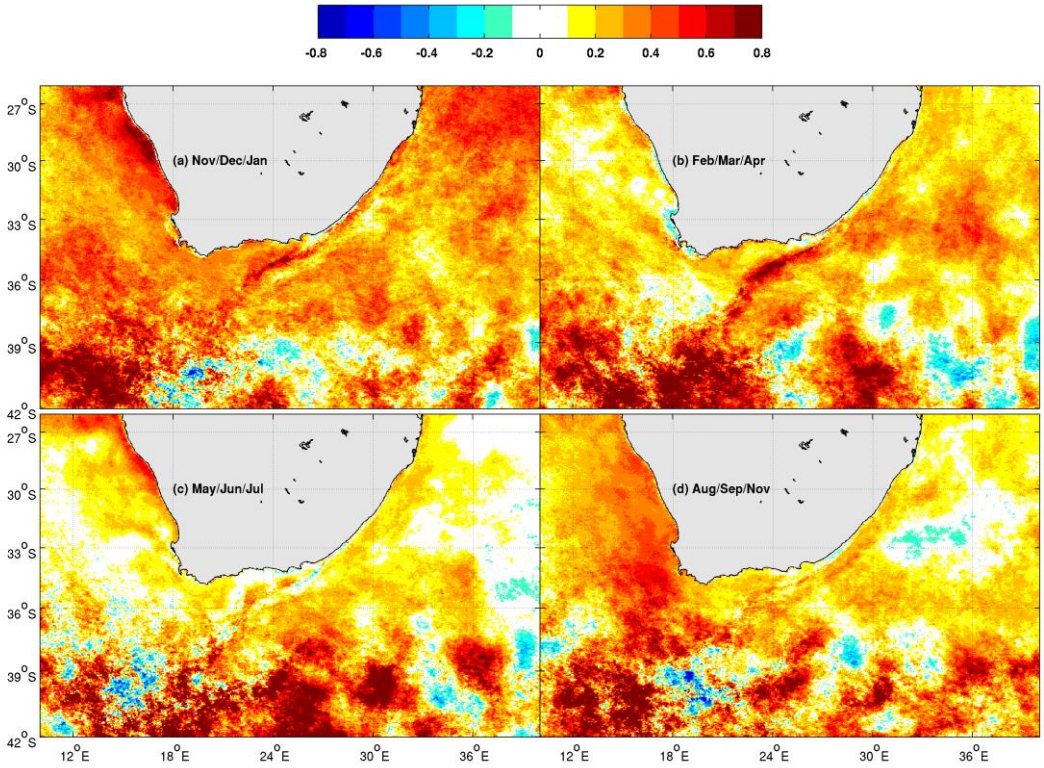

Figure 6.3: Linear trend of 4 x 4km resolution AVHRR derived Pathfinder V5.2 SST in °C per decade from 1982 to 2014.

However, Dufois et al. (2012) report a warm bias in the previous version of AVHRR Pathfinder (before version 5.2) when compared with MODIS SST, reaching up to 5 ºC in summer in the southern Benguela at the monthly scale. The latest release of Pathfinder (version 5.2) clearly improves the bias but the cooling trend described by Rouault et al. (2010) and presented in Fig. 6.1 is less evident: it is no longer present along the south coast, or north of Cape Columbine (Fig. 6.3) as previously reported. Only the late summer cooling (February-April) around the Cape Peninsula upwelling region (specifically Cape Columbine to Danger Point, see Fig. 6.3 top right panel) and the warming in the Agulhas System (Fig. 6.3) hold. The cooling in the southern Benguela is consistent with increased south-easterly winds and upwelling during the 1990s. In contrast to the Cape Peninsula upwelling region, there appears to be a warming trend all year round north of Cape Columbine/St Helena Bay (Fig. 6.3) using Pathfinder v5.2 data, although there is some uncertainty around these results given that other data show a cooling (Fig. 6.1, Rouault et al. 2010, Lima and Wethey 2012). However, off Namibia and Angola (Figs 6.1, 6.3) there has indeed been a warming and although reasons for this warming are not known, it is consistent with the southerly shift in the South Atlantic High Pressure system discussed in Jarre et al. (in press b) and summarized below. This shift could have decreased the wind off Northern Namibia leading to suppressed upwelling and hence warming.

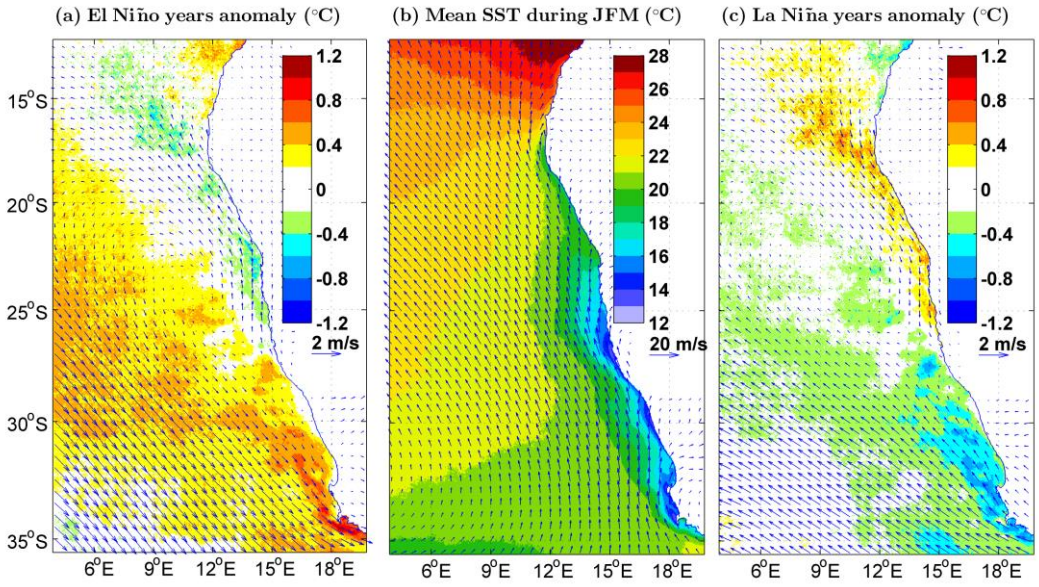

Figure 6.4: Mean summer (DJF) SST and wind speed/direction for the Benguela region (middle panel) and the respective anomalies in summer during El Niño (left) and La Niña (right). SST shown in colour and wind speed/direction indicated by arrows

It also could have deepened the thermocline off Angola leading to a warming of coastal water off Angola and an increased advection of warm tropical water in Northern Namibia by a process similar to the one discussed in Rouault (2012)**,** except at the decadal scale**.** Dufois and Rouault (2012) and Rouault et al. (2010) show that, during austral summer, El Niño events induce an equatorward shift in the South Atlantic High pressure system. This leads to a weakening of upwelling favourable south-easterly winds and warmer than average SSTs in the southern Benguela (Fig. 6.4a,b), but stronger south-easterlies and therefore cool SST anomalies in the northern Benguela. The opposite effect occurs during La Niña events, when there is a poleward shift in the South Atlantic High pressure system (Fig. 6.4c). Rouault et al. (2010) also found that the south coast and the Agulhas Current system were correlated with the El Niño Southern Oscillation (ENSO) but not with the Antarctic Annual Oscillation (AAO) also called Southern Annular Mode (SAM). Although there appears to be no change in the frequency of ENSO events, more work is required to disentangle inter-annual to decadal variability before assessing any links between ENSO frequency, SST trends and increased climate variability. Jarre et al. (in press b) used STARS to analyse the mean position of the centre of the South Atlantic High Pressure system between 1981-2013 and found a significant southerly shift of almost 2˚ latitude occurred in the late 1980s and persisted for all of the 1990s, before showing signs of retreating northwards again in the mid 2000s. This could explain the observed increase in southerly/south-easterly winds and upwelling during the 1990s and hence cooler SSTs south of 32˚ latitude (Fig. 6.2).

6.4. Discussion

Linking drivers to ecosystem change can be difficult, particularly if there are multiple drivers (as is often the case), which act in synergy and at different scales. This is further complicated if systems, such as the southern Benguela, are highly variable, and what drives ecosystem dynamics in

some years may have less of an influence in other years, as noted in Hutchings et al. (1998), where multiple factors determine recruitment success but the relative importance of factors can change from year to year. Almost all the changes we have summarized here in this either involve a temporal decline or an eastward shift in species. Most of the declines are due to overfishing (either directly or indirectly, for example due to reduction in preferred prey) or at least driven by geographically disproportionate catches in relation to abundance. In some cases changes in the physical environment seem to have played a role as well, e.g., rock lobster on the west coast. In almost all cases these changes have taken place since the 1980s/1990s, except for one or two resources, which have experienced declines since at least the mid 20th century. Spatial shifts in species have either involved an eastward expansion of cool-water species, including kelps, rock lobster and pelagic fish, or a retraction of warm water species such as the brown mussel, suggesting a cooling of inshore waters along the south-west coast since the 1980s. This suggested cooling is revealed in the SST (Pathfinder), wind and upwelling data for the Cape Peninsula and south-west coast region during the same period. Along the south coast, offshore waters have warmed while trends in the inshore depend on the data under scrutiny and thus require further investigation. Although the west coast (north of Cape Columbine) has possibly experienced a warming of ocean waters, some of the biological changes that have occurred (e.g., declines in seabirds) are most likely due to southward shifts in distributions of prey (Crawford et al. 2008b), although the shifts in prey distributions may have been a response to environmental change. In addition to the prolonged, intense exploitation of the West Coast rock lobster resource, there are three major elements, all of which occurred within a similar time frame, that are believed to have contributed to the recent spatio-temporal changes in rock lobster distribution and thus catch and effort. Firstly, a 50% reduction in rock lobster growth rates occurred during the 1980s, resulting in fewer lobsters growing beyond the minimum legal size and hence entering the fishery (Pollock et al. 1997). Evidence explaining the causes of these reduced growth rates is inconclusive. However, it was hypothesized that declines in food availability and quality due to reduced productivity resulting from shifts in the dominant upwelling-favourable winds, might be responsible (Pollock et al. 1997). Secondly, the 1990s were a period of increased rock-lobster walkouts (Cockcroft 2001). Of the five walkouts that occurred, three were severe, with one event resulting in the loss of ~ 2000 t – approximately equal to the entire annual national catch. All five events were closely linked with dense dinoflagellate blooms, most likely due to increased upwelling and quiescent periods (Cockcroft 2001). This is in contrast to the two major walkouts during the 1980s, both of which were linked to an inshore movement of low oxygen waters (Cockcroft et al. 1999, Cockcroft 2001). Thirdly, during the early 1990s there was a shift in lobster abundance east of False Bay into an area where lobster density had previously been low (Cockcroft et al. 2008). Anecdotal evidence and ecosystem modeling suggest that this increase is likely due to an abrupt arrival of adults (Tarr et al. 1996, Cockcroft et al. 2008, Blamey et al. 2013), and most likely an expansion of the False Bay population (Cockcroft et al. 2008). However, exactly why the population suddenly shifted eastwards from False Bay is not understood. Resources in the intertidal/shallow-subtidal region have been impacted by a number of different drivers. While overfishing of abalone (predominantly illegal) in the shallow-subtidal has played a large role in the spatial shifts and declines in this resource, the indirect food web effects resulting from the eastward migration of rock lobsters has also played a significant role, and in combination these two drivers have resulted in the localized collapse of some abalone stocks (Blamey et al. 2013). Direct evidence for climate change impacting inshore flora and fauna in the Benguela is sparse, although Bolton et al. (2012) attributed the

eastward shift in kelp to declining temperatures in this region and similarly Mead et al. (2013) link the retraction of the intertidal warm-water mussel along the western side of False Bay to coastal cooling. Temporal aspects of human disturbance in the rocky intertidal are also poorly documented (but see Bally and Griffiths 1989 for an example of such impacts). On sandy shores, the recent disappearance of the iconic giant isopod *Tylos granulatus* from beaches such as Hout Bay and Blouberg has been attributed to a combination of human disturbance, pollution and construction along the back beach (Brown and Odendaal 1994). Beach driving also has negative impacts on both *Tylos* populations (Brown and Odendaal 1994) and on African Black oystercatchers nesting success, with the latter showing a recovery following the ban on such driving (Leseberg et al. 2000).

One of the main difficulties in trying to identify drivers of ecosystem change, and actual ecosystem change itself, is the absence or inconsistency of long-term data. Such data can be problematic if methodology, instruments and/or scientists change over time, as is the case with most long-term fishing and climate data. While advances in technology may help improve the consistency of recent climate data, they often do not extend far back enough in time to detect long-term trends and scales may vary depending on instruments used. An example of some of these problems is especially true for ocean temperature data in the southern Benguela and these discrepancies are discussed below. Most marine ecosystems have experienced a warming of ocean waters in the last 30 years, varying from slow to rapid (Belkin 2009, Alheit et al. 2014). These include the Angolan subtropical and the northern Benguela sub-systems of the Benguela large marine ecosystem, which border the southern Benguela to the north and east, respectively. There are, however, some examples of those that are thought to have cooled e.g., Humboldt Currents (Belkin 2009, Gutiérrez et al. 2011). Both these regions are major upwelling systems and upwelling has been hypothesized to have intensified due to global warming with a subsequent cooling of coastal waters (Bakun 1990). The cooling evidenced in parts of the southern Benguela (Fig. 6.3) is in agreement with various other studies carried out at larger scales (Rouault et al. 2010, Burrows et al. 2011, Santos et al. 2012, Lima and Wethey 2012). However, looking at different periods, or other SST products at large scale, some authors found that a warming has been experienced in the entire Benguela (Belkin 2009, Morice et al.2012). It must be noted that Belkin et al. (2009) did not look at seasonal trends and averaged across the entire Benguela region. Thus it is possible that the warming trend observed is due to the warming in the northern Benguela. Figs 6.1 and 6.3 are also good examples of the differences in the temperature changes observed within the Southern Benguela when using different SST products. This discrepancy, noticeable only close to the coast, might arise for various reasons. Firstly, satellite products differ depending on the instruments and SST retrieval techniques used and this has indeed been shown for South Africa (Dufois et al. 2012, Smit et al. 2013). Secondly, some of the SST products are unable to resolve small oceanic features (e.g., an upwelling cell) due to either the resolution or the interpolation scheme used to fill in the gaps (mostly induced by clouds). For example the Reynolds SST should be applied with caution for small domains, such as an upwelling cell, or for coastal areas in the vicinity of the Agulhas Current, as the interpolation scheme employed means that each 1° resolution cell is liable to influence other cells in a 3°radius. Thirdly, SST products, which are used in the studies listed above, potentially exhibit strong SST biases in the core of the Benguela upwelling system (Dufois et al. 2012). This could impact the trend processed from satellite datasets. Therefore, a better quantification of uncertainties regarding temperature changes observed from satellite within the southern Benguela seems necessary. This could be achieved following the recommendation of Morice et al. (2012) who highlighted the need to use an ensemble of

observational estimates to quantify uncertainties and better assess temperature change. Caution should also be used when interpreting long-term trends in *in situ* data, particularly if data collection is inconsistent or suspicious, as is the case with the SAWS ocean temperature data and wind data for Cape Point. Conflicting trends may emerge between satellite and *in situ* temperature data, largely due to issues of scale. Trends based on satellite data are often for much larger scales and employ regional averages, whereas *in situ* data are usually site specific and measure temperatures at varying depths in the water column. Furthermore, satellite remote sensing is an estimate of the oceans 'skin' temperature (first few millimeters of the surface), which can be influenced by air temperature and radiation. Moreover, a considerable increase in air temperature has occurred over the last few decades (Kruger and Shongwe 2004), which could mask an increase in wind speed and upwelling intensity, which could help explain discrepancies between *in situ* and satellite data, but not between various satellite products. However, *in situ* data for Gordon's Bay correlates well with MODIS satellite data (Dufois et al. 2012). Despite this, SAWS temperature data (including Gordon's Bay) should be treated with caution due to unreported change of measuring systems, absence of a documented protocol and little information on exact timing and location of sampling. Other *in situ* inshore temperature data, measured with temperature loggers, also exist (Smit et al. 2013), but have not been used to look at long-term trends.

It is generally accepted that in the Benguela region, the complex interplay between environmental (e.g., wind, temperature, oxygen and productivity) and anthropogenic (notably fishing) drivers are responsible for the observed spatio-temporal dynamics of most resources (e.g., Jarre et al. in press b). This is true for a number of other ecosystems around the world (Halpern et al. 2008, Möllmann et al. 2009). Disentangling these combined effects will require interdisciplanary collaboration, co-ordinated ecosystem projects and the continuation of dedicated research, as well as increased modelling effort (Harley et al. 2006, Moloney et al. 2013.

6.5 References

- Alheit, J., Licandro,P., Coombs, S., Garcia, A., Giráldez, A.,Garcia Santamaría, M.T., Slotte, A., Tsikliras, A.C., 2014. Atlantic Multidecadal Oscillation (AMO) modulates dynamics of small pelagic fishes and ecosystem regime shifts in the eastern North and Central Atlantic. J Marine Syst 133, 88-102.
- Atkinson, L.J., Leslie, R.W., Field, J.G., Jarre, A., 2011a. Changes in demersal fish assemblages on the west coast of South Africa, 1986–2009. Afr J Mar Sci 33, 157-170.
- Atkinson, L.J., Field, J.G., Hutchings, L., 2011b.Effects of demersal trawling along the west coast of southern Africa: multivariate analysis of benthic assemblages. Mar Ecol Prog Ser 430, 241–255.
- Attwood, C.G., Farquhar, M., 1999. Collapse of linefish stocks between Cape Hangklip and Walker Bay, South Africa. S Afr J Mar Sci 21, 415-432.
- Backeberg, B.C., Penven, P., Rouault, M., 2012. Impact of intensified Indian Ocean winds on mesoscale variability in the Agulhas system. Nature Clim Change. Doi: 10.1038/nclimate1587.
- Bakun, A., 1990.Global climate change and intensification of coastal ocean upwelling. Science 247, 198-201.
- Belkin, I.M., 2009. Rapid warming of large marine ecosystems. Prog Oceanogr 81, 207-213.
- Bernard, S., Kudela, R.M., Franks, P.J.S., Fennel, W., Kemp, A., Fawcett, A., Pitcher, G.C., 2006. The requirements for forecasting Harmful Algal Blooms in the Benguela. Large Mar Ecosyst 14, 281-302.

- Blamey, L.K., Branch, G.M., 2012.Regime shift of a kelp-forest benthic community induced by an 'invasion' of the rock lobster *Jasus lalandii.* J Exp Mar Biol Ecol 420-421, 33-47.
- Blamey, L.K., Howard, J.A.E., Agenbag, J., Jarre, A., 2012. Regime-shifts in the southern Benguela shelf and inshore region. Prog Oceanogr 106, 80-95.
- Blamey, L.K., Plagányi, É.E., Branch, G.M., 2013.Modelling a regime shift in a kelp-forest ecosystem caused by a lobster range-expansion. Bull Mar Sci 89, 347-375.
- Blamey, L.K., Plagányi, É.E., Branch, G.M., 2014. Was overfishing of predatory fish responsible for a lobster-induced regime shift? Ecol Mod 273, 140-150.
- Bolton, J.J., Anderson, R.J., Smit, A.J., Rothman, M.D., 2012. South African kelp moving eastwards?: the discovery of *Ecklonia maxima* (Osbeck) Papenfuss at De Hoop Nature Reserve. Afr J Mar Sci 34, 147-151.
- Burrows, M.T., Schoeman, D.S., Buckley, L.B., Moore, P., Poloczanska, E.S., Brander, K.M., Brown, C., Bruno, J.F., Duarte, C.M., Halpern, B.S., Holding, J., Kappel, C.V.,Kiessling, W., O'Connor, M.I., Pandolfi, J.M., Parmesan, C., Schwing, F.B., Sydeman, W.J., Richardson, A.J., 2011. The pace of shifting climate in marine and terrestrial ecosystems. Science 334, 652-655.
- Cockcroft, A.C., 2001. *Jasus lalandii* 'walkouts' or mass strandings in South Africa during the 1990s: an overview. Mar Freshwater Res 52, 1085-1093.
- Cockcroft, A.C., van Zyl, D., Hutchings, L., 2008. Large-scale changes in the spatial distribution of South African West Coast rock lobsters: an overview. Afr J Mar Sci 30, 149-159.
- Coetzee, J.C., van der Lingen, C.D., Hutchings, L., Fairweather, T.P., 2008a. Has the fishery contributed to a major shift in the distribution of South African sardine? ICES J Mar Sci 65, 1676–1688.
- Coetzee, J. C., Merkle, D., de Moor, C. L., Twatwa, N. M., Barange, M., Butterworth, D. S.,2008b. Refined estimates of South African pelagic fish biomass from hydro-acoustic surveys: quantifying the effects of target strength, signal attenuation and receiver saturation. Afr J Mar Sci 30, 205–217.
- Crawford, R.J.M., 2009. A recent increase of Swift Terns *Thalasseus bergii* off South Africa – the possible influence of an altered abundance and distribution of prey. Prog Oceanogr 83, 398–403.
- Crawford, R.J.M., Dundee, B.L., Dyer, B.M., Klages, N.T.W., Meÿer, M.A., Upfold, L., 2007a. Trends in numbers of Cape Gannets (*Morus capensis*), 1956/57–2005/06, with a consideration of the influence of food and other factors. ICES J Mar Sci 64, 169–177.
- Crawford, R.J.M., Dyer, B.M., Kemper, J., Simmons, R.E., Upfold, L., 2007b.Trends in numbers of Cape Cormorants (*Phalacrocorax capensis*) over a 50-year period, 1956–57 to 2006–07. Emu 107, 1–9.
- Crawford, R.J.M., Cockroft, A.C., Dyer, B.M., Upfold, L., 2008a. Divergent trends in Bank Cormorants *Phalacrocorax neglectus* breeding in South Africa's Western Cape consistent with a distributional shift of rock lobsters *Jasus lalandii*. Afr J Mar Sci 30, 161–166.
- Crawford, R.J.M., Sabarros, P.S., Fairweather, T., Underhill, L.G., Wolfaardt, A.C., 2008b. Implications for seabirds off South Africa of a long-term change in the distribution of sardine. Afr J Mar Sci 30, 177–184.
- Crawford, R.J.M., Tree, A.J., Whittington, P.A., Visagie, J., Upfold, L., Roxburg, K.J., Martin, A.P., Dyer,B.M., 2008c. Recent distributional changes of seabirds in South Africa: is climate having an impact? Afr J Mar Sci 30, 189–193.
- Crawford, R.J.M, Dyer, B.M., Geldenhuys, D., Makhado, A.B., Randall, R.M., Upfold, L., Visagie, J., Waller, L., 2012.Trends in numbers of Crowned Cormorants in South Africa, with information on diet. Afr J Mar Sci 34, 411–424.
- Crawford, R.J.M., Randall, R.M., Whittington, P.A., Waller, L.J., Dyer, B.M., Allan, D., Fox, C., Martin, P.A., Upfold, L., Visagie, J., Bachoo, S., Bowker, M., Fox, R., Huisamen, J., Makhado,

A.B., Ryan, P.G., Taylor, R., Turpie, J.K., 2013. South Africa's coastal-breeding White-breasted Cormorants: population trend, breeding season and movements, and diet. Afr J Mar Sci 35, 473–490.

- De Villiers, S.,1998. Seasonal and interannual variability in phytoplankton biomass on the southern African continental shelf: evidence from satellite-derived pigment concentrations. S Afr J Mar Sci 19, 169-179.
- deYoung, B., Barange, M., Beaugrand, G., Harris, R., Perry, R.I., Scheffer, M., Werner, F., 2008. Regime shifts in marine ecosystems: detection, prediction and management. Trends Ecol Evol 23, 402-409.
- Dufois, F., Rouault, M., 2012. Sea surface temperature in False Bay (South Africa): Towards a better understanding of its seasonal and inter-annual variability. Cont Shelf Res 43, 24-35.
- Dufois, F., Penven, P., Peter Whittle, C., Veitch, J., 2012. On the warm nearshore bias in Pathfinder monthly SST products over Eastern Boundary Upwelling Systems. Ocean Model 47, 113-118.
- Evers-King, H., Bernard, S., Robertson Lain, L., Probyn, T.A., 2014. Sensitivity in reflectance attributed to phytoplankton cell size: forward and inverse modelling approaches. Opt Express 22, 11536-11551.
- Field, J.G., Attwood, C., Jarre, A., Sink, K., Petersen, S., 2013. Cooperation between scientists, NGOs and industry in support of sustainable fisheries: the South African hake *Merluccius spp*. trawl fishery experience. J Fish Biol 83: 1019–1034.
- Griffiths, C.L., van Sittert, L., Best, P.B., Brown, A.C., Clark, B.M., Cook, P.A., Crawford, R.J.M., David, J.H.M., Davies, B.R., Griffiths, M.H., Hutchings, K., Jerardino, A., Kruger, N., Lamberth, S., Leslie, R.W., Melville-Smith, R., Tarr, R., van der Lingen, C.D., 2004. Impacts of human activities on marine animal life in the Benguela: a historical overview. Oceanogr Mar Biol 42, 303-392.
- Gutiérrez, D., Bouloubassi, I., Sifeddine, A., Purca, S., Goubanova, K., Graco, M., Field, D., Méjanelle, L., Velazco, F., Lorre, A., Salvatteci, R., Quispe, D., Vargas, G., Dewitte, B.,Ortlieb, L. 2011.Coastal cooling and increased productivity in the main upwelling zone off Peru since the mid-twentieth century. Geophys Res Lett 38,doi: 10.1029/2010GL046324.
- Halpern, B.S., Walbridge, S., Selkoe, K.A., Kappel, C.V., Micheli, F., D'Agrosa, C., Bruno, J.F., Casey, K.S., Ebert, C., Fox, H.E., Fujita, R., Heinemann, D., Lenihan, H.S., Madin, E.M.P., Perry, M.T., Selig, E.R., Spalding, M., Steneck, R.,Watson, R., 2008. A global map of human impact on marine ecosystems. Science 319, 948-952.
- Harley, C.D., Randall Hughes, A., Hultgren, K.M., Miner, B.G., Sorte, C.J., Thornber, C.S., Rodriguez, L.F., Tomanek, L., Williams, S.L., 2006. The impacts of climate change in coastal marine systems. Ecol Lett9, 228-241.
- Hobday, A. J., Pecl, G. T., 2014. Identification of global marine hotspots: sentinels for change and vanguards for adaptation action. Rev Fish Biol Fisher24, 415-425.
- Hoegh-Guldberg, O., Bruno, J.F., 2010. The impact of climate change on the world's marine ecosystems.Science328, 1523-1528.
- Huggett, J., Verheye, H., Escribano, R., Fairweather, T.,2009. Copepod biomass, size composition and production in the Southern Benguela: spatio-temporal patterns of variation, and comparison with other eastern boundary upwelling systems. Prog Oceanogr 83, 197-207.
- Hutchings, L., van der Lingen, C.D., Shannon, L.J., Crawford, R.J.M., Verheye, H.M.S., Bartholomae, C.S., van der Plas, A.K., Louw, D., Kreiner, A., Ostrowski, M., Fidel, Q., Barlow, R.G., Lamont, T., Coetzee, J., Shillington, F., Veitch, J., Currie, J.C., Monteiro, P.M.S., 2009. The Benguela current: an ecosystem of four components. Prog Oceanogr 83, 15-32.
- Hutchings, L., Jarre, A., Lamont, T., van den Berg, M., Kirkman, S.P., 2012. St Helena Bay (southern Benguela) then and now: muted climate signals, large human impact. Afr J Mar Sci 34, 559-583.

- Jackson, J.B., Kirby, M.X., Berger, W.H., Bjorndal, K.A., Botsford, L.W., Bourque, B.J., Bradbury, R.H., Cooke, R., Erlandson, J., Estes, J.A., Hughes, T.P., Kidwell, S., Lange, C.B., Lenihan, H.S., Pandolfi, J.M., Peterson, C.H., Steneck, R.S., Tegner, M.J.,Warner, R.R., 2001. Historical overfishing and the recent collapse of coastal ecosystems. Science 293, 629-637.
- Jarre, A., Ragaller, S., Hutchings, L.,2013. Long-term, ecosystem-scale changes in the southern Benguela marine pelagic social-ecological system – Interaction of natural and human drivers. Ecol Soc 18, 55.
- Jennings, S., 2005. Indicators to support an ecosystem approach to fisheries. Fish Fisher 6, 212-232.
- Kruger, A.C., Shongwe, S., 2004. Temperature trends in South Africa: 1960–2003. Int J Climatol 24, 1929–1945. doi: 10.1002/joc.1096
- Laird, M., Griffiths, C.L., 2008.Present distribution and abundance of the introduced barnacle *Balanus glandula* Darwin in South Africa. Afr J Mar Sci30, 93-100.
- Leduc, G., Herbert, C. T., Blanz, T., Martinez, P., Schneider, R., 2010.Contrasting evolution of sea surface temperature in the Benguela upwelling system under natural and anthropogenic climate forcings. Geophys Res Lett 37. doi: 10.1029/2010GL044353.
- Lima F.P., Wethey, D.S.,2012. Three decades of high-resolution coastal sea surface temperatures reveal more than warming. Nat Commun 3, 704. doi:10.1038/ncomms1713.
- Ling, S.D., Johnson, C.R., Frusher, S.D., Ridgway, K.R., 2009. Overfishing reduces resilience of kelp beds to climate-driven catastrophic phase shift. Proc Nat Acad Sci USA 106, 22341-22345.
- Lloyd, P., Plagányi, E.E., Weeks, S.J., Magno-Canto, M., Plagányi, G., 2012. Ocean warming alters species abundance patterns and increases species diversity in an African sub-tropical reef-fish community. Fish Oceanogr 21, 78-94.
- McGregor, H.V., Dima, M., Fischer, H.W., Mulitza, S., 2007. Rapid 20th-century increase in coastal upwelling off northwest Africa. Science 315, 637-639.
- McGowan, J.A., Cayan, D.R., Dorman, L.M., 1998. Climate-ocean variability and ecosystem response in the Northeast Pacific. Science 281, 210-217.
- Mead, A., Carlton, J., Griffiths, C.L., Rius, M., 2011a.Introduced and cryptogenic marine and estuarine species from South Africa. J Nat Hist 45, 2463-2524.
- Mead, A., Carlton, J., Griffiths, C. L., Rius, M., 2011b. Revealing the scale of marine bioinvasions in developing regions: a South African re-assessment. Biol Invasions 13, 1991-2008
- Mead, A., Griffiths, C.L., Branch, G.M., McQuaid, C.D., Blamey, L.K., Bolton, J.J., Anderson, R., DuFois F., Rouault, M., Froneman, P.W., Whitfield, A.K., Harris, L., Nel, R., Pillay, D., Adams, J.B., 2013. Human-mediated drivers of change – impacts on coastal ecosystems and marine biota of South Africa. Afr J Mar Sci 35, 403-425.
- Melville-Smith, R., van Sittert, L., 2005. Historic commercial West Coast rock lobster *Jasus lalandii* landings in South African waters. Afr J Mar Sci 27, 33-44.
- Möllmann, C., Müller-Karulis, B., Kornilovs, G., St John, M.A., 2008. Effects of climate and overfishing on zooplankton dynamics and ecosystem structure: regime shifts, trophic cascade, and feedback loops in a simple ecosystem. ICES J Mar Sci 65, 302-310.
- Möllmann, C., Diekmann, R., Müller-Karulis, B., Kornilovs, G., Plikshs, M., Axe, P., 2009. Reorganization of a large marine ecosystem due to atmospheric and anthropogenic pressure: a discontinuous regime shift in the Central Baltic Sea. Glob Change Biol 15, 1377-1393.
- Moloney, C.L., Jarre, A., Arancibia, H., Bozec, Y.M., Neira, S., Roux, J.P., Shannon, L.J., 2005. Comparing the Benguela and Humboldt marine upwelling ecosystems with indicators derived from inter-calibrated models. ICES J Mar Sci 62, 493-502.

- Moloney, C.L., Fennessy, S.T., Gibbons, M.J., Roychoudhury, A., Shillington, F.A., von der Heyden, B.P., Watermeyer, K., 2013. Reviewing evidence of marine ecosystem change off South Africa. Afr J Mar Sci 35, 427-448.
- Morice, C.P., Kennedy, J.J., Rayner, N.A., Jones, P.D., 2012. Quantifying uncertainties in global and regional temperature change using an ensemble of observational estimates: The HadCRUT4 data set. J Geophys Res-Atmos (1984–2012)117,doi: 10.1029/2011JD017187.
- Perry, A.L., Low, P.J., Ellis, J.R., Reynolds, J.D., 2005. Climate change and distribution shifts in marine fishes. Science 308, 1912-1915.
- Pitcher, G.C., Calder, D.A., 2000. Harmful algal blooms of the southern Benguela Current: a review and appraisal of monitoring from 1989 to 1997. S Afr J Mar Sci 22, 255-271.
- Pitcher, G.C., Probyn, T.A., 2011. Anoxia in southern Benguela during the autumn of 2009 and its linkage to a bloom of the dinoflagellate *Ceratium balechii*. Harmful Algae 11, 23-32.
- Pitcher, G.C., Bernard, S., Ntuli, J., 2008. Contrasting Bays and Red Tides in the Southern Benguela Upwelling System. Oceanography 21, 82-91.
- Poloczanska, E.S., Brown, C.J., Sydeman, W.J., Kiessling, W., Schoeman, D.S., Moore, P. J., Brander, K., Bruno, J.F., Buckley, L.B., Burrows, M.T., Duarte, C.M., Halpern, B.S.,Holding, J., Kappel, C.V., O'Connor, M.I., Pandolfi, J.M., Parmesan, C., Schwing, F., Thompson, S.A., Richardson, A.J., 2013. Global imprint of climate change on marine life. Nat Clim Change 3, 919-925.
- Polovina, J.J.,2005. Climate variation, regime shifts, and implications for sustainable fisheries. Bull Mar Sci 76, 233-244.
- Rademeyer, R. A., Butterworth, D. S., Plagányi, É. E., 2008. Assessment of the South African hake resource taking its two-species nature into account. Afr J Mar Sci 30, 263-290.
- Reynolds, R.W., Rayner, N.A., Smith, T.M., Stokes, D.C., Wang, W., 2002. An improved *in situ* and satellite SST analysis for climate. J Climate15, 1609–1625.
- Rice, J.C., Rochet, M.J., 2005. A framework for selecting a suite of indicators for fisheries management. ICES J Mar Sci 62, 516-527.
- Robinson, T.B., Branch, G.M., Griffiths, C.L., Govender, A., Hockey, P.A.R., 2007. Changes in South African rocky intertidal invertebrate community structure associated with the invasion of the mussel *Mytilus galloprovincialis.* Mar Ecol Prog Ser 340, *163-171*.
- Rochet, M.J., Trenkel, V.M.,2003. Which community indicators can measure the impact of fishing? A review and proposals. Can J Fish Aquat Sci 60, 86-99.
- Rouault, M., 2012.Bi-annual intrusion of tropical water in the northern Benguela upwelling. Geophys Res Lett 39, L12606 doi: 10.1029/2012GL052099.
- Rouault, M., Penven, P., Pohl, B., 2009. Warming in the Agulhas Current system since the 1980's. Geophys Res Lett 36, L12602 doi: 10.1029/2009GL037987.
- Rouault, M., Pohl, B., Penven, P., 2010. Coastal oceanic climate change and variability from 1982 to 2009 around South Africa. Afr J Mar Sci 32, 237-246.
- Roy, C., van der Lingen, C.D., Coetzee, J.C., Lutjeharms, J.R.E., 2007. Abrupt environmental shift associated with changes in the distribution of Cape anchovy *Engraulis encrasicolus* spawners in the southern Benguela. Afr J Mar Sci 29, 309–319.
- Sagarin, R.D., Barry, J.P., Gilman, S.E., Baxter, C.H., 1999. Climate-related change in an intertidal community over short and long time scales. Ecol Monogr 69, 465-490.
- Scheffer, M., Carpenter, S., Young, B.D., 2005. Cascading effects of overfishing marine systems.Trends Ecol Evol 20, 579-581.
- Schwartzlose, R.A., Alheit, J., Bakun, A., Baumgartner, T.R., Cloete, R., Crawford, R.J.M., Fletcher, W.J., Green-Ruiz, Y., Hagen, E., Kawasaki, T., Lluch-Belda, D., Lluch-Cota, S.E., MacCall, A.D., Matsuura, Y., Nevárez-Martínez, M.O., Parrish, R.H., Roy, C., Serra, R., Shust, K.V., Ward, M.N., Zuzunaga, J.Z., 1999. Worldwide large-scale fluctuations of sardine and anchovy populations. Afr J Mar Sci 21, 289-347.

- Shannon, L.J., Neira, S., Taylor, M., 2008. Comparing internal and external drivers in the southern Benguela and the southern and northern Humboldt upwelling ecosystems. Afr J Mar Sci 30, 63-84.
- Shannon, L.V., Crawford, R.J.M., Pollock, D.E., Hutchings, L., Boyd, A.J., Taunton-Clark, J., Badenhorst, A., Melville-Smith, R., Augustyn, C.J., Cochrane, K.L., Hampton, I., Nelson, G., Japp, D.W., Tarr, R.J.Q., 1992. The 1980s – a decade of change in the Benguela ecosystem. S Afr J Mar Sci 12, 271-296.
- Stephen, V.C., Hockey, P.A.R., 2007.Evidence for an increasing incidence and severity of Harmful Algal Blooms in the southern Benguela region. S Afr J Sci 103, 223-231.
- Troell, M., Robertson-Andersson, D., Anderson, R.J., Bolton, J.J., Maneveldt, G., Halling, C., Probyn, T., 2006. Abalone farming in South Africa: An overview with perspectives on kelp resources, abalone feed, potential for on-farm seaweed production and socio-economic importance. Aquaculture 257,266-281.
- van der Lingen, C.D., 2011. The biological basis for hypothesizing multiple stocks in South African sardine. International Stock Assessment Workshop document, MARAM IWS/DEC11/P/OMP/P7, 10pp.
- Verheye, H.M., 2000.Decadal-scale trends across several marine trophic levels in the southern Benguela upwelling system off South Africa. Ambio 29, 30-34.